Cancer stromal cells and lymphovascular invasion

Jamie Lynn Null
Manassas, Virginia

Bachelor of Arts in Biology, University of Virginia, 2016
Master of Science in Biological and Physical Sciences, University of Virginia, 2018

A Dissertation presented to the Graduate Faculty of the University of Virginia in Candidacy for the Degree of Doctor of Philosophy

Department of Microbiology, Immunology, and Cancer Biology

University of Virginia
May 2023

Abstract

Breast cancer is the most commonly diagnosed cancer worldwide and is the leading cause of cancer-related mortality among women. Although existing therapeutic strategies are relatively effective at controlling localized disease, metastatic breast cancer that has spread to distant organs remains incurable and is responsible for the overwhelming majority of breast cancer-related deaths. In breast cancer metastasis, cancer cells escape from the primary tumor and enter circulation via the vasculature, allowing them to reach distant organs such as the lymph nodes, lungs, liver, bones, and brain and colonize these tissues. Standard therapies often fail to eliminate metastatic lesions, allowing for cancer outgrowth at these sites that compromises organ function and causes patient mortality. The lack of therapeutic options for metastatic disease can be attributed to the biological complexity of the metastatic process. Cancer cell invasion and entry into vessels is dynamic and driven by cross-talk between cancer cells and stromal cells within the tumor microenvironment, but the specific contributions of stromal populations are diverse and not fully understood. Therefore, we used in vivo genetic tools and in vitro functional assays to label and deplete a population of stromal cells marked by the expression of periostin, a matrisomal protein associated with metastasis, in order to characterize their functions during breast cancer progression. We report that highly-metastatic cancer cells activate periostin-expressing cells in the primary tumor site that promote collagen remodeling and lymphovascular invasion of cancer cells into lymphatic vessels, allowing for their colonization of the sentinel lymph node.

Acknowledgments

First and foremost, I have to thank my entire family for their unwavering love and support. Without their endless encouragement this work would not be possible, and I consider myself so lucky to live my life surrounded by such wonderful people. I would especially like to thank my parents and my sister who have supported me in every phase of life and are always there for me when I need them. I love them dearly and would not be where I am today without their love and support, so this work is dedicated to them.

Next, I would like to thank my amazing friends. Their friendship means the world to me and brings me such joy. I'm so grateful to know each and every one of them, and their presence in my life is invaluable. A special thanks to the "lunch crew" who provided daily distractions and listening ears that made the sometimes-difficult graduate school journey all the more enjoyable.

I would also like to thank my mentor, Dr. Andrew Dudley, for all of his guidance and encouragement during my PhD studies. His enthusiasm for cancer biology is contagious, and he has undoubtedly made me a better scientist and critical thinker. I could not have asked for a better mentor. Further, I would like to thank the members of my thesis committee, Dr. Amy Bouton, Dr. Hui Zong, Dr. David Kashatus, and Dr. Thomas Barker for their incredibly helpful feedback and advice. I'm also grateful to the members of the Dudley lab past and present for their valuable feedback and help over the years and for creating a great lab environment. Finally, I would like to give special thanks to Dr. Jay Fox for his guidance and support and acknowledge the collaborators who have helped

generate the data presented within this dissertation including Dr. Stacey Criswell, Dr. Adrian Halme, and Natalia Dworak of the UVA Advanced Microscopy Facility, Marya Dunlap-Brown of the UVA Molecular Immunologic and Translational Sciences Core, Jeremy Gatesman of the UVA Center for Comparative Medicine, Dr. Pankaj Kumar of the UVA Genome Sciences Core, the University of Minnesota Genomics Core, and Angela Miller and Dr. Patcharin Pramoonjago of the UVA Biorepository and Tissue Research Facility. Their contributions were essential to my project, and I am immensely grateful for their hard work.

Table of Contents

List of figures

List of abbreviations

ADC – antibody-drug conjugate

α-SMA – alpha-smooth muscle actin

CAF – cancer-associated fibroblast

CTD – carboxy-terminal domain

DCIS – ductal carcinoma *in situ*

DDR1 - discoidin domain receptor 1

DTA – diphtheria toxin A chain

ECM – extracellular matrix

EMT – epithelial-mesenchymal transition

EVs – extracellular vesicles

FAS1 – fasciclin1-like

HER2 – human epidermal growth factor receptor 2

HSPGs – heparan sulfate proteoglycans

iCAFs – inflammatory-like CAFs

LAIRs - leukocyte-associated Ig-like receptors

LOX – lysyl oxidase

myCAFs – myofibroblast-like CAFs

PDAC – pancreatic ductal adenocarcinoma

SHG – second harmonic generation

SPARC – secreted protein acidic and cysteine rich

TGFβ – transforming growth factor beta

TNC – tenascin-C

Chapter 1: Introduction

Breast cancer is the most commonly diagnosed cancer worldwide and is the leading cause of cancer-related mortality among women (1). In the United States, breast cancer accounts for nearly one-third of all cancer diagnoses in women and is expected to cause more than 43,000 deaths in 2023 (2). Although localized disease is often successfully treated, metastatic breast cancer that has spread to distant organs remains incurable and is responsible for virtually all breast cancer-related deaths (3). Standard therapies frequently fail to control metastatic growth, leading to a five-year survival rate for patients with distant disease of only 29% (4). Therefore, metastatic breast cancer poses a critical clinical challenge, and functionally characterizing metastasis-promoting features of the tumor microenvironment to inform the design of more effective therapeutic strategies is essential for improving patient outcomes.

The primary aim of this thesis is to determine how periostin-expressing stromal cells within the tumor microenvironment contribute to the metastatic dissemination of breast cancer cells. This chapter will provide an overview of breast cancer development and diagnosis, followed by a description of the current standards of care for breast cancer patients. Next is a discussion of the metastatic process and how breast cancer cells can enter circulation through lymphovascular invasion and disseminate to secondary sites. This is followed by a review of the breast tumor microenvironment and the contributions of diverse cell types, especially cancer-associated fibroblasts (CAFs), during primary tumor growth and metastasis. Finally, this chapter provides a review of the concepts and questions that will be addressed by the research compiled in this thesis and

how this information may be of clinical significance for the treatment of metastatic breast cancer.

1.1 Clinical overview of breast cancer

1.1.1 Mammary gland architecture and breast cancer progression

Mammary glands develop during puberty into branching ductal structures consisting of two tissue compartments: the epithelium and stroma. The epithelium is comprised of a central layer of luminal epithelial cells surrounded by a layer of myoepithelial cells attached to the basement membrane. These epithelial structures are embedded in connective tissue stroma consisting of the extracellular matrix (ECM) and diverse stromal cells including adipocytes, fibroblasts, macrophages and other immune cells, blood vessels, and lymphatic vessels (5, 6). Breast cancers develop from transformed, hyperproliferative epithelial cells and progress sequentially to *in situ*, invasive, and metastatic carcinomas (7). Ductal carcinoma *in situ* (DCIS) lesions are confined to the duct whereas invasive carcinomas are characterized by loss of the integrity of the myoepithelial cell layer and basement membrane (6). Once the basement membrane is breached, cancer cells can invade into the surrounding stroma and enter blood and lymphatic vessels, resulting in metastatic disease in which breast cancer cells spread to distant sites including the lymph nodes, lungs, liver, bone, and brain (8-11) (Figure 1.1).

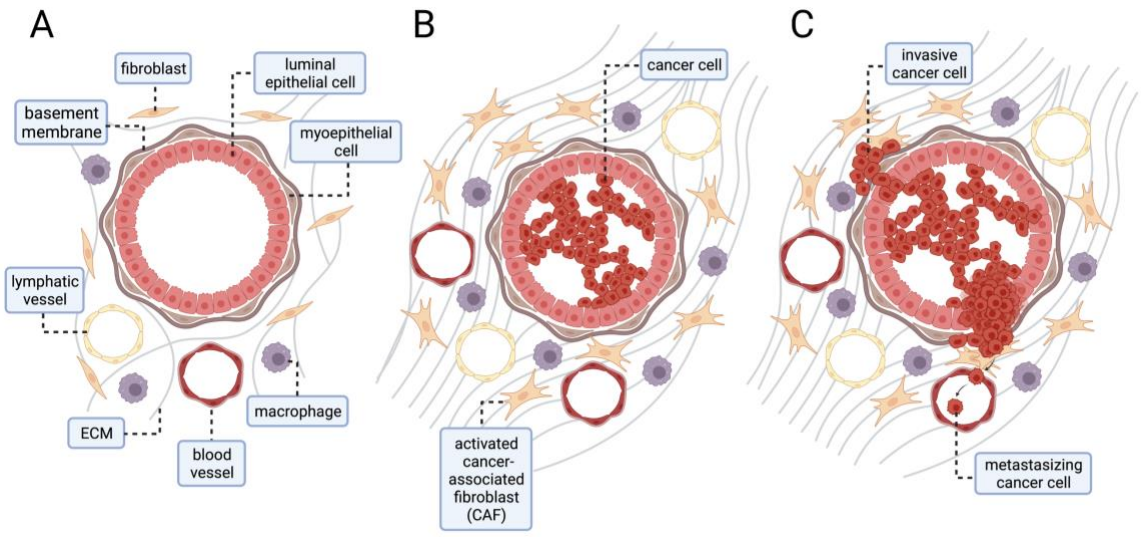

Figure 1.1. Breast cancer progression. (A) Normal breast ducts consist of a layer of luminal epithelial cells surrounded by a second layer of myoepithelial cells and enclosed by a continuous basement membrane. Ducts are embedded in an extracellular matrix (ECM) primarily composed of collagen and surrounded by fibroblasts, immune cells such as macrophages, and a vascular network consisting of lymphatic and blood vessels (B) Progression to ductal carcinoma *in situ* is characterized by the hyperproliferation of transformed epithelial cells (cancer cells) within the duct, activation of fibroblasts into cancer-associated fibroblasts (CAFs), proliferation of CAFs and immune cell infiltrates, and enhanced angiogenesis and lymphangiogenesis. (C) Invasive breast carcinoma is defined by breakdown of the basement membrane surrounding the duct and invasion of cancer cells into the surrounding stroma and vasculature. Cancer cells that reach lymphatic and blood vessels can then disseminate to secondary sites, leading to metastatic disease. This figure is adapted from Cichon *et al*. (2010) (12) and was made using BioRender.

1.1.2 Breast cancer diversity and classification

Since invasive breast cancers are phenotypically and molecularly diverse, tumors are classified according to multiple parameters including histologic grade, molecular subtype, and stage. These classifications are subsequently used to inform treatment decisions and predict prognosis. Clinicians use histology of biopsied tissues from the primary tumor to visualize ductal structures, assess the extent of cancer cell invasion, and assign the cancer a grade based on the nuclear appearance of the cancer cells. Grades are numerically categorized from low to high, with a higher grade indicating that the cancer cells are less differentiated, more proliferative, and, therefore, more likely to spread (13, 14).

Breast cancers are assigned to three primary molecular subtypes based on the expression of pro-proliferative target genes within the biopsied tissues: hormone-receptor positive, human epidermal growth factor receptor 2 (HER2)-enriched, and triple-negative (15, 16). Hormone-receptor positive cancers display high expression of the estrogen and/or progesterone hormone receptors which have been shown to regulate cell cycle progression and cell proliferation (17-19). HER2-enriched breast cancers are characterized by high expression of HER2/neu, a cell-surface receptor of the ErbB family of receptor tyrosine kinases that promotes cell proliferation and survival by signaling through the Ras/MAPK and PI3K/Akt pathways (20). Finally, triple-negative breast cancers are marked by a lack of target gene expression as they display low expression of both hormone receptors and HER2 (21). Breast cancers may be further divided into intrinsic subtypes according to additional gene expression information, but the

three primary molecular subtypes listed above are most commonly used for clinical decision-making and disease management (22-24).

Disease stage is an assessment of primary tumor size, regional lymph node involvement, and distant metastases based on physical examination, pathologic classification, and imaging via mammography, ultrasound, and/or MRI (25-27). Primary tumor size is assigned a score from T0-T3 based on its greatest dimension. In addition, a tumor of any size that has directly extended into the chest wall and/or the skin is assigned a score of T4. Regional lymph nodes are often the initial sites of metastasis and can indicate disease spread, which is why they are used for breast cancer staging. Lymph nodes can be assessed clinically or pathologically, and the regional lymph node classifications range from N0-N3 based on how many lymph nodes contain evidence of cancer cells and the area of cancer growth within those nodes. Distant metastasis is classified as M0 or M1, with M0 indicating that there is no clinical or radiographic evidence of distant metastases and M1 indicating that there are detectable distant metastases present (26). Once each of these factors has been scored, the information is combined to assign an overall stage which then informs patient treatment and prognosis.

1.1.3 Current standards of care

Molecular subtype and stage are used to develop therapeutic plans for breast cancer patients. For non-metastatic breast cancer, the main goal of treatment is to use a combination of local and systemic therapies to eradicate the

primary tumor from the breast and eliminate any cancer growth in regional lymph nodes. Local therapy consists of surgery (either lumpectomy to remove the tumor or mastectomy to remove the entire breast), sampling and/or removal of axillary lymph nodes, and radiation (3). Systemic therapy is guided by molecular subtype and includes endocrine therapy, chemotherapy, and targeted therapies. The timing of systemic therapy varies and may be neoadjuvant (administered before surgical resection of the tumor), adjuvant (postoperative), or both. Hormone receptor positive cancers are treated with endocrine therapies that reduce estrogen signaling-mediated tumor growth by either competitive antagonism for the estrogen receptor (tamoxifen) or by reducing circulating estrogen levels by preventing the conversion of androgens into estrogen by the enzyme aromatase (aromatase inhibitors). Patients with hormone receptor positive cancers that have received endocrine therapy may also be treated with chemotherapy which consists of drugs that are cytotoxic to proliferating cells. Chemotherapy is also typically administered to patients with HER2-enriched breast cancer in addition to targeted therapies, which limit tumor growth by disrupting HER2 signaling (28, 29). Triple-negative breast cancers are especially clinically challenging as they do not display hormone receptor positivity or HER2-enrichment and display extensive genomic and clinical heterogeneity (30-32). Therefore, therapeutic options for patients with triple-negative breast cancer are limited, and chemotherapy remains the primary treatment for both early-stage and advanced-stage triple-negative disease (3, 33). In contrast to non-metastatic breast cancer where the goal is to eradicate cancer cells and achieve remission, metastatic

disease is considered incurable so the primary therapeutic goal when treating patients is to prolong life and provide palliative care. Systemic therapies are most commonly used in metastatic breast cancer cases, though local therapies may be employed to treat painful symptoms or prevent complications from tumor growth.

1.1.4 Prognoses and limitations

Current therapies are generally effective in treating non-metastatic breast cancers, with survival rates of ~ 93% at four years post-diagnosis for patients with hormone receptor-positive breast cancer, ~83% for patients with HER2-enriched breast cancer, and ~77% for patients with triple-negative breast cancer (34). However, a major limitation of breast cancer treatment is the frequency of disease recurrence, as nearly 30% of women initially diagnosed with early-stage breast cancer ultimately develop recurrent metastatic disease for which there is a significantly worse prognosis (11). Recurrent metastatic disease results from dormant disseminated cancer cells that are re-activated into a proliferative state and grow-out at secondary sites into clinically-detectable metastatic lesions (8, 35-40), and this process can occur over a wide-ranging time frame, from months to decades following initial treatment of the primary tumor (41, 42). Triple-negative disease is the most likely to recur within five years of diagnosis, and metastatic triple-negative disease has a significantly shorter median overall survival compared to the other subtypes (one year versus five years, respectively) (3, 33). As previously mentioned, metastatic breast cancer is

considered incurable and is responsible for the overwhelming majority of breast cancer-related deaths. Therefore, the lack of effective therapeutic options for metastatic disease, especially of the triple-negative subtype, is a significant unmet clinical need that can be partially attributed to the biological complexity of the metastatic process.

1.2 Metastasis

1.2.1 The metastatic cascade

Metastasis is a multi-step process in which cancer cells egress from the primary tumor and disseminate throughout the body to colonize distant organs. Throughout the metastatic process, cancer cells display phenotypic plasticity as they undergo a series of transcriptional and morphological changes that allow them to progress through the metastatic cascade. First, cancer cells breach the basement membrane and locally invade into surrounding tissue stroma. This local invasion coincides with transcriptional changes within the cancer cells, often referred to as epithelial-mesenchymal transition (EMT), that allow them to migrate, remodel the surrounding extracellular matrix, and survive as individual cells or small cellular clusters as they navigate the surrounding tissue (43-48). Cancer cells then transmigrate across the endothelial barrier and intravasate into lymphatic and blood vessels which serve as routes for their transit to distant tissues (49). Cancer cells must survive in circulation, then arrest at a distant organ site and cross the endothelium again to extravasate through the vascular walls and basement membrane into the parenchyma of the tissue (50, 51).

Cancer cells first form micrometastases within the parenchyma and often enter dormancy during which they must survive and adapt to the new tissue microenvironment. These latent micrometastases can later be re-activated into a proliferative state and grow out into overt metastatic colonies that form clinically detectable lesions (37, 39, 52-57) (Figure 1.2).

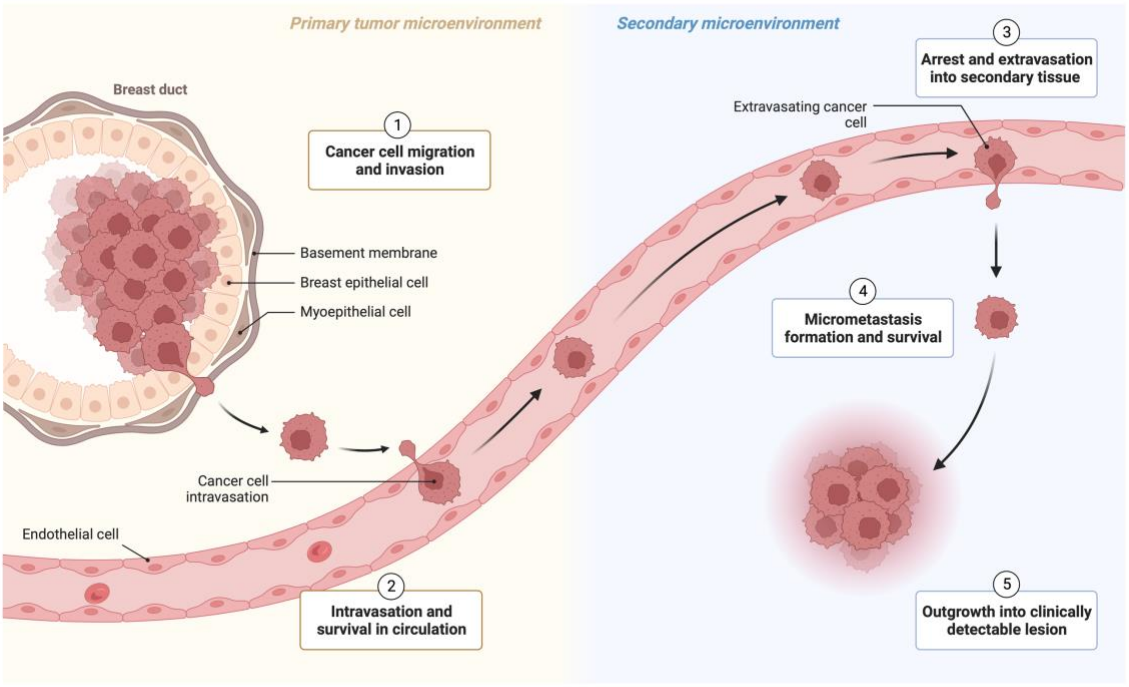

Figure 1.2. The metastatic cascade. During metastatic progression, cancer cells locally invade and intravasate into blood and lymphatic vessels. They then must survive in systemic circulation and arrest in a distant organ. Following arrest, cancer cells extravasate out of the vasculature into the parenchyma of the secondary tissue where they must adapt to a new microenvironment in order to survive and expand from micrometastases into clinically detectable macrometastases. This figure is adapted from Valastyan *et al*. (2011) (12, 54) and was made using BioRender.

1.2.2 The metastatic microenvironment

Although the metastatic cascade is considered a linear progression as cancer cells physically translocate from the primary tumor to distant organs, the process is dynamic and further complicated by the involvement of the diverse cellular populations and other microenvironmental factors that can both limit and promote metastatic progression. Each step of the metastatic cascade involves cross-talk between cancer cells and their microenvironment, so the process includes both cell-intrinsic and cell-extrinsic determinants of successful metastasis. This idea was first captured by Stephen Paget's "seed and soil hypothesis" proposed in 1889, which includes three key points: metastases can only form in tissues with biologically compatible microenvironments, primary tumors and metastases consist of both cancer cells and host cells, and metastases result from the interactions between disseminated cancer cells (seeds) and the surrounding milieu (soil) (8, 53, 58, 59). The ability of the primary tumor microenvironment to promote early steps in the metastatic cascade, including invasion and dissemination, will be discussed later in this chapter and is a primary focus of this thesis, but it is important to first consider how the tissue microenvironment of distant organs informs metastatic colonization as well as the ways in which disseminated cancer cells adapt to and modulate their surrounding microenvironment to support their survival and growth at secondary sites.

Patterns of metastases are non-random, with different cancers displaying preferential tropism for certain secondary organs. In the case of breast cancer, primary tumors most often metastasize to the lungs, liver, bone, and brain. This

can be attributed to the fact that the microenvironments within different organs are structurally and molecularly distinct, so cancer cells will only successfully colonize biologically compatible microenvironments (52, 53, 60). In other words, a receptive tissue microenvironment is required for disseminated cancer cells to form metastases. There is growing evidence that primary tumors can release systemic signals such as soluble factors and extracellular vesicles (EVs) that can modify the ECM, vasculature, and immune landscape of distant tissues and establish a premetastatic niche in these organs, rendering them more permissive to cancer cell colonization (54, 61-71). Additionally, once cancer cells have reached secondary sites they can modulate the surrounding microenvironment by remodeling the ECM, inducing angiogenesis, activating tissue-resident fibroblasts into cancer-associated fibroblasts (CAFs), and mobilizing immune-suppressive cells in order to survive and support their outgrowth into macrometastases (10, 39, 72-78).

1.2.3 Lymphatic involvement

Before breast cancer cells can reach distant organs and establish metastases, they often first transit to the axillary lymph nodes as these are typically the first nodes in the lymphatic basin that receive drainage from the anatomic region in which the primary tumor resides. Axillary lymph node status is one of the most significant prognostic factors in women with early stage breast cancer and is therefore used for disease staging as described above (79, 80). A study of more than 24,000 breast cancer patients demonstrated that as lymph

node involvement increased, five-year survival status decreased regardless of primary tumor size (81). Thus, lymphatic metastasis is considered an indication of how likely a tumor is to spread to distant sites and can lead to regional recurrence as well as distant metastases as cancer cells often metastasize regionally through the lymphatics before ultimately metastasizing systemically through the blood (82-85). In fact, lymph node involvement may have a functional bearing on subsequent metastatic colonization of distant tissues. It was recently shown that exposure to the lymphatic environment can promote distant metastases by protecting disseminated cancer cells from ferroptosis as they enter circulation, thereby increasing the ability of metastasizing cancer cells to survive as they transit to secondary sites (86). Additionally, lymph node colonization can promote distant metastases by inducing broad alterations in the immune repertoire that drive tumor-immune tolerance and allow for survival and outgrowth of metastatic colonies (87). These findings contradict the previous notion that metastatic deposits in the regional lymph nodes are primarily dead ends for cancer cells and simply function as markers of parallel dissemination from the primary tumor into the general circulation (52); instead, they demonstrate that lymph node involvement is not just an indication of disease spread but rather a process that functionally contributes to disease progression.

1.2.4 Lymphovascular invasion

In order to reach regional lymph nodes, cancer cells must first escape from the primary tumor and intravasate into lymphatic vessels – a process called

lymphovascular invasion. Lymphovascular invasion is the predominant method of vascular invasion in breast cancer, and is a significant independent prognostic factor associated with increased risk of recurrence, distant metastasis, and death from the disease (85, 88-91). Lymphatic vessels function to regulate interstitial fluid pressure, facilitate macromolecule transport, and serve as an entry point for immune cell trafficking (82, 92-95). The architecture of the lymphatic endothelium is reflective of its role in absorbing interstitial fluid and allowing immune cells to transit between the lymphatic vasculature and the tissue parenchyma, distinguishing lymphatic vessel structure from that of blood vessels and making lymphatic vessels inherently more amenable to the intravasation of cancer cells (82). For example, unlike blood capillaries, lymphatic capillaries lack pericyte coverage and are surrounded by an incomplete basement membrane. Additionally, lymphatic capillaries have discontinuous intercellular junctions that open as a result of increased interstitial pressure in order to permit the passage of fluid and particles into the vessels to normalize the pressure balance within the tissue (92, 96). Whereas high intratumoral interstitial fluid pressure can compress and collapse blood vessels (97), preventing intravasation, the discontinuous intercellular junctions of lymphatic vessels and the anchoring of the lymphatic endothelium to the surrounding extracellular matrix allow lymphatic lumens to remain open despite increased interstitial pressure and enhance the intravasation of cancer cells (85, 98) (Figure 1.3). Once cancer cells enter the lymphatic vasculature, they experience lower shear stress and oxidative stress than they would encounter in blood circulation, further supporting the survival of

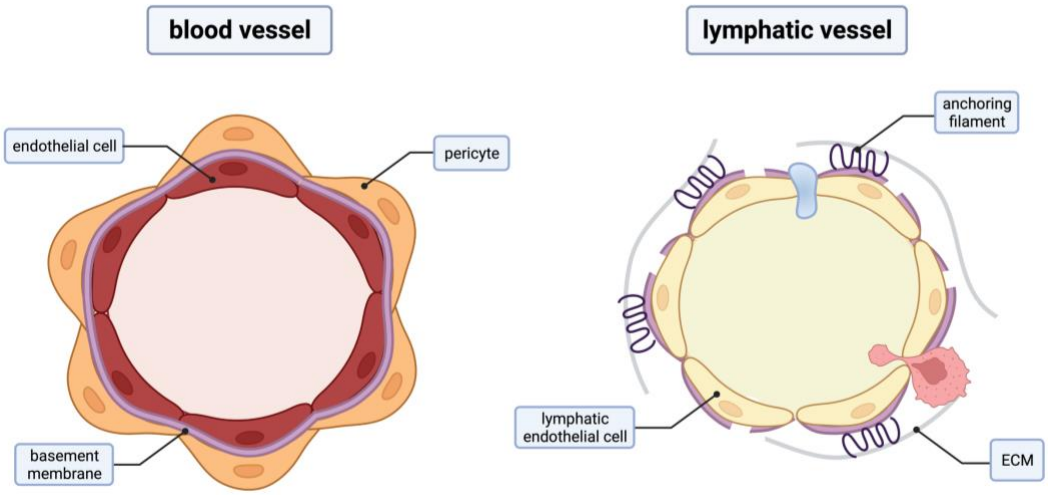

Figure 1.3. Structural differences between blood vessels and lymphatic vessels. Cross sections of a blood capillary (left) and initial lymphatic vessel (right). Blood vessels are surrounded by a continuous basement membrane and pericytes whereas lymphatic vessels lack pericyte coverage and are characterized by a discontinuous basement membrane. Lymphatic endothelial cells are anchored to the extracellular matrix which stretches as interstitial fluid pressure increases, allowing for the entry of fluid (shown in blue) and cells (shown in pink) into lymphatic vessels. This figure is adapted from Stacker *et al*. (2014) (95) and was made using BioRender.

metastasizing cancer cells (85). Together, these structural and physiological features allow the lymphatic vasculature to serve as the predominant route of cancer cell dissemination in breast cancers (88). In addition to the structural and physiological differences that distinguish blood and lymphatic vessels, there are also molecular features including chemokines and growth factor receptors that are selectively upregulated in the lymphatic vasculature that function as chemo-attractants for cancer cells and promote their directional migration towards lymphatic vessels (94, 99-107). While these physiological processes and molecular mechanisms underlying lymphovascular invasion have been elucidated, the process of cancer cell invasion and intravasation into lymphatic vessels is likely also driven by the heterotypic interactions between cancer cells and the diverse auxiliary cells in the breast tumor microenvironment, though these contributions remain largely unknown.

1.3 Breast tumor microenvironment

Solid tumors are communities of heterogeneous cell populations whose interactions play key roles in tumor progression and metastasis. The breast tumor microenvironment consists of neoplastic epithelial cells, which make up the bulk of the tumor, surrounded by diverse cellular populations including immune cells, cancer-associated fibroblasts (CAFs), and a vascular network consisting of both lymphatic and blood vessel endothelium (108). Molecular characterization of the breast cancer microenvironment has shown that each of these cell populations undergo gene expression changes during tumor progression, and cellular cross-talk among these altered populations can shift the landscape of the

tumor microenvironment and promote early steps in the metastatic cascade by contributing to basement membrane degradation, cancer cell invasion, CAF activation, ECM-remodeling, enhanced angiogenesis and lymphangiogenesis, and immune suppression (5, 6, 67, 95, 109-133). The immune milieu consists of distinct cell populations that display complex and dynamic functions within the tumor microenvironment. While the immune system has been implicated in both promoting and preventing tumor growth, tumor-associated immune populations have been shown to largely suppress the host anti-tumor immune response and promote tumor growth and dissemination by remodeling the ECM and producing pro-angiogenic and pro-invasive growth factors, cytokines, and enzymes (76, 104, 129). Therefore, these cells directly contribute to tumor progression and are of significant interest in the investigation of cancer metastasis. However, the focus of this thesis is the interface between cancer cells, CAFs, and the ECM and how these interactions drive critical steps in the early metastatic cascade by promoting lymphovascular invasion and lymphatic metastasis.

1.4 Cancer-associated fibroblasts (CAFs)

1.4.1 Origin and activation

CAFs are the most abundant stromal cell type in breast cancers and can arise from multiple sources including quiescent tissue-resident fibroblasts that are activated into a proliferative and synthetic state in response to the parenchymal tissue injury caused by tumor growth (68, 134, 135). During acute wound healing, fibroblasts are activated by growth factor signaling to proliferate,

secrete growth factors, and deposit a provisional matrix to mediate tissue repair. The ECM consists of structural proteins that provide flexibility and support tissue integrity during mechanical stress like collagens, laminins, elastins, and fibronectins and non-structural proteins including proteoglycans and hyaluronan which bind to and stabilize growth factors as well as glycoproteins such as integrins that regulate cell adhesion, cytoskeletal re-organization, and signaling between cells and the ECM (136-139). Following matrix synthesis, the ECM molecules secreted by fibroblasts are re-aligned and cross-linked to form a mature matrix which, over time, allows for the injury to resolve and restores tissue integrity. Once the injury is resolved, activated fibroblasts either undergo apoptosis and are cleared or return to a quiescent state. This process is recapitulated in solid tumors, but since tumor growth causes a chronic wound that does not heal, the process becomes dysregulated and does not resolve, resulting in abundant persistently activated CAFs within the tumor microenvironment (140-142). Once activated, CAFs are characterized by enhanced expression of alpha-smooth muscle actin (α-SMA), a cytoskeletal protein that confers contractile properties to cells, thereby giving CAFs their classic stellate morphology and an increased capacity for migration. CAFs also display an enhanced secretory phenotype and are synthetically active – serving as a source of growth factors, cytokines, metabolites, and matrix components within the tumor (135). The resulting biochemical crosstalk between CAFs and cancer cells as well as CAF-driven matrix remodeling are important contributors to cancer progression and are implicated in multiple hallmarks of cancer

including sustaining proliferative signaling, evading growth suppressors, and activating invasion and metastasis (139, 143, 144).

1.4.2 Roles in ECM remodeling

Just as fibroblasts are arbiters of the ECM in normal tissues, CAFs also deposit, assemble, and modulate the ECM within tumors by synthesizing a number of structural and non-structural ECM components. However, given their aberrant activation, CAFs secrete increased levels of structural proteins including collagens, fibronectins, tenascins, and elastin and exhibit enhanced expression of lysyl oxidases, the family of enzymes responsible for collagen cross-linking, as well as matrix-degrading metalloproteinases, leading to changes in the composition, organization, and mechanical properties of the intratumoral ECM (140). The collagen fibers surrounding the epithelial structures within the normal mammary gland are typically anisotropic and curly in structure, but many of the fibers thicken and linearize over the course of tumor progression (145, 146). Linearized fibers are more rigid than curly fibers, and the resulting increase in ECM stiffness can enhance cancer cell proliferation, plasticity, migration, and metastasis (122, 127, 147-151). CAFs serve as leader cells in the collective invasion of cancer cells and fibroblasts, as they remodel the ECM at the leading edge and promote migration by creating “tracks” in the collagen matrix that cancer cells then exploit for directional invasion, aiding their intravasation into vessels and dissemination to distant organs (152-154). Therefore, the ECM-remodeling function of CAFs directly contributes to tumor progression and has

clinical consequences for patients. In human breast cancer samples, a higher density of activated CAFs and stromal desmoplasia are consistent aspects of invasive progression and distinguish tumors that are “non-progressors” from those that recur and spread (121). Additionally, tumor-associated collagen signature analysis of biopsied human breast cancer tissues has revealed that a matrix characterized by bundles of straightened and aligned collagen fibers that are oriented perpendicular to the tumor boundary is an independent prognostic indicator of patient outcome as it significantly correlates with poor patient survival (155). Although these roles of CAFs in ECM remodeling, cancer cell migration, and metastasis position them as attractive therapeutic targets, preclinical depletion studies have yielded unexpected results with indiscriminate CAF depletion leading to more aggressive, undifferentiated tumors (156, 157). This indicates that diverse CAF subpopulations play opposing roles in the tumor microenvironment, with some CAFs restraining tumor growth while others are tumor-supportive.

1.4.3 Molecular and functional diversity of CAFs

Single-cell transcriptomic studies have begun to uncover the extent of molecular heterogeneity among CAF subpopulations, revealing spatially distinct CAF populations that perform diverse context-dependent functions within the tumor microenvironments of different cancers (120, 158-166). Though CAFs are mainly characterized by expression of contractile proteins such as alpha smooth muscle actin (α-SMA) and extracellular matrix (ECM) proteins including collagens

and fibronectin, single-cell transcriptomic analysis has identified additional subpopulations of CAFs that display expression profiles associated with proliferation, vascular development and angiogenesis, and immune modulation (67, 124, 163). A recent single-cell and spatially resolved atlas of human breast cancers identified five distinct subclasses of CAFs that exhibit diverse differentiation states. These subclasses include immune modulatory "MSC/inflammatory-like CAFs (iCAFs)" that display high expression of mesenchymal stem cell markers and inflammatory markers and "myofibroblast-like CAFs (myCAFs)" that are characterized by increased expression of *ACTA2* (α-SMA) and *COL1A1* (type I collagen) (162). These CAF subsets are often spatially segregated within the tissue, indicating that signals from the local microenvironment likely drive CAF differentiation and that CAFs may transition between these differentiation states depending on heterotypic cellular interactions. Importantly, CAF composition is not only dependent on spatial distribution but is also temporally regulated. Human breast cancer specimens show that CAF populations are dynamic and shift over the course of tumor progression, which can have direct clinical implications as CAF composition has been shown to directly contribute to treatment response and patient outcome (120, 167). Given the complexity of CAF heterogeneity, functional classification of molecularly-defined CAF subpopulations is necessary to overcome the limitations of broadly targeting CAFs so that specific tumor-promoting and/or metastasis-promoting CAFs can be identified and tracked over the course of tumor progression. A challenging but critical first step in this process is identifying

reliable biomarkers that distinguish pro-tumorigenic and pro-metastatic CAFs from their counterparts. This thesis explores the possibility that periostin, a matricellular protein induced by tissue injury and enriched in myofibroblasts in the heart, could serve as a marker of pro-metastatic CAFs in the breast tumor microenvironment.

1.5 Periostin

1.5.1 Structure, function, and expression

Periostin, originally named osteoblast-specific factor 2, is a TGFβ-induced matricellular protein first discovered in murine osteoblasts with ~90% homology in mice and humans (168-170). Periostin is a secreted protein with a multi-domain structure consisting of an amino-terminal signal peptide, a cysteine-rich EMI domain, four repeated fasciclin-like (FAS1) domains, a variable hydrophilic carboxy-terminal domain (CTD), and a heparin-binding site (170-173) (Figure 1.4). The EMI domain is named after a domain first described in the EMILIN family and binds directly to collagen I and fibronectin. The FAS1 domains are homologous to the protein fasciclin 1 which is an evolutionarily ancient adhesion domain found in extracellular proteins and common to all living species (168). Therefore, periostin belongs to the fasciclin family. The FAS1 domains bind tenascin-C (TNC), integrins αvβ3 and αvβ5, and bone morphogenetic protein-1 (BMP-1) (170, 172, 174). The CTD undergoes alternative splicing to generate

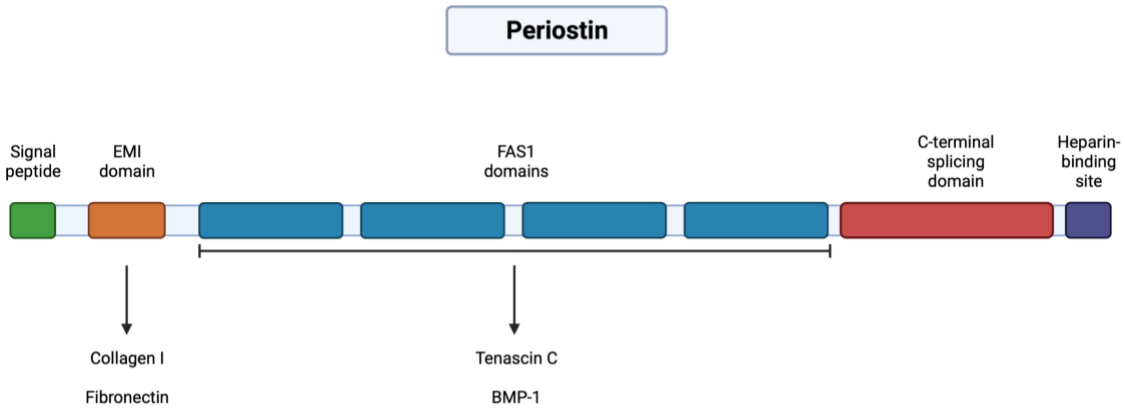

Figure 1.4. Protein structure of human periostin. Periostin has a multi-domain structure consisting of an amino-terminal signal peptide, a cysteine-rich EMI domain that binds to ECM proteins including collagen I and fibronectin, four repeated fasciclin-like (FAS1) domains that bind to tenascin C and BMP-1, a variable hydrophilic carboxy-terminal splicing domain, and a heparin-binding site. This figure is adapted from Sonnenberg-Riethmacher *et al*. (2021) (172) and was made using BioRender.

different protein isoforms and is known to bind heparin and heparan sulfate proteoglycans (HSPGs) (172, 175).

The adjacent binding domains of periostin allow for interacting matrix proteins to be in close proximity, thereby serving as a protein scaffold for mediators of matrix assembly and promoting intermolecular interactions that drive the assembly of extracellular architectures (175, 176). Therefore, although it is a nonstructural matrix protein, periostin's interactions with other ECM components directly affect matrix structure. For example, periostin regulates collagen fibrillogenesis by binding to BMP-1 and promoting BMP-1-mediated cleavage of the propeptide of lysyl oxidase (LOX) into its mature, activated form which catalyzes the intra- and intermolecular covalent cross-linking of collagen molecules, an essential process for the stabilization of collagen fibrils (174, 175, 177, 178). Periostin can also regulate cellular processes such as cell survival, proliferation, adhesion, and migration by engaging integrin signaling and binding to cell-surface heparin and HSPGs (175, 179, 180). Thus, periostin modulates both the biomechanical properties of the ECM as well as intracellular signaling driven by cell-matrix interactions.

Periostin is generally present at low levels in most adult tissues and is typically found in collagen-rich connective tissues that experience mechanical stress such as heart valves, tendons, and the periodontal ligament (177). Periostin is frequently induced at sites of inflammation and injury, and is expressed by activated myofibroblasts during wound repair (181-185). Thus, its expression is often elevated in pathological conditions compared to normal

physiological conditions (170). Since the CTD of the periostin protein can be alternatively spliced to generate three isoforms in mice and ten isoforms in humans, it has been proposed that full-length periostin and its variable isoforms may be differentially expressed across tissues and in various diseases (186-192).

1.5.2 Roles in cancer

Periostin has been shown to play multi-faceted roles in a number of pathologies including allergic asthma (172, 193-195), pulmonary fibrosis (196-198), scleroderma (171, 199, 200), chronic kidney disease (201-204), atherosclerotic cardiovascular disease (205, 206), and cancer (72, 179, 190, 191, 207-212). High expression of periostin protein and/or mRNA is detected in multiple cancer types including breast cancer, pancreatic ductal adenocarcinoma, non-small-cell lung carcinoma, oral squamous-cell carcinoma, melanoma, head and neck cancer, gastric cancer, and colon cancer (210). In these solid tumors, periostin is primarily secreted by stromal populations, though there is evidence that tumor cells can express periostin in certain cancers (213-216). It has been implicated in diverse pro-tumorigenic processes including angiogenesis, invasion, anchorage-independent growth, tumor cell proliferation and survival, ECM-remodeling, and chemoresistance (184, 210, 217-221).

In breast cancer, periostin has primarily been characterized in the context of the metastatic niche. In addition to establishing an immunosuppressive microenvironment in the lungs during breast cancer metastasis, periostin has

also been reported to recruit Wnt ligands in pulmonary metastases of breast tumors, thereby increasing Wnt signaling in the infiltrating cancer stem cells and promoting their self-renewal and expansion (72, 208). Similarly, periostin is associated with the perivascular niche of disseminated breast cancer cells where it is reported to promote micrometastatic outgrowth of dormant tumor cells (39). In a mouse model of breast cancer, periostin knockout results in a significant decrease in lung metastases but does not affect primary tumor growth (72). Therefore, periostin has been largely classified as a critical pro-tumorigenic component within the metastatic niche.

1.5.3 Limitations of previous studies of periostin

Though previous studies have elucidated important functions of periostin in metastatic breast cancer, their methods include technical limitations that affect the interpretation of the results. For example, the studies of periostin in pulmonary metastases of breast cancer relied on the use of periostin null mice, which are now understood to display some embryonic lethality. Surviving periostin null mice often display severe growth retardation and skeletal defects postnatally and frequently die before weaning due to valvular insufficiency in the heart (222). Given these significant anatomical abnormalities, a conditional depletion strategy would be a more valid approach to characterize the role of periostin specifically during tumor progression. The study of periostin in the perivascular niche used organotypic microvascular niche cultures to show that periostin expression is enhanced in cultures with abundant neovascular tips, but

provided limited evidence that periostin is enriched within the perivascular micrometastatic niche in vivo (39). Further, each of these studies of periostin relied on immunohistochemical staining to characterize its abundance and distribution within tumors and metastatic microenvironments. However, periostin is a secreted protein so this technique does not reveal the cellular source of periostin within each tissue. Though in vitro studies and single cell transcriptomic analyses indicate that stromal cells are likely the source of periostin in these contexts, molecularly-defined periostin-expressing stromal populations have not been studied in situ using genetic tools to elucidate their specific functions during breast cancer progression. Therefore, we set out to study periostin-expressing cells in the context of the tumor microenvironment by adapting a genetic lineage-tracing strategy that had previously been used to define the origin and function of periostin-expressing myofibroblasts in the injured heart (223).

1.6 Significance and overview

Given the previously stated limitations of studies of periostin in tumor progression, there are several outstanding questions that this dissertation aimed to address. First, we used a lineage tracing mouse model to characterize periostin$^+$ cells in tumor-naïve mammary glands and tracked their activation in primary tumors, premetastatic niches, and metastatic sites. Since previous studies have established a connection between periostin and metastasis, we compared periostin$^+$ populations in low- versus highly-metastatic tumors to determine whether the metastatic potential of cancer cells within the primary

tumor affects the activation of periostin-expressing cells across primary and secondary tissues. We demonstrated that periostin^{+} cells are more abundant in mice bearing highly-metastatic tumors and that this differential activation coincides with ECM remodeling and collagen organization within the primary tumor. Therefore, we next examined whether periostin expression regulates the ability of CAFs to generate an organized collagen matrix. Using primary human breast CAFs, we performed a series of in vitro knock down experiments to establish a functional connection between periostin expression and collagen matrix deposition. We found that knocking down periostin reduced the expression of collagens, matrisomal proteins, and ECM regulators and reduced the ability of CAFs to spread and migrate. Additionally, periostin knock down in CAFs limited the ability of co-cultured cancer cells to invade through a 3D collagen matrix and reduced the transmigration of cancer cells across a lymphatic endothelial cell barrier. Given this role for periostin-expressing CAFs in collagen-mediated collective cell invasion in vitro, we then performed in vivo depletion studies to determine how periostin^{+} cells contribute to primary tumor growth and metastasis. Using a diphtheria toxin A chain (DTA) mouse model in which specific cell populations undergo Cre-dependent selective depletion through expression of the diphtheria toxin, we ablated periostin-expressing cells in vivo and measured tumor growth and metastatic burden in the lymph nodes and lungs. Surprisingly, we found that depleting periostin-expressing cells accelerated primary tumor growth but reduced lymphatic metastasis. These findings are detailed in Chapter 2 and provide a new understanding of stromal

contributions to the lymphovascular invasion and metastatic colonization of breast cancer cells. In Chapter 3, remaining questions regarding periostin^{+} cell activation during tumor progression are explored as well as future experimental directions to address these gaps in knowledge. Finally, the clinical relevance of our findings is discussed and our work is put into broader context within the cancer biology field.

Chapter 2: Periostin^{+} stromal cells guide lymphovascular invasion by cancer cells

**This chapter is a modified version of a manuscript under review at Cancer Research, "Periostin^{+} stromal cells guide lymphovascular invasion by cancer cells". JL Null, DJ Kim, JV McCann, P Pramoonjago, JW Fox, P Kumar, L Edatt, CV Pecot, and AC Dudley. (2023).*

All data presented in this chapter were generated by JL Null unless otherwise indicated

2.1 Abstract

Cancer cell dissemination to the sentinel lymph node associates with poor patient outcomes, particularly in breast cancers. How cancer cells egress the primary tumor upon interfacing with the lymphatic vasculature is complex and driven by dynamic interactions between cancer cells and stromal cells including cancer associated fibroblasts (CAFs). The matricellular protein periostin can distinguish CAF subtypes in breast cancer and is associated with increased desmoplasia and disease recurrence in patients. However, since periostin is secreted, periostin-expressing CAFs are difficult to characterize in situ, limiting our understanding of their specific contribution to cancer progression. Here, we used in vivo genetic labelling and ablation to lineage trace periostin^{+} cells and characterize their function(s) during tumor growth and metastasis. We report that periostin-expressing CAFs are spatially found at periductal and perivascular margins, are enriched at lymphatic vessel peripheries, and are differentially activated by highly-metastatic cancer cells versus low-metastatic counterparts. Surprisingly, genetically depleting periostin^{+} CAFs slightly accelerated primary tumor growth but impaired intratumoral collagen organization and inhibited lymphatic, but not lung, metastases. Periostin ablation in CAFs impaired their ability to deposit aligned collagen matrices and inhibited cancer cell invasion through collagen and across lymphatic endothelial cell monolayers. Thus, highly-metastatic cancer cells mobilize periostin-expressing CAFs in the primary tumor site which promote collagen remodeling and collective cell invasion within lymphatic vessels and ultimately to sentinel lymph nodes.

2.2 Introduction

The overwhelming majority of cancer-associated deaths, including those of breast cancer patients, are caused by metastatic burden rather than primary tumor growth. However, the complex process of cancer cell dissemination and colonization of distant tissues is incompletely understood and largely incurable using existing therapies (11). Metastatic disease is particularly intractable because metastasis is not solely driven by cancer cell-intrinsic properties but is instead a consequence of dynamic crosstalk between cancer cells and other cell types in the tumor microenvironment including vascular cells, immune cells, and cancer-associated fibroblasts (CAFs). A critical early step in the metastatic cascade is the intravasation of cancer cells into blood and lymphatic vessels which serve as routes for cancer cells to spread to secondary sites. Lymphovascular invasion of cancer cells into lymphatic vessels is a predominant method of vascular invasion in breast cancer and is significantly associated with the presence of lymph node metastasis, development of distant metastasis, and decreased disease-free interval and overall survival (85, 88-91). Despite the frequency of lymphovascular invasion in breast cancer and its association with poor clinical outcomes, the heterotypic cell interactions that drive lymphovascular invasion are not well characterized. Many studies of lymphovascular invasion focus on paracrine signaling between cancer cells and lymphatic endothelial cells with limited consideration given to the contributions of other auxiliary cells in the tumor microenvironment (TME) such as CAFs.

CAFs are an abundant stromal cell in the breast tumor microenvironment and primarily originate from tissue-resident fibroblasts that become persistently activated by a dysregulated “wound-healing” process recapitulated in solid tumors (224). They are important during multiple stages of tumor development though their specific contributions to disease progression are contradictory and context-dependent (125, 126, 156, 157, 166, 225, 226). The paradoxical functions of CAFs during tumor progression can be attributed to their extensive molecular diversity both within and across tumor types as revealed by a number of single-cell RNA sequencing studies (120, 158-161, 163, 227). Though CAFs are mainly characterized by expression of contractile proteins such as alpha smooth muscle actin (SMA) and extracellular matrix (ECM) proteins including collagens and fibronectin, single-cell transcriptomic analysis has identified additional subpopulations of CAFs that display expression profiles associated with proliferation, vascular development and angiogenesis, and immune modulation (124, 163). Although these purported functions of CAF subpopulations position them as attractive therapeutic targets, in vivo depletion studies have yielded unexpected results with SMA^+ CAF depletion leading to more aggressive, undifferentiated tumors (156, 157). These data suggest that CAF subpopulations play opposing roles in the tumor microenvironment, with some CAFs restraining tumor growth whereas others are tumor-supportive. Therefore, functional classification of molecularly-defined CAF subpopulations is necessary to overcome the limitations of broadly targeting CAFs so that specific tumor-promoting and/or metastasis-promoting CAFs can be identified. A

challenging but critical first step in this process is identifying reliable biomarkers that distinguish pro-tumorigenic and pro-metastatic CAFs from their counterparts.

A recent single-cell RNA sequencing study demonstrated that periostin, a TGFβ-induced matricellular protein, is expressed by CAF populations in human triple negative breast cancers (124). As a nonstructural matrix component, periostin directly interacts with other ECM proteins including lysyl oxidase, collagen I, and fibronectin, serving as a protein scaffold for mediators of collagen cross-linking and ECM stiffening (174). It is typically present at low levels in most tissues but induced at sites of inflammation and tissue injury. Periostin's role in pathologies including cancer have been noted, including its ability to promote immunosuppressive niche formation, mediate interactions between disseminated cancer cells and the ECM, and support cancer stem cell expansion at metastatic sites (72, 207, 208). In human breast cancer samples, periostin is associated with a higher density of activated CAFs and stromal desmoplasia. This stromal desmoplasia is a consistent aspect of invasive progression and distinguishes tumors that are "non-progressors" from those that recur and spread (121). Although these studies characterize periostin as a tumor-supportive factor of metastatic disease, its source in the primary tumor microenvironment and the specific contributions of periostin-expressing cells during tumor progression have not been well-studied in vivo. Previous studies of periostin have relied on immunostaining to characterize its abundance and distribution in primary and secondary sites. However, given that periostin is a secreted factor, immunostaining is unable to link the source of periostin to specific cell types in

the tumor microenvironment. Therefore, we have adapted an in vivo lineage tracing strategy previously used to study activated myofibroblasts in the heart (223) to track, characterize, and ablate periostin-expressing cells in the breast TME. We reveal that highly-metastatic cancer cells mobilize periostin-expressing perivascular-like CAFs (PVL-CAFs) in the TME which promote collagen-mediated collective cell invasion of cancer cells across the endothelial barrier of nearby lymphatic vessels and ultimately to the proximal lymph node.

2.3 Materials and Methods

2.3.1 In vivo animal studies

All tumor studies were performed in 8- to 12-week old female mice with a C57BL/6 genetic background. *Postn*^{iZSGreen} lineage tracing mice were generated by crossing *Postn*^{MCM} mice (Jax Stock No. 029645) with *ZSGreen*$^{l/s/l}$ mice (Jax Stock No. 007906). *Postn*^{iZSGreen} mice were injected intraperitoneally (IP) with 75 mg/kg tamoxifen 3 times over the course of 7 days to induce ZSGreen labelling of periostin-expressing cells. In the low-versus highly-metastatic tumor studies, one million EO771^{mCherry} or EO771.LMB^{mCherry} cancer cells were orthotopically injected into the third mammary fat pad of tamoxifen-induced heterozygous *Postn*^{iZSGreen} lineage tracing mice. Tumor volumes were measured with calipers, and tumors were surgically removed when they averaged ~400 mm^3. Mice were euthanized and mammary glands, lymph nodes, and lungs were harvested ~2 weeks following tumor resection surgery. For the tail vein model of experimental metastasis, tamoxifen-induced *Postn*^{iZSGreen} mice were injected with one million

EO771^{mCherry} or EO771.LMB^{mCherry} cancer cells into their tail vein. Mice were sacrificed and lungs were harvested 2 weeks following tumor cell injection. *Postn*^{iZSGreen} lineage tracing mice were crossed with ROSA-DTA mice (Jax Stock No. 009669) to generate *Postn*^{DTA} mice that allow for selective depletion of periostin-expressing cells. *Postn*^{DTA} mice were injected IP with 75 mg/kg tamoxifen 3 times over the course of 7 days to induce depletion of periostin-expressing cells. 500,000 mCherry-labelled EO771.LMB or PyVMT cells were orthotopically injected into the third mammary fat pad of heterozygous tamoxifen-induced (or vehicle-injected control) mice. Tumor volumes were measured with calipers, and tumors were surgically removed when they averaged ~400 mm^3. Mice were euthanized and mammary glands, lymph nodes, and lungs were harvested 2 weeks (PyVMT-injected mice) or 4 weeks (EO771.LMB-injected mice) following tumor resection surgery. *Postn-Cre:Tgfbr2*$^{fl/fl}$ mice were generated by crossing *Postn*^{iZSGreen} mice with *Tgfbr2*$^{fl/fl}$ mice (Jax Stock No. 012603). *Postn-Cre:Tgfbr2*$^{fl/fl}$ mice were injected IP with 75 mg/kg tamoxifen 3 times over the course of 7 days to induce *Tgfbr2* knockout in periostin-expressing cells. 500,000 mCherry-labelled EO771.LMB cells were orthotopically injected into the third mammary fat pad of tamoxifen-induced *Postn-Cre:Tgfbr2*$^{fl/fl}$ mice or *Postn*^{iZSGreen} control mice. Tumor volumes were measured with calipers, and tumors were surgically removed when they averaged ~400 mm^3. Mice were euthanized and lymph nodes were harvested 3 weeks following tumor resection surgery. All experiments were performed in accordance with the University of Virginia guidelines for animal handling and care.

2.3.2 Immunohistology

Resected tissues were fixed overnight in 4% PFA/PBS and moved to a 30% sucrose solution for an additional 24 hours before embedding in OCT. Cryosections were DAPI stained and mounted in Vectashield (Vector Labs H-1700-10), then imaged using a Nikon Eclipse Ti-E inverted microscope and NIS-Elements software. Fluorescent populations were quantified using the thresholding function in FIJI (Figure 2.4).

2.3.3 Cell lines, cell culture, and media

EO771 cells were obtained from CH3 Biostystems (940001) and transfected with mCherry. EO771.LMB cells were a gift from Dr. Chad Pecot at UNC Chapel Hill and transfected with mCherry. EO771^{mCherry} and EO771.LMB^{mCherry} cells were cultured in 4.5 g/l D-glucose DMEM (HG-DMEM) with 10% FBS. Metastatic PyVMT cells were a gift from Dr. Melanie Rutkowski at UVA. They were transfected with mCherry and cultured in RPMI1640 with 2mM L-Glutamine, 10% FBS, 0.5% sodium pyruvate, and 0.09% β-mercaptoethanol. MDA-MB-231 human breast cancer cells were purchased from ATCC (HTB-26) and transfected with mCherry. MDA-MB-231^{mCherry} cells were cultured in HG-DMEM with 10% FBS. Primary human breast CAFs were isolated and gifted to us by Dr. Melissa Troester at UNC Chapel Hill (228) and were cultured on 0.5% gelatin-coated plates in HG-DMEM with 20% FBS and 10 ng/mL bFGF. Primary human lymphatic endothelial cells (Cell Biologics H-6092) were cultured in Complete Human Endothelial Cell Medium (Cell Biologics H1168) on 0.5%

gelatin-coated plates. HUVECs (Lonza C2517A) were cultured in Endothelial Cell Growth Media (R&D Systems CCM027) on 1% gelatin-coated plates. Primary mouse mammary fibroblasts and CAFs were isolated from mammary glands and primary tumors by digesting tissues in a cocktail of collagenase/dispase/DNAse for 40 minutes with shaking at 37° C, filtering through a 100 µm filter, and seeding cells on 0.5% gelatin-coated plates in HG-DMEM with 20% FBS and 10 ng/mL bFGF. All cell media included Plasmocin (Invivogen ant-mpt) to prevent mycoplasma growth and antibiotics/antimycotics to prevent bacterial and fungal contamination. Cells were maintained at 37° C in 5% CO_2 plus 20% O_2.

2.3.4 Breast tumor tissue microarray analysis

Antigen-retrieval was performed on a tissue microarray of paraffin-embedded breast tumor cores (US Biomax BR20829) at 95° C for 20 minutes. The microarray slide was rinsed in DI water then incubated with blocking buffer (5% BSA + 5% goat serum in TBS) for 1 hour at room temperature. The slide was then incubated with rabbit anti-periostin antibody (Abcam ab215199, 1:1000) overnight at 4° C. The next day, the slide was rinsed 3 times with TBS and incubated for 30 minutes at room temperature with Biocare's MACH 3 Rabbit Probe (M3R533 G). Following another three TBS washes, the slide was incubated for 30 minutes at room temperature with Biocare's MACH 3 Rabbit AP-Polymer (M3R533 G). The slide was then rinsed in TBS and developed using Biocare's Warp Red Chromogen Kit (WR 806 H) for 8 minutes at room temperature. The slide was washed in TBS, counterstained for 3 seconds with

hematoxylin QS, then rinsed in water and TBS. Finally, the microarray slide was dipped in 100% ethanol then xylene and mounted using Biocare's Ecomount (EM897L). Fluorescent AP signal was imaged using a Nikon Eclipse Ti-E inverted microscope and NIS-Elements software and percent periostin positive area (by pixel) was quantified by thresholding in FIJI.

2.3.5 Immunoblotting

Collection of cell lysates and Western blotting were carried out as previously described using standard methods (229). For analysis of secreted proteins, conditioned media was collected and concentrated 10X using Microsep Advance Centrifugal Filters (Pall Laboratory MCP010C41). Samples probed for collagen I were prepared and run under non-reducing conditions in a 7.5% gel. Primary antibodies: rabbit anti-periostin (Abcam ab14041, 1:1000), rabbit anti-collagen I (Abcam ab34710, 1:1000). Secondary HRP-conjugated antibody: peroxidase goat anti-rabbit IgG (Vector Laboratories PI-1000, 1:10,000).

2.3.6 Real-time quantitative PCR (RT-qPCR)

Total RNA isolation was performed using a Quick-RNA Miniprep Kit (Zymo Research R1055) according to the manufacturer's instructions. cDNA synthesis was completed using an iScript cDNA Synthesis Kit (Bio-Rad 1708891EDU), and qPCR reactions were carried out using a QuantStudio 12K Flex Real-time PCR System.

2.3.7 Immunofluorescence

Fixed frozen tissue sections were stained using the following antibodies and concentrations: Cy3-SMA (TCF C6198, 1:100), CD31 (BD Biosciences 550274, 1:50), F4/80 (BioRad MCA497, 1:50), CK14 (Biolegend 905301, 1:250), Pdpn (R&D Systems AF3244, 1:200). Antibodies were diluted in blocking buffer with 5% BSA, 5% goat serum, and 1% Triton X-100. Primary incubations were performed overnight at 4° C and secondary incubations were performed for 1 hour at room temperature. Nuclei were counterstained with DAPI and slides were mounted using Vectashield (Vector Labs H-1700-10). Slides were imaged using a Nikon Eclipse Ti-E inverted microscope and NIS-Elements software.

2.3.8 GeoMx Digital Spatial Profiling (DSP)

NanoString GeoMx DSP was used to quantify transcript numbers in spatially distinct populations of periostin-expressing cells in the naïve mammary glands of *Postn*^{iZSGreen} lineage tracing mice. Fixed frozen mammary glands were incubated with the NanoString mouse Whole Transcriptome Atlas (WTA) panel probes overnight, then stained with Cy3-SMA (TCF C6198), Pdpn (R&D Systems AF3244;Cy5 secondary), and the DNA stain Syto83 (Thermo S11364) as morphology markers to visualize tissue architecture. Stained slides were loaded onto the GeoMx instrument and scanned for region of interest (ROI) selection. Due to the filters in the optical system of the DSP platform, ZSGreen^{+} cells appear blue, SMA staining appears in green, and Pdpn staining appears in red in the ROIs. ROIs of ZSGreen^{+} cells near thin-walled Pdpn^{+} structures were

selected to represent lymphatic-adjacent populations, and ROIs of ZSGreen^{+} cells near SMA^{+} structures were selected to represent duct- and blood vessel-adjacent populations. After UV illumination of the ROIs, the eluent was collected via microcapillary aspiration and transferred into individual wells of a microtiter plate. The collected aspirates in the microtiter plate were then transferred to a PCR plate for library prep with Seq Code primers. PCR products were pooled and purified, then subjected to Illumina NGS Sequencing (Next Seq 2000). FASTQ sequencing files obtained from the NGS run were processed into digital count conversion (DCC) files by NanoString's GeoMx NGS Pipeline software. The DCC files were then uploaded onto the GeoMx DSP, and quality control checks and differential gene expression analysis were performed.

2.3.9 Second harmonic generation

Fixed frozen tumor sections were imaged using a Zeiss 710 Multiphoton Confocal microscope and collagen fiber length measurements were performed in FIJI. The FIJI plug-ins TWOMBLI (230) and OrientationJ (http://bigwww.epfl.ch/demo/orientation/) (231) were used to analyze the collagen area (abundance), curvature (measured as mean change in angle along fibers), and directionality of the collagen fibers.

2.3.10 siRNA transfection

For in vitro periostin knockdown studies, primary human breast CAFs were transfected with 75 nm human periostin-targeting stealth siRNA (si-*POSTN)*

(ThermoFisher siRNA ID: HSS116400) or 75 nm non-targeting control siRNA (si-Control) (DHARMACON D-001810-02-05) for 5 hours, then media was replaced. This siRNA transfection was repeated after 24 hours, and media was replaced with low-serum media. Cells were then used for functional assays.

2.3.11 Bulk RNAseq and analysis

Primary human breast CAFs were transfected with siRNA in quadruplicate as described above. RNA samples were harvested from cells and sent to Novogene for bulk RNA sequencing. Sequencing analysis was performed by the UVA Bioinformatics Core. On average we received 30 million paired ends for each of the replicates. RNAseq libraries were checked for their quality using the fastqc program **(**http://www.bioinformatics.babraham.ac.uk/projects/fastqc/). The results from fastqc were aggregated using multiqc software. In-house developed programs were used for adaptor identification, and any contamination of adaptor sequence was removed with cutadapt (https://cutadapt.readthedocs.io/en/stable/). Reads were mapped with the “splice aware” aligner ‘STAR’ to the transcriptome and genome of mm10 genome build. The HTseq software was used to count aligned reads that map onto each gene. The count table was imported into R to perform differential gene expression analysis using the DESeq2 package. Low expressed genes (genes expressed only in a few replicates and had low counts) were excluded from the analysis before identifying differentially expressed genes. Data normalization, dispersion estimates, and model fitting (negative binomial) were carried out with the DESeq

function. The log-transformed, normalized gene expression of 500 most variable genes was used to perform an unsupervised principal component analysis. The differentially expressed genes were ranked based on the log2fold change and FDR corrected p-values. The ranked file was used to perform pathway analysis using GSEA software. The enriched pathways were selected based on enrichment scores as well as normalized enrichment scores.

2.3.12 ECM deposition assay

Primary human breast CAFs were seeded (30,000 cells per well) on a gelatin-coated chamber slide and transfected with siRNA as described above. 48 hours after the second siRNA treatment, cells were lysed using ammonium hydroxide-based extraction buffer. The deposited ECM was washed in PBS and fixed with 2% PFA for 20 minutes. The ECM was then rinsed in PBS and incubated in blocking buffer with 1% Triton for 30 minutes to reduce non-specific antibody binding. The ECM was then incubated with primary antibody (rabbit anti-collagen I ab34710, 1:200) for 1 hour at room temperature and secondary antibody (goat anti-rabbit IgG Alexa Fluor 594 1:100) for 1 hour at room temperature. Slides were mounted using Vectashield (Vector Labs H-1700-10) and imaged using a Nikon Eclipse Ti-E inverted microscope and NIS-Elements software. Collagen fiber length measurements were performed using FIJI.

2.3.13 Cell spreading assay

Primary human breast CAFs were seeded (1 x 10^5 cells/mL) in a 6-well gelatin coated dish and transfected with siRNA as described above. 24 hours following knockdown, CAFs were detached and re-seeded at 10,000 cells per well on a gelatin-coated chamber slide. The “rescue” wells were treated with 0.8 ug/mL recombinant human periostin (BioLegend 770506). After 24 hours, cells were fixed in 4% PFA and stained with Alexa Fluor 594 Phalloidin (ThermoFisher Scientific A12381). Cells were imaged using a Nikon Eclipse Ti-E inverted microscope and NIS-Elements software, and cell area measurements were performed in FIJI.

2.3.14 Wound closure scratch assay

Primary human breast CAFs were seeded (1 x 10^5 cells/mL) in a 6-well gelatin coated dish and transfected with siRNA as described above. The next day, a P1000 pipette tip was used to create a scratch down the middle of the cell monolayer in each well. Each well was washed once with PBS to removed detached cells and low serum media was then added. “Rescue” wells were treated with 0.8 ug/mL recombinant human periostin (BioLegend 770506). Scratches were imaged at 0 hours, 12 hours, and 24 hours using a Nikon Eclipse Ti-E inverted microscope and NIS-Elements software, and percent wound closure was calculated using area measurements in FIJI.

2.3.15 3D CAF/cancer cell spheroid invasion assay

Primary human breast CAFs were seeded (1 x 10^5 cells/mL) in a 6-well gelatin coated dish and transfected with siRNA as described above. The next day, CAFs were co-cultured 1:1 with MDA-MB-231^{mCherry} human breast cancer cells in 20 uL hanging droplets containing 5% methylcellulose on the inverted lid of a 100 mm tissue culture dish containing PBS. The CAF/cancer cell co-cultures were incubated for 24 hours to allow aggregation of cells into a spheroid, as confirmed under light microscopy. The CAF/cancer cell spheroids were then embedded in either Matrigel (Corning 356237) or rat-tail collagen type I (Ibidi 50201) according to manufacturer's instructions in a 96-well plate. Spheroids were imaged at 12 and 24 hours using a Nikon Eclipse Ti-E inverted microscope and NIS-Elements software, and invasive area was quantified using FIJI. Representative images of spheroids were taken using a Zeiss LSM 880 confocal microscope.

2.3.16 Trans-well migration assay

Primary human breast CAFs were seeded (1.5 x 10^5 cells/mL) in a 6-well gelatin coated dish and transfected with siRNA as described above. The next day, CAFs were co-cultured with MDA-MB-231^{mCherry} human breast cancer cells into spheroids as described above. Transwell membrane inserts (Fisher Scientific 07-200-150) were coated with 0.5% gelatin and seeded with 60,000 primary human lymphatic endothelial cells or 60,000 primary human umbilical vein endothelial cells (HUVECs). After 24 hours, CAF/cancer cell spheroids were

embedded in rat-tail collagen type I (Ibidi 50201) in the transwell membrane inserts above the monolayer of endothelial cells. Inserts were cleared with a cotton swab and washed in PBS after 24 hours, so that only cells that had migrated across the lymphatic endothelial cell barrier and reached the bottom surface of the transwell insert remained. These cells were fixed in 4% PFA for 10 minutes at room temperature and washed in PBS. Transwell inserts were placed on slides and imaged using a Nikon Eclipse Ti-E inverted microscope and NIS-Elements software. Trans-migrated cancer cells were counted in FIJI.

2.3.17 Kaplan-Meier Analysis

Kaplan-Meier Plotter was used to generate survival curves for lymph node positive breast cancer patients from the Tang_2018 patient cohort that were stratified based on low versus high periostin protein expression.

2.3.18 Statistical analysis

All data points are shown, and horizontal lines on graphs represent median values. Descriptive numerical values in the text are expressed as mean value ± standard error of the mean (SEM). All statistical analyses were performed using GraphPad Prism software, and P values less than 0.05 were considered significant.

2.4 Results

2.4.1 Periostin is enriched in CAFs and cycling perivascular-like cells in breast cancers and is associated with advanced disease stage and lymph node metastasis

As periostin has previously been shown to distinguish CAFs in triple negative breast cancer samples (124), we turned to a comprehensive, spatially-resolved single-cell transcriptional atlas of molecularly diverse breast tumors to determine with greater resolution which cellular populations express periostin in human breast cancers (162). We found that periostin is not detected in breast cancer cells of any molecular subtype but is expressed by multiple stromal populations (Figure 2.1A). Periostin and associated matrix proteins are enriched in CAFs, including mesenchymal stem cell-like inflammatory CAFs (MSC iCAF-like) and myofibroblast-like CAFs (myCAF-like) populations as well as cycling perivascular-like (PVL) cells (Figure 2.1B). Despite its expression being restricted to the tumor stroma, periostin may have important functional consequences during tumor progression as it is associated with disease recurrence in human breast cancer patients (121). Therefore, we hypothesized that its expression in human breast cancer tissues would correlate with disease stage and lymph node status. Indeed, when we stained a human breast tissue microarray of 200 tumor cores for periostin and measured the positive fluorescent area, we found that periostin abundance positively associated with advanced disease stage (Figure 2.1C,D) and lymph node metastasis (Figure 2.1E). These data indicate that

periostin is almost exclusively expressed by CAFs or CAF-like cells in the breast TME and its abundance associates with disease progression.

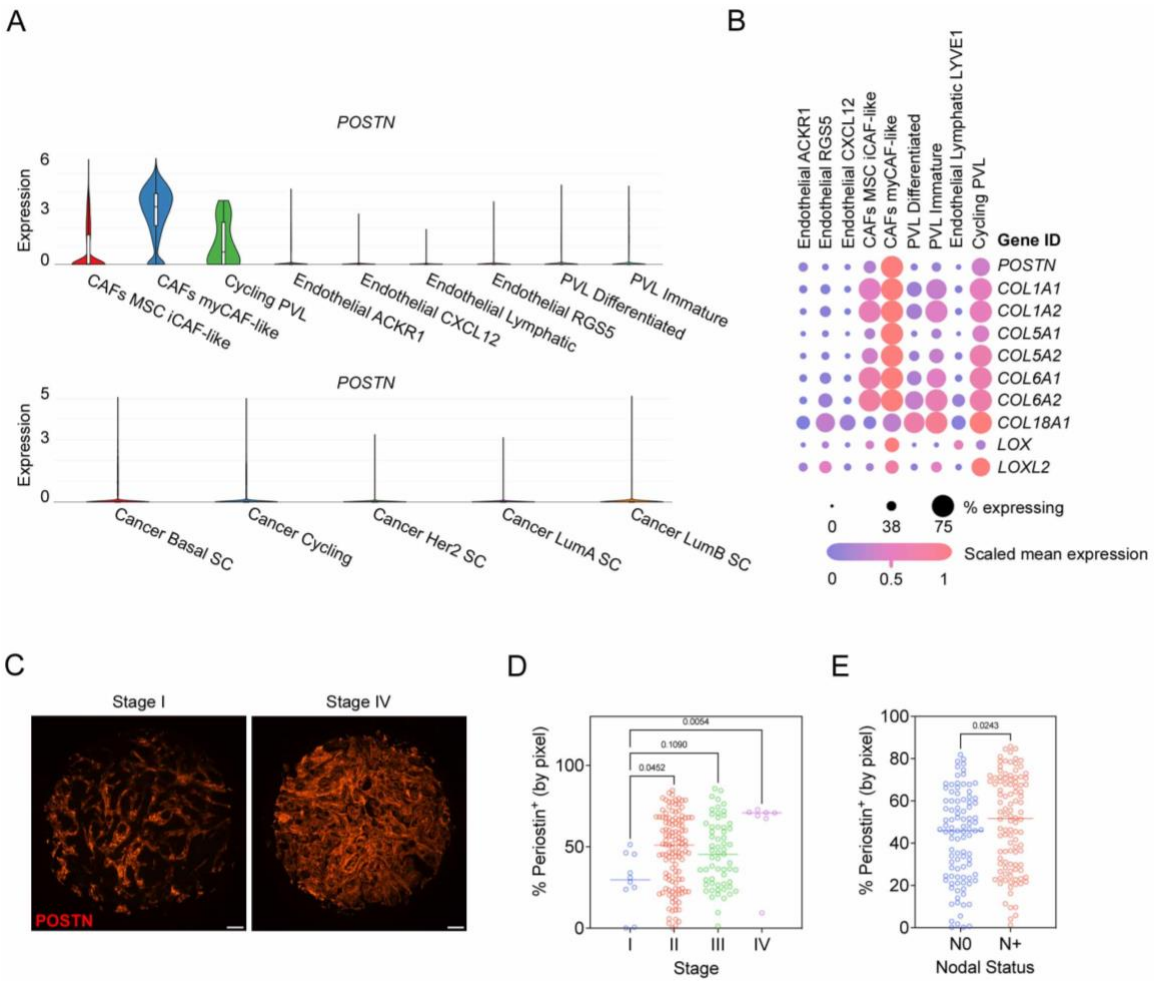

Figure 2.1. ***Periostin is enriched in CAFs and cycling perivascular-like cells in breast cancers and is associated with advanced disease stage and lymph node metastasis.*** (A) Single-cell RNAseq data were downloaded from the Wu et al dataset (162) and analyzed for periostin expression. Violin plots of differential expression of periostin (*POSTN)* in stromal populations (top) and breast cancer cells (bottom) in this patient cohort are shown. MSC = mesenchymal stem cells, PVL = perivascular-like cells, and SC = subclass. (B) Expression of periostin and associated matrix proteins in distinct stromal populations derived from the Wu et al. cohort. (C) Representative immunofluorescence images of human breast cancer tissues stained for periostin (in red). Scale bars: 100 μm. (D) Percentage of tissue area positive for periostin staining (by pixel), grouped by tumor stage (D) and patient's lymph node status (N0 = no nodal involvement, N+ = nodal involvement) (E). Each data point represents an individual tumor core (N = 200). Statistics shown for Kruskal-Wallis test (D) and Mann-Whitney test (E).

2.4.2 Periostin-expressing cells surround tumor-naïve mammary ducts and blood vessels and are enriched at the lymphatic vessel periphery

Our human data support existing murine studies linking periostin to metastasis (72, 207, 208). However, previous characterizations of periostin in primary and metastatic environments have primarily relied on immunostaining to characterize its abundance and distribution. Since periostin is a secreted factor, immunostaining is unable to link periostin to a cellular source in the TME. While single-cell RNAseq data indicate that periostin expression is restricted to stromal populations in human breast cancers, these populations have not been studied in situ in murine tumor models. Thus, in vivo approaches to label periostin-expressing cells are required to characterize periostin's source in the tumor microenvironment and to determine how these periostin-expressing populations function during tumor growth. We generated reporter mice (*Postn*^{iZSGreen} lineage tracing mice) to genetically mark periostin-expressing cells by crossing *Postn*^{MCM} mice with *ZSGreen*$^{l/s/l}$ mice (Figure 2.2A). Upon tamoxifen administration, periostin-expressing cells and their progeny are genetically labelled with ZSGreen and can be quantified using fluorescence microscopy which allowed us to spatially track the status of these cells across different tissues. After generating *Postn*^{iZSGreen} mice, we first characterized the spatial distribution of ZSGreen^{+} cells in tumor-naïve mammary glands. We harvested mammary glands from tumor-naïve *Postn*^{iZSGreen} mice and stained for the following cell lineage markers: SMA (fibroblast and pericyte marker), Ck14 (myoepithelial marker), F4/80 (macrophage marker), CD31 (endothelial marker), and Pdpn

(lymphatic endothelial marker) (Figure 2.2B). We found that periostin-expressing cells were relatively sparse in the naïve tissues and surrounded mammary ducts and blood vessels as revealed by the CK14 and CD31 staining, respectively. Intriguingly, we also found that periostin-expressing cells localized to the lymphatic vessel periphery and were more enriched along thin-walled lymphatic vessels compared to large vessel endothelium marked by abundant SMA (Figure 2.2C), with an average of ~ one ZSGreen^{+} cell per large blood vessel (± 0.6 cells/vessel) compared to ~ four ZSGreen^{+} cells per lymphatic vessel (± 0.9 cells/vessel). These data are consistent with the spatially resolved expression of periostin by cycling perivascular-like (PVL) stromal cells in human breast cancers as noted above using comprehensive single cell transcriptomics.

Given the spatially distinct populations of periostin-expressing cells observed along the ducts, blood vessels, and lymphatic vessels in the naïve mammary gland, we used GeoMx Digital Spatial Profiling (DSP) to molecularly characterize the subpopulations in situ and reveal heterogeneity among periostin-expressing cells. Using SMA and Pdpn as morphology markers to select regions of interest within the mammary glands, we performed whole transcriptome analysis on ZSGreen-labelled periostin-expressing cells within these regions (Figure 2.2D) and compared expression profiles of SMA-adjacent ZSGreen^{+} cells (near ducts and blood vessels) and Pdpn-adjacent ZSGreen^{+} cells (near lymphatic vessels). Spatial transcriptomics identified a number of genes that are differentially expressed between the periostin-expressing subpopulations (Figure 2.2E), and Gene Set Enrichment Analysis (GSEA)

indicated that periostin-expressing cells located near ducts and blood vessels are enriched in genes involved in ECM organization as well as collagen synthesis and remodeling while lymphatic-adjacent periostin-expressing cells are enriched in genes related to the activation of matrix metalloproteinases that degrade the ECM (Figure 2.2F). However, cluster analysis of the individual subpopulations based on collagen-related genes revealed that there is diversity among lymphatic-adjacent periostin-expressing cells, with multiple lymphatic-adjacent samples enriched in collagens and collagen cross-linking genes suggesting they also play a role in collagen synthesis and organization (Figure 2.2G). In sum, the spatial transcriptomic analysis suggests that these spatially distinct populations of periostin-expressing cells function together to remodel, synthesize, and organize the extracellular matrix within the mammary gland.

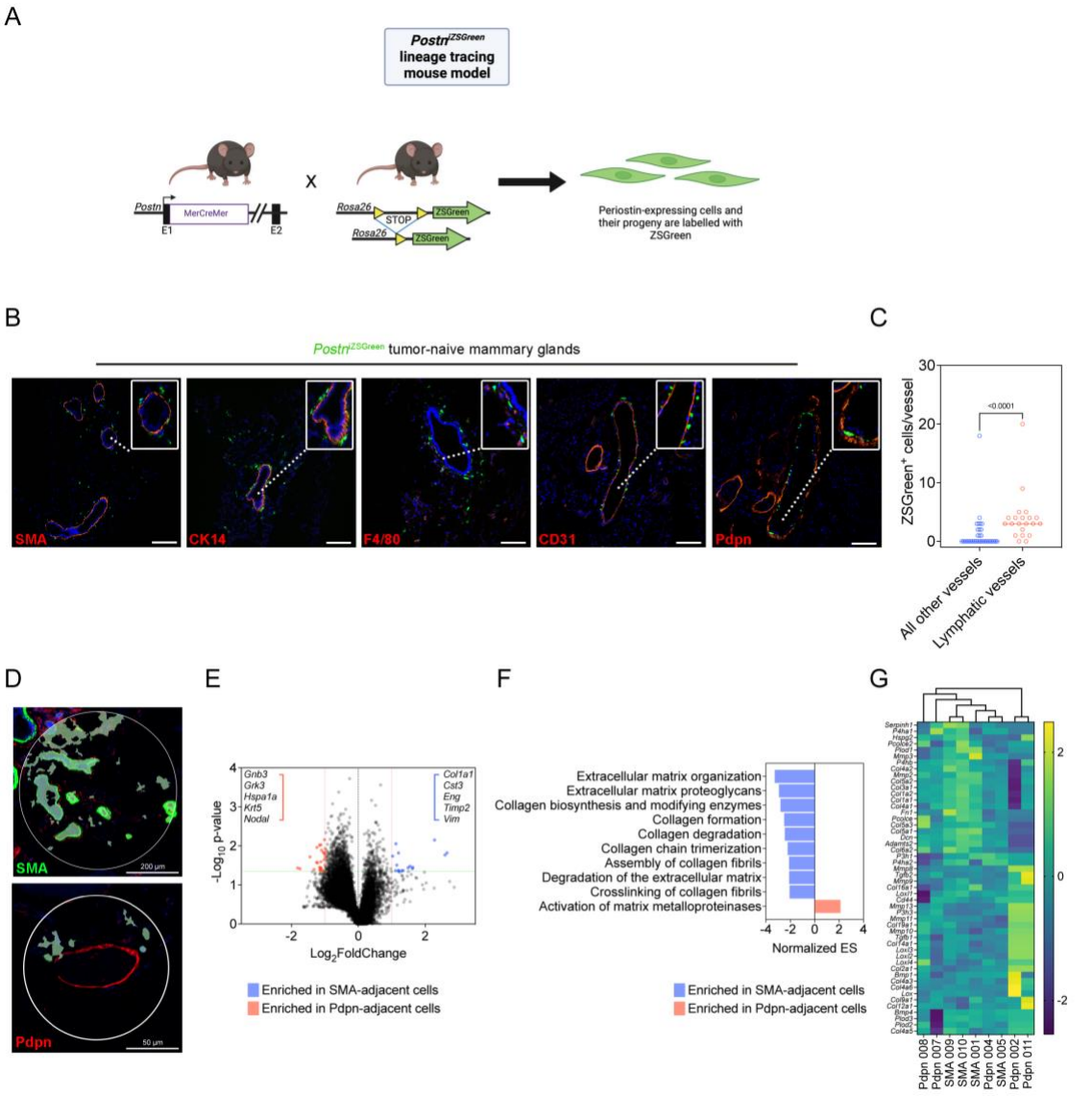

Figure 2.2. ***Periostin-expressing cells surround tumor-naïve mammary ducts and blood vessels and are enriched at the lymphatic vessel periphery.*** (A) Schematic representing the generation of *Postn*^{iZSGreen} lineage tracing mice. Adapted from Kanisicak *et al*. (2016) (223) and created using BioRender. (B) Immunofluorescence images of tumor naïve mammary glands from *Postn*^{iZSGreen} lineage tracing mice stained for the following markers (in red): SMA, CK14, F4/80, CD31, and Pdpn. Nuclei counterstained with DAPI. Scale bars: 200 μm, insets are 3x zoom. (C) Quantification of ZSGreen^{+} periostin-expressing cells per vessel (large vessel endothelium marked by abundant SMA versus thin-walled endothelium marked by Pdpn) in serial tissue sections of tumor naïve mammary glands (n = 3 mammary glands per group). Each data point represents an individual vessel. Statistics shown for Mann-Whitney test. (D) Representative images of regions of interest (ROIs) used to select ZSGreen^{+} periostin-expressing cells for spatial RNA profiling (n = 4-5 ROIs per group, from the mammary glands of 3 mice). (E) Volcano plot of differential gene expression in ZSGreen^{+} cells located near ducts and

blood vessels (SMA-adjacent) and ZSGreen^{+} cells located near lymphatic vessels (Pdpn-adjacent). Green line represents a p-value of 0.05 and red line represents the significance threshold. (F) Gene Set Enrichment Analysis (GSEA) showing upregulated pathways in spatially-defined ZSGreen^{+} populations. (G) Cluster analysis of ZSGreen^{+} cells from individual ROIs based on collagen-related genes. GeoMx spatial RNA profiling was performed by Dr. Patcharin Pramoonjago of the UVA BTRF Core, and Illumina NGS sequencing was performed by the University of Minnesota Genomics Center.

2.4.3 Highly-metastatic mammary tumors differentially activate periostin-expressing CAFs

Following characterization of periostin-expressing cells in the naïve mammary gland, we next used a mammary tumor model to assess the abundance, morphology, and spatial distribution of periostin-expressing cells in the primary TME and secondary sites of spontaneous metastasis. We used paired, differentially metastatic triple negative mammary cancer cell lines EO771 and EO771.LMB to classify differences in periostin-expressing cell activation in low- versus highly-metastatic tumor contexts. These cell lines have been molecularly and functionally characterized and shown to have differential capacities for spontaneous metastasis, with the poorly metastatic parental EO771 line rarely reaching secondary sites and the highly-metastatic derivative EO771.LMB tropic to the lungs and lymph nodes (232). Importantly, the EO771 and EO771.LMB lines express negligible periostin compared to murine mammary CAFs (Figure 2.3A), so our lineage tracing strategy successfully captures the predominant host-derived sources of periostin. Following tamoxifen administration to label periostin-expressing cells, *Postn*^{iZSGreen} mice were orthotopically injected with either EO771^{mCherry} or EO771.LMB^{mCherry} cells into the third mammary gland (Figure 2.3B). According to the previous characterization of the cancer cell lines, the difference in metastatic capacity is observed following primary tumor resection. Therefore, we incorporated this into our study design and harvested secondary tissues 3-4 weeks after tumor resection, allowing more time for disseminated cells to reach and grow out at secondary sites. This

experimental setup recapitulates human disease as human breast cancer patients often undergo a lumpectomy but may still progress to metastatic disease as a result of previously disseminated cancer cells emerging from dormancy and expanding in secondary sites. Since the periostin-expressing cells are genetically labelled with ZSGreen and the cancer cells are labelled with mCherry, we could spatially quantify these populations using a thresholding strategy for positive fluorescence in histological sections (Figure 2.4).

When we examined the low-metastatic EO771^{mCherry} tumors and highly-metastatic EO771.LMB^{mCherry} tumors in the *Postn*^{iZSGreen} mice, we found that periostin-expressing cells were more abundant in highly-metastatic tumors with an ~ 84-fold increase in the percentage of tissue area positive for ZSGreen in EO771.LMB tumors compared to EO771 tumors (1.68% ± 0.2% versus 0.02% ± 0.01%) (Figure 2.3C,D). We also examined a second highly-metastatic variant of PyVMT in the *Postn*^{iZSGreen} mice and found a 24-fold increase in the percentage of tissue area positive for ZSGreen in these tumors compared to low-metastatic EO771 tumors (0.48% ± 0.2%) (Figure 2.3D). This difference in periostin-expressing cell abundance in low- versus highly-metastatic mammary tumors correlated as expected with differences in secreted periostin in situ (Figure 2.3E). In addition to the difference in abundance of periostin-expressing cells in the low- versus highly-metastatic primary tumors, we observed a difference in the morphology of the ZSGreen^{+} cells between the two groups. Periostin-expressing cells in highly-metastatic EO771.LMB and PyVMT tumors exhibited the typical stellate-shaped morphology of activated myofibroblasts and were 2-3-times

larger on average compared to those found in low-metastatic EO771 tumors (509.7 ± 23.6 μm^2 and 334.2 ± 12.6 μm^2 versus 146.3 ± 12.0 μm^2, respectively) (Figure 2.3F,G). These data suggest that highly-metastatic cancer cells may differentially activate periostin-expressing CAFs in the primary tumor compared to their low-metastatic counterparts.

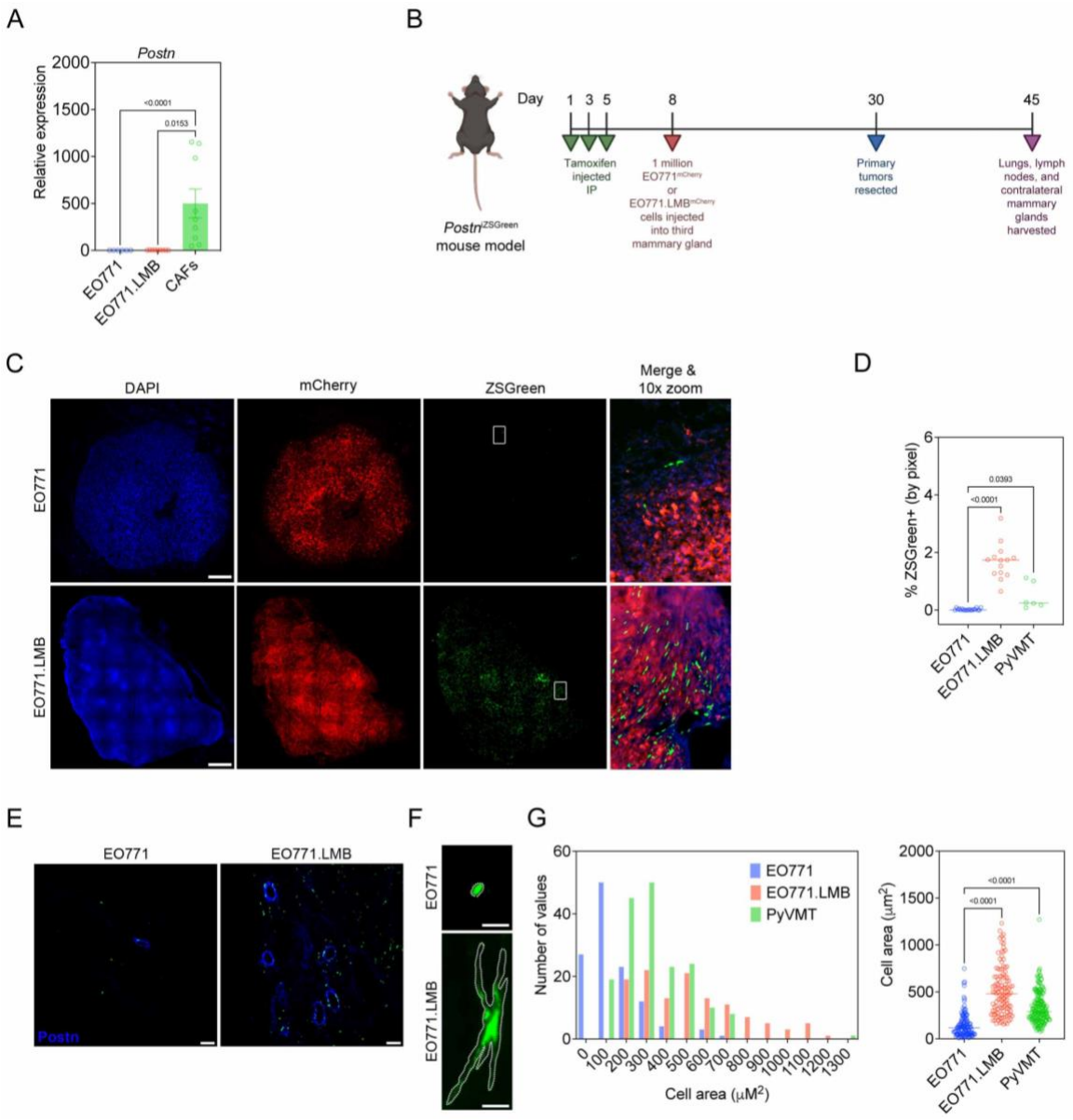

Figure 2.3. ***Highly-metastatic mammary tumors differentially activate periostin-expressing CAFs.*** (A) qPCR analysis of periostin expression in mammary tumor cell lines EO771 and EO771.LMB and murine mammary CAFs. Data represent the mean ± SEM. The experiments were performed in triplicate, and results compared using Kruskal-Wallis test. (B) Study design including tamoxifen treatment and orthotopic mammary tumor injections for EO771 vs EO771.LMB experiment in *Postn*^{iZSGreen} lineage tracing mice. (C) Tissue tilescans of primary mammary tumors from *Postn*^{iZSGreen} lineage tracing mice. Tumor cells labelled with mCherry and periostin-expressing cells genetically labelled with ZSGreen. Nuclei counterstained with DAPI. Scale bars: 500 μm. (D) Percentage of tissue area positive for ZSGreen in low metastatic (EO771) tumors versus high metastatic (EO771.LMB and PyVMT) tumors (n = 3-7 mice per group). Each data point represents a different histological section. Statistics shown for Kruskal-Wallis,

Dunn's multiple comparisons test. (E) Representative immunofluorescence images of mammary tumors from *Postn*^{iZSGreen} lineage tracing mice stained for periostin (in blue), with periostin-expressing cells genetically labelled with ZSGreen. Scale bars: 100 μm. (F) Representative immunofluorescence images of individual ZSGreen-labelled periostin-expressing cells in low metastatic (EO771) and high metastatic (EO771.LMB) mammary tumors. Scale bars: 10 μm. (G) Area of individual ZSGreen-labelled cells in primary tumors represented as a histogram (left) and scatter plot (right). Each data point in the scatter plot represents an individual cell. Between 120 and 180 cells were measured from multiple tumor sections (n = 3-6 mice per group) and results compared using Kruskal-Wallis, Dunn's multiple comparisons test. Marya Dunlap-Brown performed mammary tumor resection surgeries for samples shown in panel (C).

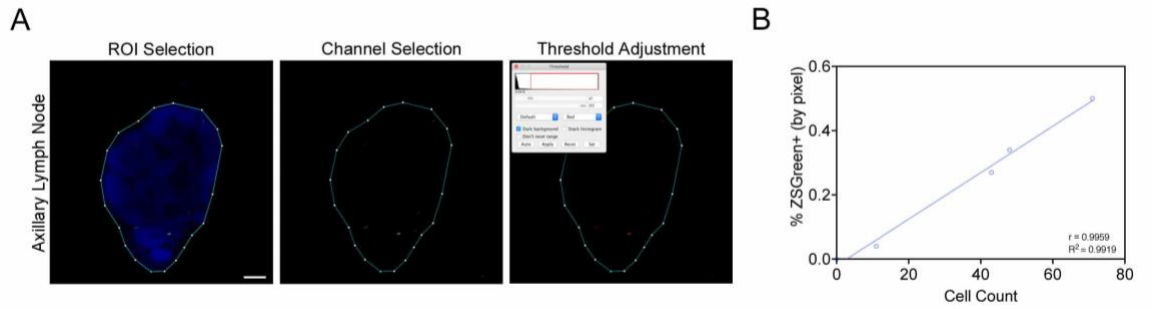

Figure 2.4. ***Thresholding strategy for fluorescent area quantification.*** (A) Workflow in FIJI to quantify fluorescent area by thresholding. First, a region of interest (ROI) is selected around the tissue boundary using DAPI nuclear counterstain as a guide so that background pixels are excluded from quantification. Next, a fluorescent channel is selected to quantify the population of interest. Finally, the threshold is adjusted so that all fluorescent cells are captured with minimal noise. Positive areas are highlighted in red by thresholding tool, and percent positive measurement is displayed in the threshold window. (B) Correlation between individual cell count and percentage of tissue area positive for ZSGreen (by pixel) measured by thresholding. Pearson r and R squared values are shown.

2.4.4 Periostin-expressing CAFs are more abundant in the metastatic niches of mice bearing highly-metastatic mammary tumors

Next, we examined the distribution of periostin-expressing CAFs in common metastatic sites of breast tumors, beginning with the draining axillary lymph nodes of the tumor-bearing mice as regional lymph nodes are often the first site of metastatic spread in breast cancers. Periostin-expressing cells were ~ 14-times more abundant in the axillary lymph nodes of mice bearing highly-metastatic EO771.LMB tumors, with 0.8% (± 0.1%) of the tissue area positive for ZSGreen compared to 0.06% (± 0.03%) in the lymph nodes of mice bearing low-metastatic EO771 tumors (Figure 2.5A,C). We then assessed the abundance of periostin-expressing cells in the lungs of mice as this is another common site of breast cancer metastasis. Similar to the lymph nodes, we observed a significant increase in the percentage of lungs positive for ZSGreen in mice bearing highly-metastatic mammary tumors compared to those bearing low-metastatic tumors (0.2% ± 0.03% versus 0.08% ± 0.04%) (Figure 2.5B,D). Interestingly, we observed ZSGreen$^+$ cells in a number of histological sections of lymph nodes (Figure 2.5C) and lungs (Figure 2.5D) without evidence of mCherry$^+$ cancer cells in these same tissues, suggesting that periostin-expressing cells are present in the premetastatic niche. In support of this possibility, we also observed differential activation of periostin-expressing cells in the contralateral mammary glands of tumor-bearing mice, another common metastatic site for breast cancers (233, 234). Though we did not detect mCherry$^+$ cancer cells at these sites, there was an ~ 8-fold increase in the percentage of tissue area positive for ZSGreen in

mice bearing highly-metastatic tumors compared to those bearing low-metastatic tumors (1.6% ± 0.2% versus 0.2% ± 0.1%) (Figure 2.6).

Since the spontaneous metastases we observed in the lungs resembled micrometastases, we hypothesized that a tail vein model of experimental metastasis would yield greater activation of periostin-expressing cells in the lungs, especially in the EO771.LMB-injected mice, as this would allow a greater number of tumor cells to colonize the lungs and activate periostin expression in tissue-resident cells via growth factor signaling. Surprisingly, though we found macrometastases of both the low-metastatic and highly-metastatic mammary cancer cells in the lungs following tail vein injection (Figure 2.5E), there was a lack of periostin activation in these tissues (Figure 2.5F), suggesting that the primary tumor must be established prior to activation of periostin at secondary sites.

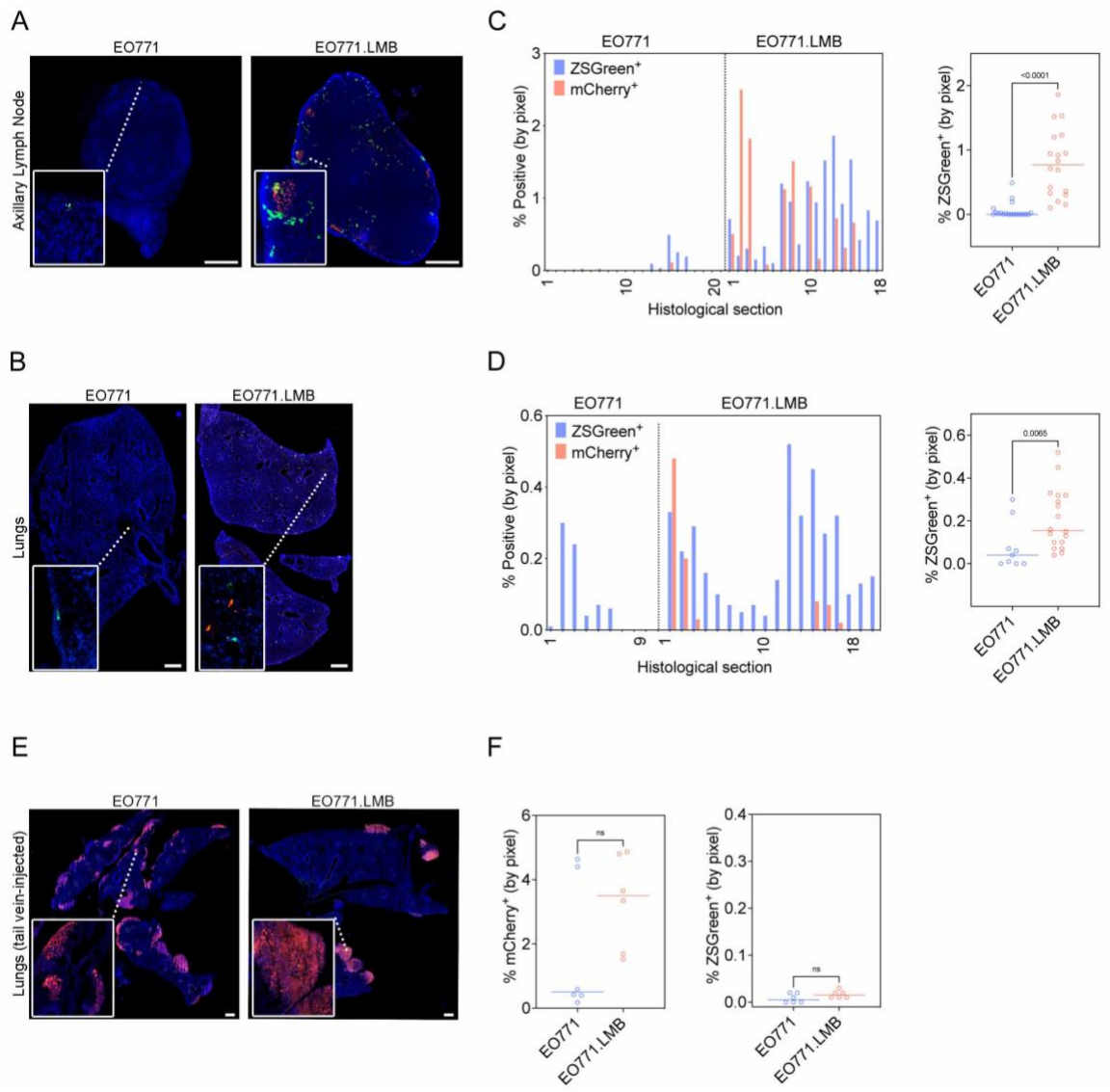

Figure 2.5. ***Periostin-expressing CAFs are more abundant in the metastatic niches of mice bearing highly-metastatic mammary tumors.*** (A,B) Tissue tilescans of axillary lymph nodes (A) and lungs (B) from *Postn*^{iZSGreen} lineage tracing mice bearing either low metastatic (EO771) or highly metastatic (EO771.LMB) mammary tumors. Tumor cells labelled with mCherry and periostin-expressing cells genetically labelled with ZSGreen. Nuclei counterstained with DAPI. Scale bars: 500 μm, insets are 3x zoom (A) and 6x zoom (B). (C,D) Percentage of tissue area positive for ZSGreen in serial sections of axillary lymph nodes (C) and lungs (D) from mice bearing EO771 or EO771.LMB mammary tumors represented as a histogram (left) and scatter plot (right). Each bar of the histogram represents a different histological section with matched mCherry and ZSGreen measurements. The scatter plot shows individual ZSGreen measurements with each point representing a different histological section (n = 6-7 lymph nodes and 3-6 lungs per group). Statistics shown for Mann-Whitney test. (E)

Tissue tilescans of lungs from *Postn*^{iZSGreen} lineage tracing mice injected via the tail vein with EO771 or EO771.LMB mammary tumor cells in a model of experimental metastasis. Tumor cells labelled with mCherry and periostin-expressing cells genetically labelled with ZSGreen. Nuclei counterstained with DAPI. Scale bars: 500 μm, insets are 6x zoom. (F) Percentage of tissue area positive for mCherry (left) and ZSGreen (right) in serial sections of lungs from tail vein-injected mice. Each data point represents a different histological section (n = 3 mice per group). Statistics shown for Mann-Whitney test. Tail vein injections were performed by Jeremy Gatesman of the UVA Center for Comparative Medicine.

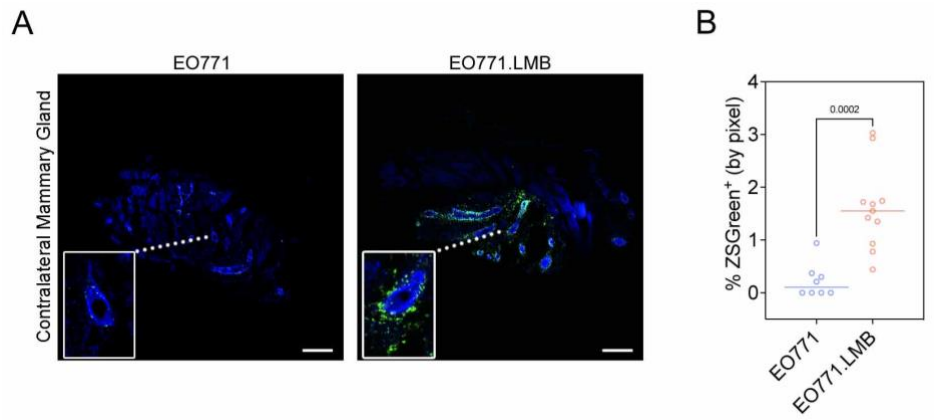

Figure 2.6. ***Periostin-expressing CAFs are more abundant in the premetastatic niches of mice bearing highly metastatic mammary tumors.*** (A) Tissue tilescans of contralateral mammary glands from *Postn*^{iZSGreen} lineage tracing mice bearing low-metastatic (EO771) or highly-metastatic (EO771.LMB) mammary tumors. Periostin-expressing cells genetically labelled with ZSGreen, and tumor cells labelled with mCherry (not detected in these tissues). Nuclei counterstained with DAPI. Scale bars: 200 μm, insets are 3x zoom. (B) Percentage of tissue area positive for ZSGreen in serial sections of contralateral mammary glands of mice bearing EO771 or EO771.LMB mammary tumors. Each data point represents a different histological section (n = 4-5 mice per group). Statistics shown for Mann-Whitney test.

2.4.5 Collagen fibers are longer and more aligned in highly-metastatic (periostin^{high}) breast tumors

Because periostin has been shown to promote ECM remodeling by binding to other matrix proteins including collagen, tenascin-C, and fibronectin to enable collagen cross-linking through a mechanism dependent on BMP-1-mediated activation of lysyl oxidase (LOX) (174, 177), we next used second harmonic generation (SHG) imaging to visualize collagen fibers in low- versus highly-metastatic mammary tumors to determine whether differences in periostin^{+} cell abundance associated with intratumoral collagen structure. Coincident with an increase in periostin-expressing CAFs in highly-metastatic breast tumors, we observed global changes to collagen matrix abundance and architecture in these tumors (Figure 2.7A). Total collagen fiber area was greater in highly-metastatic tumors (Figure 2.7B), and these fibers were straighter (Figure 2.7C) and more aligned (Figure 2.7D) when compared to low-metastatic counterparts whose collagen matrices were less dense and more closely resembled the “curly” collagen fiber structures associated with normal mammary glands (147). Additionally, there was a 3.7-fold increase in collagen fiber length in highly-metastatic mammary tumors compared to low-metastatic mammary tumors (342.6 ± 14.9 μm versus 93.4 ± 5.4 μm) (Figure 2.7E). Taken together, these differences indicate that the collagen matrix is more organized in highly-metastatic (periostin^{high}) mammary tumors compared to the randomly distributed and shorter collagen fibers found in low-metastatic (periostin^{low}) mammary tumors.

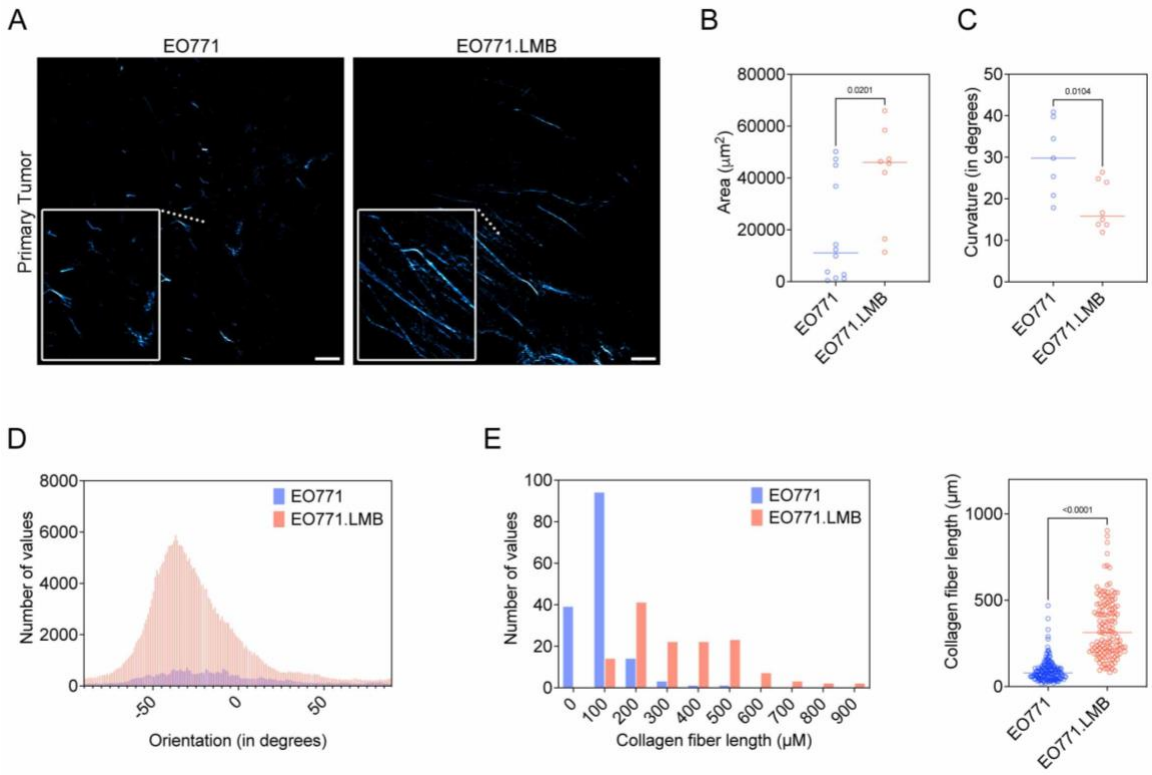

Figure 2.7. ***Collagen fibers are longer and more aligned in highly-metastatic (periostin^{high}) breast tumors.*** (A) Second harmonic generation (SHG) images of collagen fibers (pseudo-colored in cyan) in EO771 or EO771.LMB mammary tumors. Scale bars: 150 μm, insets are 3x zoom. (B) Total collagen area in histological sections of primary tumors (n = 3-4 mice per group). Each data point represents a different histological section. Statistics shown for Mann-Whitney test. (C) Curvature of collagen fibers, measured as mean change in angle along fibers, in histological sections of primary tumors (n = 3-4 mice per group). Each data point represents a different histological section. Statistics shown for unpaired Student's t test. (D) Representative histogram of collagen fiber orientation in primary tumors. A peaked histogram represents aligned fibers whereas a flat histogram represents random organization. (E) Quantification of collagen fiber length in primary tumors, represented as a histogram (left) and scatter plot (right). Each point represents an individual fiber. Between 130 and 160 fibers quantified from multiple histological sections (n = 3 mice per group) and results compared using a Mann-Whitney test. Second harmonic generation was performed in collaboration with Dr. Adrian Halme, Dr. Stacey Criswell, and Natalia Dworak of the UVA Advanced Microscopy Core.

2.4.6 Periostin knockdown in primary human breast CAFs alters collagen matrix architecture and inhibits collective cell invasion

Given that an aligned collagen matrix is a signature of more advanced breast tumors and can promote local invasion of cancer cells (122, 127, 155, 235, 236), we hypothesized that the difference in collagen matrix structure we observed in vivo was related to differences in the pool of intratumoral periostin and could have consequences for cancer cell migration. Thus, we knocked down periostin in primary human breast CAFs in vitro (Figure 2.8A-C) to determine whether periostin expression itself confers functional properties to CAFs including their ability to deposit an organized collagen matrix. RNAseq of primary human breast CAFs showed that periostin knockdown secondarily reduced expression of matrisomal proteins, ECM regulators, and collagens among other matrix-related genes found in the NABA Gene Set Enrichment Analysis (GSEA) (Figure 2.9A, Figure 2.8D). Secreted collagen I protein levels were reduced ~3-fold following periostin knockdown (Figure 2.9B), and the collagen fibers deposited by periostin-knockdown CAFs were significantly shorter than collagen fibers deposited by CAFs treated with non-targeting control siRNA (201.6 ± 7.6 μm versus 120.0 ± 4.8 μm) (Figure 2.9C,D). Coupled with our in vivo observations that periostin-expressing cell area and matrix organization were associated with increased intratumoral periostin, these in vitro matrix alterations prompted us to test whether knocking down periostin would affect cell area in vitro, as the stellate-shaped morphology that is characteristic of CAFs is attributed to their ability to engage the ECM and form focal adhesions. Primary

human breast CAF cell area was significantly reduced following periostin knockdown (2,199 ± 100.2 μm^2 versus 1643 ± 72.1 μm^2), and this effect was rescued by addition of recombinant human periostin (2,534 ± 131.4 μm^2) (Figure 2.9E, Figure 2.8E). The ability of CAFs to spread and form focal adhesions is critical for their motility, so we used migration assays to assess whether periostin knockdown would also impede their ability to migrate. Indeed, periostin knockdown in human breast CAFs reduced migration ~ 3-fold at 12 hours and 2-fold at 24 hours, and addition of recombinant human periostin restored the migratory capacity of periostin-knockdown CAFs at both time points (Figure 2.8F). Given this observed deficit in CAF migration following periostin knockdown, we hypothesized that ablating periostin in CAFs would also inhibit their ability to promote collective cell invasion. Therefore, we performed a 3D co-culture spheroid assay in which human breast CAFs were treated with either periostin-targeting siRNA (si-*POSTN)* or non-targeting control siRNA (si-Control) and co-cultured in spheroids with MDA-MB-231^{mCherry} human breast cancer cells. CAF/cancer cell spheroids were then embedded in 3D matrices and the percent change in invasive area was measured over time. We observed a selective impairment of collective cell invasion through a collagen matrix, as spheroids with periostin knockdown CAFs were significantly less invasive at 24 hours compared with control spheroids when embedded in type I collagen, but there was no difference in invasion when embedded in Matrigel (Figure 2.9F,G). Taken together, these data suggest that the ability of periostin-expressing CAFs to drive collective cell invasion is selectively dependent on collagen remodeling as there

was no invasion deficit following periostin knockdown when spheroids were embedded in Matrigel which primarily consists of laminins and other basement membrane proteins.

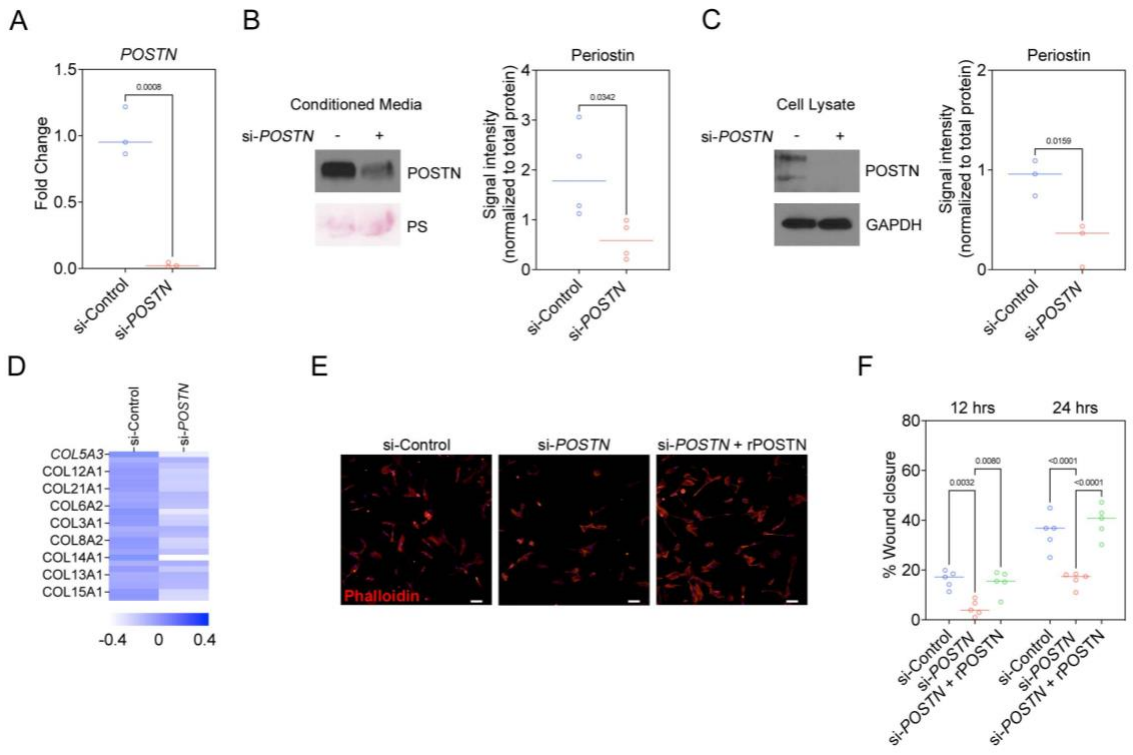

Figure 2.8. ***Periostin knockdown in primary human breast CAFs inhibits cell spreading and migration.*** (A) qPCR analysis to confirm periostin expression is reduced in primary human breast CAFs treated with periostin-targeting siRNA (si-*POSTN*) compared to cells treated with a non-targeting control siRNA (si-Control). Performed in triplicate. Statistics shown for unpaired Student's t test. (B) Western blot for secreted periostin in primary human breast CAFs treated with si-Control or si-*POSTN.* Ponceau stain (PS) shown as loading control. Protein signal intensity quantified on the right, performed in quadruplicate. Statistics shown for unpaired Student's t test. (C) Western blot for intracellular periostin in primary human breast CAFs treated with si-Control or si-*POSTN.* GAPDH shown as loading control. Protein signal intensity quantified on the right, performed in triplicate. Statistics shown for unpaired Student's t test. (D) Heat map of gene expression of collagen family proteins in primary human breast CAFs treated with si-Control or si-*POSTN.* (E) Immunofluorescence images of phalloidin staining of primary human breast CAFs treated with si-Control or si-*POSTN* ± recombinant human periostin (rPOSTN). Nuclei counterstained with DAPI. Scale bars: 100 μm. (F) Scratch assay quantification of percent wound closure over time by primary human breast CAFs treated with si-Control or si-*POSTN* ± recombinant human periostin (rPOSTN) to measure cell migration. Each data point represents a different scratch replicate. Statistics shown for 2-way ANOVA, Tukey's multiple comparisons test. RNA seq analysis in panel (D) performed by Dr. Pankaj Kumar of the UVA Genomics Core.

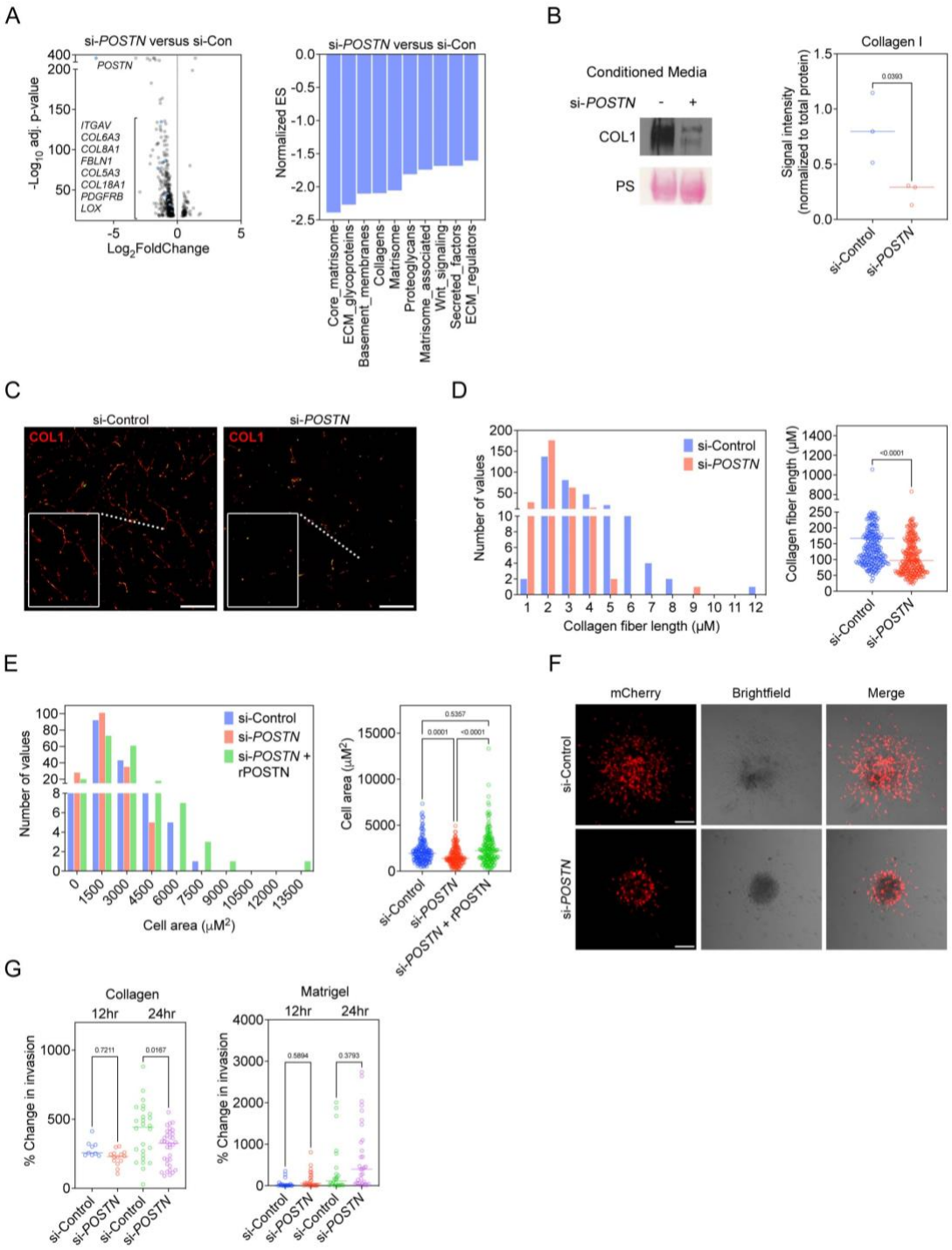

Figure 2.9. ***Periostin knockdown in primary human breast CAFs alters collagen matrix architecture and inhibits collective cell invasion.*** (A) Volcano plot of genes with significantly altered expression detected by bulk RNAseq following periostin knockdown in primary human breast CAFs (left) and NABA Gene Set Enrichment Analysis (GSEA) showing downregulated pathways in periostin knockdown cells (right). Periostin knockdown in human breast CAFs done in quadruplicate. (B) Western blot of

secreted collagen I following periostin knockdown. Ponceau stain (PS) shown as loading control. Signal intensity quantified at right and compared using unpaired Student's t test. Performed in triplicate. (C) Immunostaining of deposited collagen I by si-Control- vs. si-*POSTN*-treated human breast CAFs. Scale bars: 100 μm, insets are 2x zoom. (D) Lengths of collagen fibers deposited by control versus periostin knockdown human breast CAFs represented as a histogram (left) and scatter plot (right). Each data point represents an individual continuous collagen fiber (n = 285-305 fibers per group). Experiments performed in triplicate and results compared using a Mann-Whitney test. (E) Cell area measurements of phalloidin-stained primary human breast CAFs treated with si-Control or si-*POSTN* ± recombinant human periostin (rPOSTN) represented as a histogram (left) and scatter plot (right). Experiment performed in triplicate with each data point representing an individual cell (n = 160-190 cells per group). Statistics shown for Kruskal-Wallis, Dunn's multiple comparisons test. (F) Confocal images at the 24 hr timepoint of tumor cell/CAF co-culture spheroids consisting of MDA-MB-231^{mCherry} human breast cancer cells and unlabeled primary human breast CAFs embedded in type I collagen. Scale bars: 100 μm. (G) Percent change in invasive area of tumor cell/CAF co-culture spheroids embedded in type I collagen (left) or Matrigel (right). Each data point represents an individual spheroid, carried out in biological triplicates. Statistics shown for ordinary one-way ANOVA, Tukey's multiple comparisons test (left) and Kruskal-Wallis, Dunn's multiple comparison's test (right). RNAseq analysis in panel (A) performed by Dr. Pankaj Kumar of the UVA Genomics Core.

2.4.7 Periostin-expressing CAFs promote lymphatic metastasis by remodeling the extracellular matrix and directing lymphovascular invasion along organized collagen fibers

Taken together, our in vitro data implicated periostin-expressing CAFs in collagen-mediated collective invasion. To further explore the specific role of this population during tumor progression and metastasis, we used a DTA depletion strategy to ablate periostin-expressing CAFs in vivo. We generated *Postn*^{DTA} mice by crossing *Postn*^{iZSGreen} lineage tracing mice with *Rosa*-DTA mice. In this model, tamoxifen administration drives expression of diphtheria toxin in periostin-expressing cells resulting in their selective ablation. To confirm ablation of periostin-expressing cells in our *Postn*^{DTA} mouse model, we quantified ZSGreen^{+} cells in the primary mammary tumors of control (*Postn*^{iZSGreen}) mice compared to periostin^{+} cell-depleted (*Postn*^{DTA}) mice. There was a 75% reduction in the percentage of tissue area positive for ZSGreen in the mammary tumors of the *Postn*^{DTA} mice (1.68% ± 0.2% versus 0.41% ± 0.1%), indicating successful ablation of the majority of periostin-expressing cells (Figure 2.10). We then used these *Postn*^{DTA} mice in our mammary tumor model to measure changes in matrix architecture and metastasis following ablation of periostin-expressing cells (Figure 7A). *Postn*^{DTA} mice were treated with either tamoxifen to induce periostin^{+} cell depletion or vehicle-only control, then injected with highly-metastatic EO771.LMB^{mCherry} mammary cancer cells. Primary tumors were resected and a booster dose of tamoxifen (or vehicle-only control) was administered to ablate any periostin-expressing cells that may have been activated as a result of

surgery as periostin is induced by tissue injury and inflammation. Finally, secondary sites were harvested and evaluated for metastatic burden.

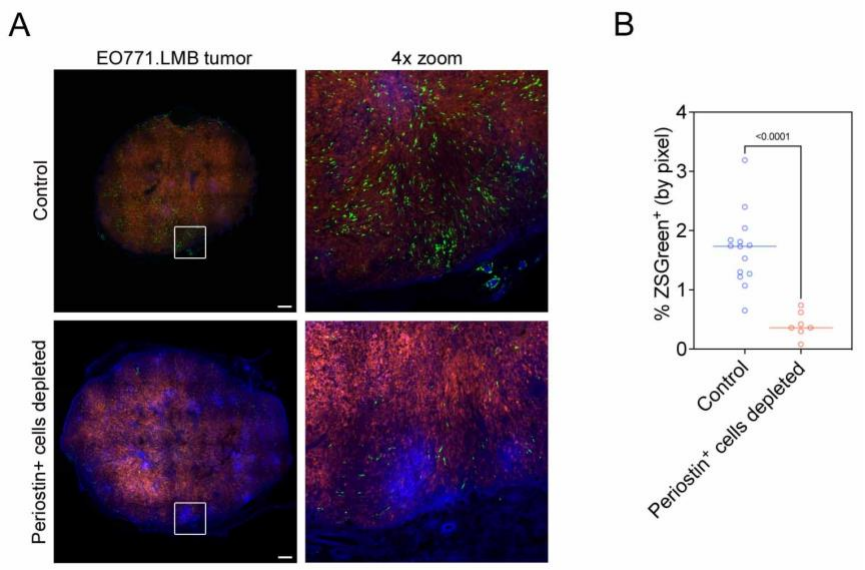

Figure 2.10. ***Confirmation of periostin-expressing cell depletion in mammary tumors of Postn^{DTA} mice.*** (A) Tissue tilescans of EO771.LMB mammary tumors from *Postn*^{iZSGreen} control mice (left) and *Postn*^{DTA} mice (right). Tumor cells labelled with mCherry and periostin-expressing cells genetically labelled with ZSGreen. Nuclei counterstained with DAPI. Scale bars: 500 μm. (B) Percentage of tissue area positive for ZSGreen in EO771.LMB tumors (n = 3-5 mice per group). Each data point represents a different histological section. Statistics shown for unpaired Student's t test. Tumors shown in panel (A) were surgically resected by Marya Dunlap-Brown.

Surprisingly, depleting periostin-expressing cells accelerated the growth of primary mammary tumors which would indicate a growth-restraining feature of periostin-expressing cells at sites of primary growth by breast cancer cells (Figure 2.11B). In line with our previous observations, mammary tumors in which periostin-expressing cells had been depleted displayed impaired intratumoral collagen organization as detected by SHG imaging (Figure 2.11C), as collagen fibers were less aligned (Figure 2.12A) and shorter in the tumors of periostin^{+} cell-depleted mice (235.0 ± 8.0 μm versus 154.9 ± 5.5 μm) (Figure 2.12B). As expected, total collagen area was significantly reduced following periostin^{+} cell depletion (Figure 2.12C), but we unexpectedly found that the curvature of the collagen fibers in the periostin^{+} cell depleted tumors was reduced as well (Figure 2.12D). This indicates that depleting periostin^{+} cells reduced overall collagen abundance, fiber length, and alignment, but did not revert the collagen fibers to the “curly” phenotype associated with normal mammary tissues and observed in the periostin^{low} EO771 primary tumors. Instead, the shorter collagen segments remained straight but disorganized.

Periostin^{+} cell depletion also dramatically reduced lymphatic metastasis of highly metastatic EO771.LMB^{mCherry} mammary cancer cells. The metastatic burden in the draining axillary lymph nodes of periostin^{+} cell-depleted mice was reduced ~3-fold (2% ± 0.3% versus 0.8% ± 0.1%) (Figure 2.11D,E), suggesting that periostin-expressing cells might enable lymphatic metastasis. Consistent with our previous results, very few EO771.LMB^{mCherry} mammary cancer cells reached the lungs in both the vehicle-control mice and periostin^{+} cell-depleted

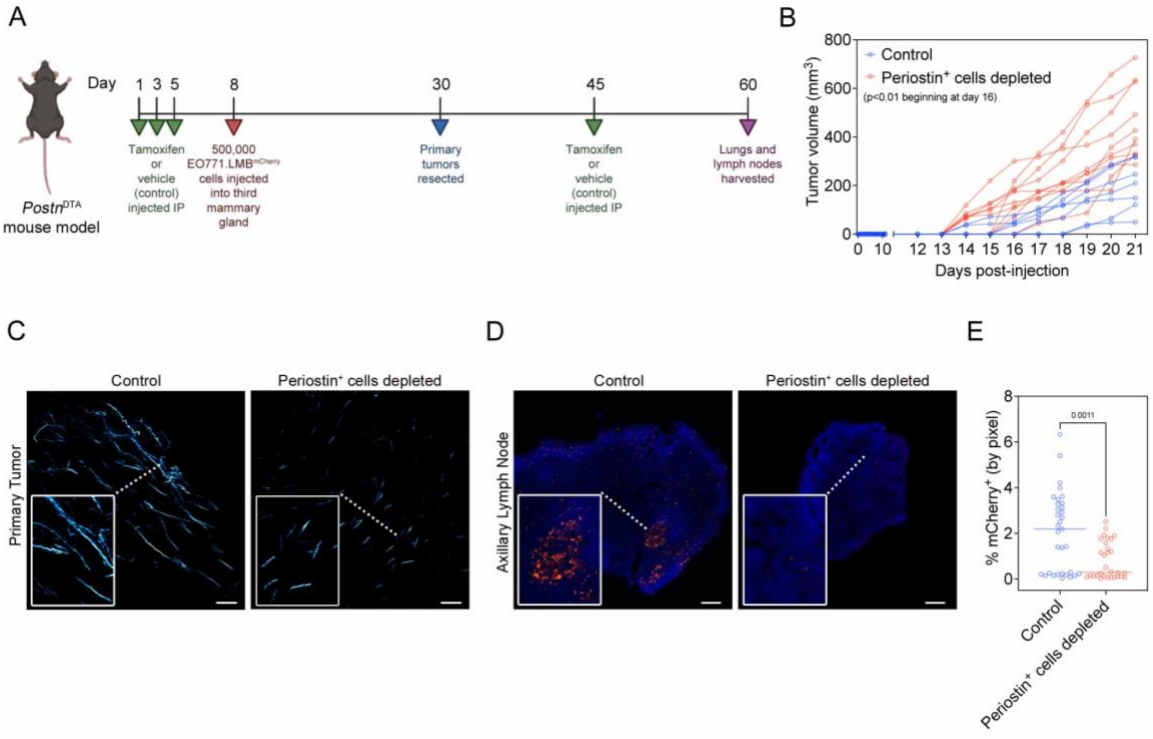

Figure 2.11. ***Periostin-expressing CAFs promote lymphatic metastasis by remodeling the extracellular matrix and directing lymphovascular invasion along organized collagen fibers.*** (A) Study design including tamoxifen (or vehicle-only control) treatment and orthotopic EO771.LMB mammary tumor injections in *Postn*^{DTA} mice. (B) Tumor volume measurements of highly metastatic EO771.LMB mammary tumors in control versus periostin+ cell-depleted mice. Each line represents an individual mouse (n = 8-10 mice per group). Statistics shown for multiple Mann-Whitney tests. (C) Second harmonic generation (SHG) images of intratumoral collagen fibers (pseudo-colored in cyan) in control versus periostin^{+} cell-depleted mice. Scale bars: 150 μm, insets are 3x zoom. (D) Tissue tilescans of axillary lymph nodes from control versus periostin^{+} cell-depleted mice bearing highly metastatic EO771.LMB mammary tumors. Tumor cells labelled with mCherry and nuclei counterstained with DAPI. Scale bars: 200 μm, insets are 3x zoom. (E) Percentage of tissue area positive for mCherry in serial sections of axillary lymph nodes from control versus periostin^{+} cell-depleted mice bearing highly metastatic EO771.LMB mammary tumors. Each data point in the scatter plot represents an individual histological section (n = 8-10 mice per group). Statistics shown for Mann-Whitney test. Second harmonic generation shown in panel (C) was performed in collaboration with Dr. Adrian Halme, Dr. Stacey Criswell, and Natalia Dworak of the UVA Advanced Microscopy Core.

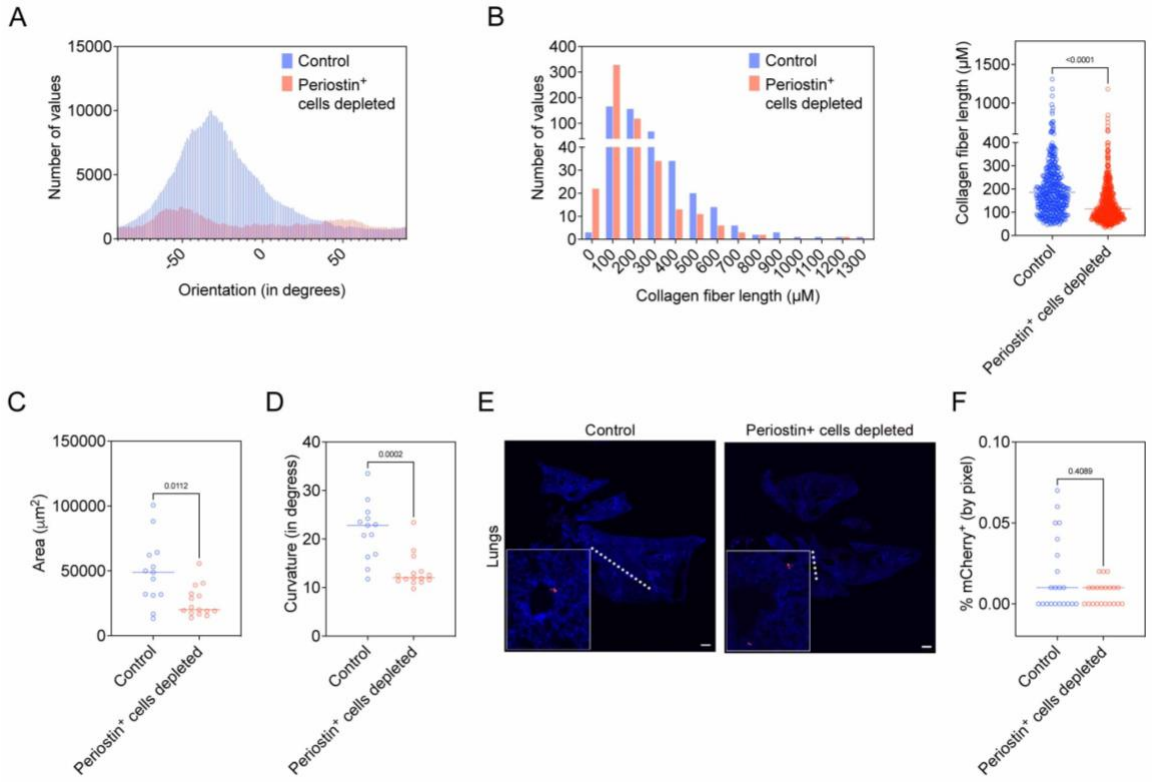

Figure 2.12. ***Depleting periostin-expressing CAFs alters matrix architecture in primary tumors but does not significantly reduce metastatic burden in the lung.*** (A) Representative histogram of collagen fiber orientation in EO771.LMB tumors from vehicle-only injected control mice and periostin$^+$ cell-depleted mice. A peaked histogram represents aligned fibers whereas a flat histogram represents random organization. (B) Quantification of collagen fiber length in EO771.LMB tumors from vehicle-only injected control mice and periostin$^+$ cell-depleted mice, represented as a histogram (left) and scatter plot (right). Each point represents an individual fiber. Between 475 and 540 fibers quantified from multiple histological sections (n = 3-4 mice per group) and results compared using Mann-Whitney test. (C) Total collagen area in histological sections of EO771.LMB tumors from vehicle-only injected control mice and periostin$^+$ cell-depleted mice. (n = 4-5 mice per group). Each data point represents a different histological section. Statistics shown for Mann-Whitney test. (D) Curvature of collagen fibers, measured as mean change in angle along fibers, in histological sections of EO771.LMB tumors from vehicle-only injected control mice and periostin$^+$ cell-depleted mice. (n = 4-5 mice per group). Each data point represents a different histological section. Statistics shown for Mann-Whitney test. (E) Tissue tilescans of lungs from either vehicle-only injected control mice or periostin$^+$ cell-depleted mice bearing EO771.LMB mammary tumors. Tumor cells labelled with mCherry and nuclei counterstained with DAPI. Scale bars: 500 μm, insets are 6x zoom. (F) Percentage of tissue area positive for mCherry in serial sections of lungs from either vehicle-only injected control mice or periostin$^+$ cell-depleted mice bearing EO771.LMB mammary tumors. Each point represents a different histological section (n = 7 mice per group). Statistics shown for Mann-Whitney test.

mice, and we did not observe a statistically significant reduction in pulmonary metastases following periostin^{+} cell depletion (Figure 2.12E,F). Similarly, we found that periostin^{+} cell depletion reduced lymphatic metastasis (Figure 2.13A,B) but did not affect pulmonary metastasis (Figure 2.13C,D) when we repeated the periostin^{+} cell depletion study using highly-metastatic PyVMT cells. Since targeting periostin on the cellular level reduced lymphatic metastasis, we then asked whether attenuating periostin expression on a molecular level would have a similar effect. Periostin expression in mouse mammary fibroblasts is regulated by TGFβ (Figure 2.14A), and we hypothesized that reducing TGFβ-mediated periostin activation by conditionally knocking out a receptor in the TGFβ pathway (*Tgfbr2)* in periostin-expressing cells would similarly reduce lymphatic metastasis. Using *Postn-Cre:Tgfbr2*$^{fl/fl}$ mice, we found a significant reduction in metastasis of highly-metastatic EO771. LMB^{mCherry} mammary cancer cells to the draining axillary lymph node following *Tgfbr2* knockout (Figure 2.14B,C).

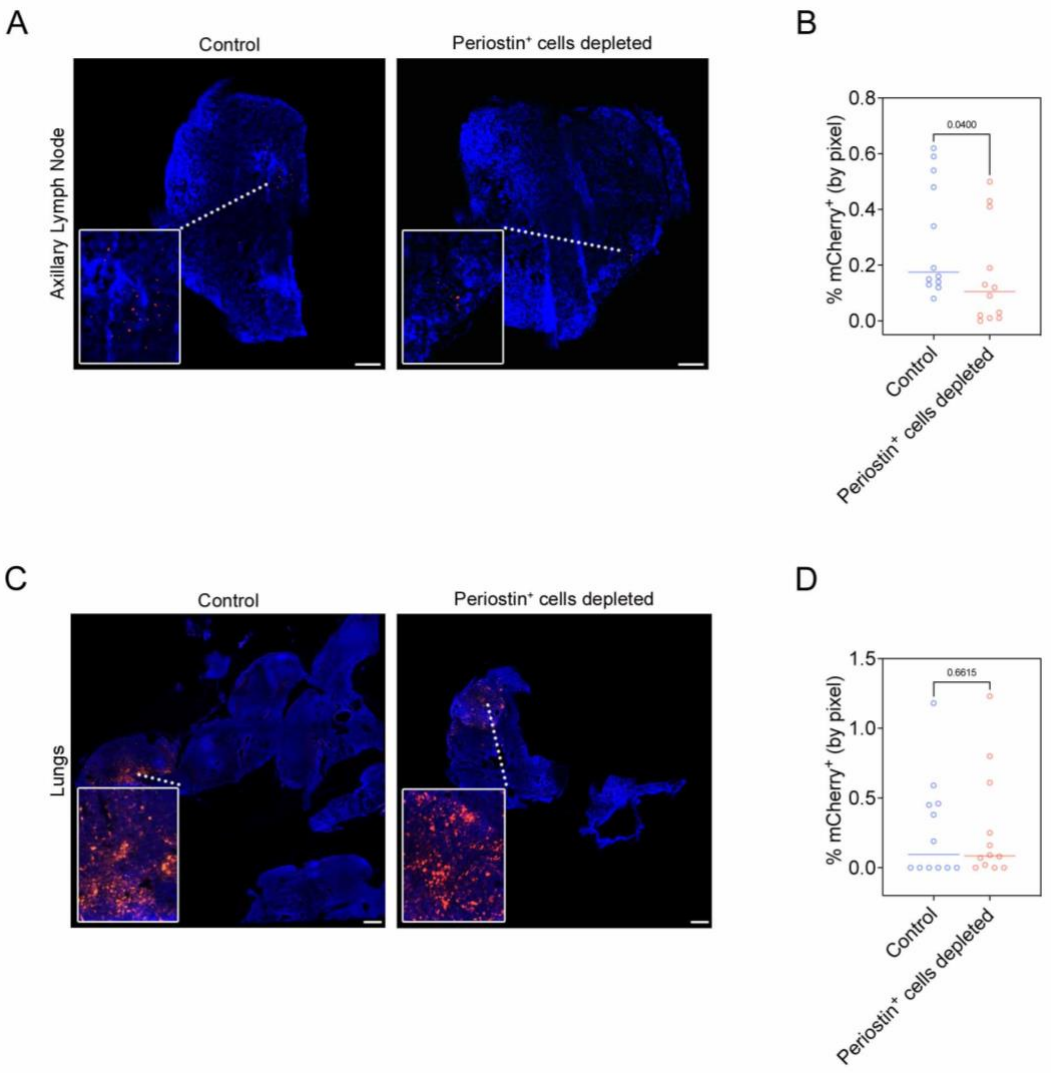

Figure 2.13. ***Depleting periostin-expressing CAFs reduces lymphatic metastasis of highly-metastatic PyVMT tumors but does not significantly reduce metastatic burden in the lung.*** (A) Tissue tilescans of axillary lymph nodes from control mice or periostin$^+$ cell-depleted mice bearing highly-metastatic PyVMT mammary tumors. Tumor cells labelled with mCherry and nuclei counterstained with DAPI. Scale bars: 200 μm, insets are 3x zoom. (B) Percentage of tissue area positive for mCherry in serial sections of axillary lymph nodes from either control mice or periostin$^+$ cell-depleted mice bearing highly-metastatic PyVMT mammary tumors. Each point represents a different histological section (n = 4 mice per group). Statistics shown for Mann-Whitney test. (C) Tissue tilescans of lungs from control mice or periostin$^+$ cell-depleted mice bearing highly-metastatic PyVMT mammary tumors. Tumor cells labelled with mCherry and nuclei counterstained with DAPI. Scale bars: 500 μm, insets are 6x zoom. (D) Percentage of tissue area positive for mCherry in serial sections of lungs from either control mice or periostin$^+$ cell-depleted mice bearing highly-metastatic PyVMT mammary tumors. Each point represents a different histological section (n = 4 mice per group). Statistics shown for Mann-Whitney test.

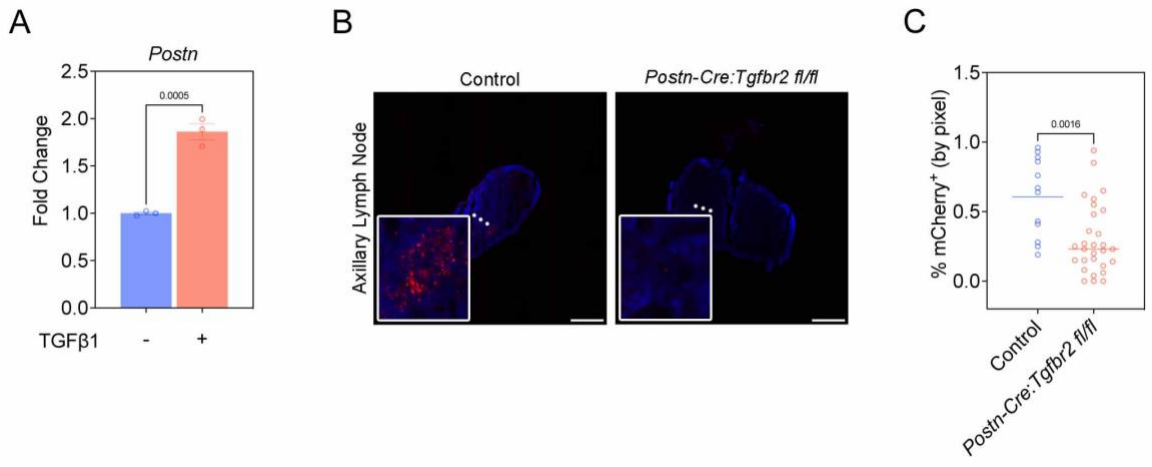

Figure 2.14. ***Tgbfr2 knockout in periostin-expressing cells reduces lymphatic metastasis.*** (A) qPCR analysis of periostin expression in primary mouse mammary fibroblasts treated with 10 ng/mL TGFβ1. Statistics shown for unpaired Student's t test. (B) Tissue tilescans of axillary lymph nodes from control mice or *Postn-Cre:Tgfbr2*$^{fl/fl}$ mice. Tumor cells labelled with mCherry and nuclei counterstained with DAPI. Scale bars: 200 μm, insets are 6x zoom. (C) Percentage of tissue area positive for mCherry in serial sections of axillary lymph nodes from either control mice or *Postn-Cre:Tgfbr2*$^{fl/fl}$ mice bearing EO771.LMB mammary tumors. Each point represents a different histological section (n = 4-10 mice per group). Statistics shown for Mann-Whitney test.

Given the reduction in lymphatic metastasis following periostin depletion in vivo, we then modelled lymphovascular invasion in vitro to determine whether there is a role for periostin^{+} CAFs in guiding the intravasation of cancer cells across the lymphatic endothelial cell barrier. Using a modified spheroid/transwell migration assay (Figure 2.15A), we found that treating primary human breast CAFs with periostin-targeting siRNA inhibited their ability to promote the invasion of MDA-MB-231^{mCherry} human breast cancer cells through a collagen matrix and across a primary human lymphatic endothelial cell barrier (Figure 2.15B). Following periostin knockdown in CAFs, significantly fewer mCherry-labelled cancer cells crossed the lymphatic endothelial cell barrier compared to control (144 ± 24 cells versus 81 ± 17 cells) (Figure 2.15C), indicating that periostin-expressing CAFs promote lymphovascular invasion of breast cancer cells. This effect of periostin knockdown on cancer cell invasion appears to be specific to lymphatic vessels, as it did not reduce cancer cell invasion across a blood endothelial cell barrier when we repeated the spheroid/transwell migration assay using a layer of human umbilical vein endothelial cells (HUVECs) (Figure 2.16A,B).

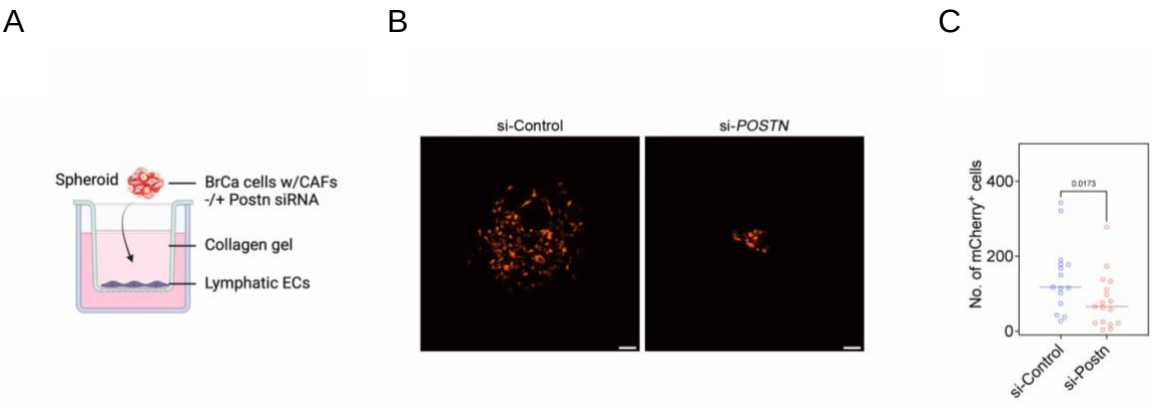

Figure 2.15*. Periostin knockdown in primary human breast CAFs reduces breast cancer cell invasion across a lymphatic endothelial cell barrier.* (A) Experimental setup for in vitro lymphovascular invasion assay using MDA-MB-231^{mCherry} human breast cancer cells, primary human breast CAFs, and primary human lymphatic endothelial cells. (B) Representative fluorescent images of transmigrated MDA-MB-231^{mCherry} tumor cells that have invaded across the lymphatic endothelial cell barrier in the in vitro lymphovascular invasion assay. Breast cancer cells were co-cultured in spheroids with primary human breast CAFs that were pre-treated with either non-targeting control siRNA (si-Control) or periostin-targeting siRNA (si-*POSTN).* Scale bar: 100 μm. (C) Quantification of the number of MDA-MB-231^{mCherry} tumor cells that have invaded across the lymphatic endothelial cell barrier in the in vitro lymphovascular invasion assay. Each data point represents an individual spheroid. Experiment performed in triplicate. Statistics shown for Mann-Whitney test.

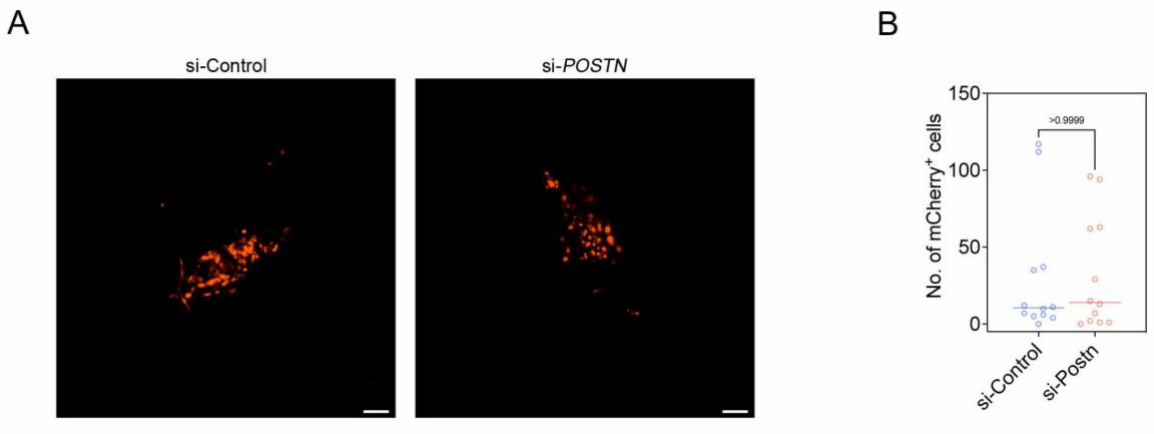

Figure 2.16. ***Periostin knockdown in primary human breast CAFs does not affect breast cancer cell invasion across a blood endothelial cell barrier.*** (A) Representative fluorescent images of transmigrated MDA-MB-231^{mCherry} tumor cells that have invaded across the blood endothelial cell barrier of HUVECs in the in vitro lymphovascular invasion assay. Breast cancer cells were co-cultured in spheroids with primary human breast CAFs that were pre-treated with either non-targeting control siRNA (si-Control) or periostin-targeting siRNA (si-*POSTN).* Scale bar: 100 μm. (B) Quantification of the number of MDA-MB-231^{mCherry} tumor cells that have invaded across the blood endothelial cell barrier in the in vitro lymphovascular invasion assay. Each data point represents an individual spheroid. Statistics shown for Mann-Whitney test.

Taken together, our in vivo depletion studies and in vitro functional assays reveal a role for periostin-expressing CAFs in driving collagen-mediated lymphovascular invasion of cancer cells, resulting in lymphatic metastasis to the draining lymph node. To assess whether this pro-metastatic role for periostin within the primary tumor is reflected in clinical specimens, we used RT-qPCR analysis to measure relative periostin expression in paired primary breast tumors and lymph node metastases from 28 metastatic breast cancer patients obtained from the UNC Chapel Hill tissue biorepository. We found that periostin expression was higher in the primary tumors compared to their paired lymph node samples in 68% of patients (Figure 2.17A), which is consistent with periostin functioning within the primary TME to promote breast cancer cell escape and eventual metastasis. To determine if periostin abundance is associated with poor patient outcome, we used the Kaplan-Meier Plotter to perform survival analysis of lymph node positive breast cancer patients stratified based on high or low periostin protein expression (Figure 2.17B) (237). As predicted, periostin expression significantly correlated with decreased overall survival probability in this patient cohort, further supporting a clinically-relevant role for periostin in driving disease progression.

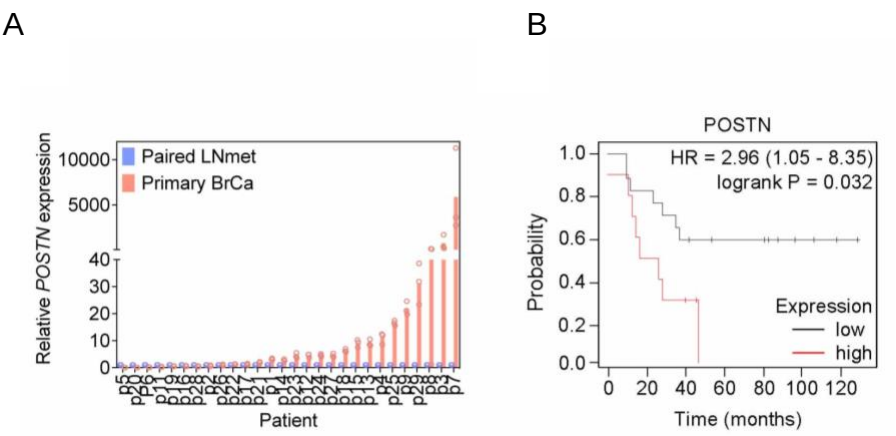

Figure 2.17. ***Periostin is enriched in primary human breast cancers and is associated with reduced overall survival.*** (A) RT-qPCR analysis of periostin expression in paired primary breast cancer specimens (Primary BrCa) and lymph node metastases (Paired LNmet) from human breast cancer patients (n = 28 patients). qPCR performed in triplicate. (B) Kaplan-Meier plot of overall survival in lymph node positive breast cancer patients stratified based on periostin protein expression (n = 27 patients). qPCR data in panel A provided by Lincy Edatt and Dr. Chad Pecot.

2.5 Discussion

Considerable progress has been made in the field of CAF biology using single-cell sequencing technologies to identify molecularly diverse CAF subpopulations. While expression profiles can indicate potential functional roles for these subclasses of CAFs, the clustering algorithms used to analyze sequencing data can yield subpopulations that are not necessarily spatially or pathologically relevant. Therefore, there remains a need to track these cells in situ and validate the functions of CAF subpopulations both in vitro and in vivo to determine their biological importance during tumor progression. In the present study, we have used lineage tracing strategies to functionally characterize a population of cells marked by expression of periostin which is a matricellular protein associated with metastasis and is expressed by the desmoplastic stroma of human breast cancers. We show that periostin is expressed by CAFs and perivascular-like cells and is enriched in advanced stage and lymph node positive human breast cancer samples. Our work also identifies a population of periostin-expressing CAFs that are enriched at the lymphatic vessel periphery and are differentially activated in highly-metastatic mammary tumors compared to their low-metastatic counterparts. In addition to quantitative differences, we observe phenotypic variation in the periostin-expressing cells between tumor types. The ZSGreen-labelled periostin-expressing cells in highly-metastatic tumors are larger and resemble the classical stellate shape of activated myofibroblasts whereas the periostin-expressing cells in low-metastatic tumors are smaller and rounded, reflecting the different activation states between the

two populations. Together, this shows that the metastatic potential of cancer cells informs the activation of periostin-expressing cells in the primary tumor microenvironment. Interestingly, we find that the same is true at metastatic and premetastatic sites. We show that periostin-expressing cells are more abundant in the draining lymph nodes, lungs, and contralateral mammary glands of mice bearing highly-metastatic mammary tumors compared to those implanted with low-metastatic mammary tumors. A limitation of our spontaneous metastasis model is that relatively few mammary cancer cells reach the lungs before primary tumors re-grow to the maximum volume at which time mice must be sacrificed. In order to address this, we used an experimental model of metastasis in which mammary cancer cells were injected into the tail vein of lineage tracing mice. Both low- and highly-metastatic mammary cancer lines established macrometastases in the lungs but marginally activated periostin-expressing cells despite a greater number of cancer cells present in these tissues. This indicates that periostin activation in a primary tumor is critical for robust activation of periostin at secondary sites rather than activation occurring at the secondary site once cancer cells have already colonized the tissue. These findings support previous reports that periostin is activated in premetastatic (208) and metastatic niches (72) where it may function to promote cancer cell survival and outgrowth, though our study focuses on an earlier pro-metastatic role for periostin within the primary tumor.

We find that periostin-expressing cell abundance is associated with intratumoral collagen abundance and organization, with straighter, longer, and

more aligned collagen fibers in highly-metastatic (periostin^{high}) tumors. Our in vitro functional assays reveal that this difference in collagen matrix architecture is due to differences in intratumoral periostin abundance, as knocking down periostin expression in primary human breast CAFs reduces expression of a number of matrix-related proteins including collagens. This reduction in collagen secretion leads to a deficient and unorganized matrix, which impairs the ability of primary human breast CAFs to engage the matrix, spread, and migrate. These spreading and migratory defects are rescued by treatment with recombinant human periostin, suggesting that the differences in periostin-expressing cell morphology we observe in vivo in low- versus highly-metastatic tumors are directly related to differences in intratumoral periostin levels. We also show that periostin knockdown selectively inhibits collective cell invasion of primary human breast CAFs and breast cancer cells through collagen matrices. Though the timing of our in vitro assay is too short for CAFs to remodel collagen into the highly organized fibrillar networks we observe in periostin^{high} tumors in vivo, our results reflect that the inhibitory effect of periostin knockdown on early steps of collagen remodeling is sufficient to reduce collective cell invasion. Additionally, we cannot rule out that proliferation of the human breast cancer cells could contribute to the differences in the area of invasion that we observed, although we used low serum conditions and a 24-hour timepoint to minimize this effect. If CAF-derived periostin promotes collagen cross-linking as proposed, then it's possible that cancer cells could engage the resulting matrix differently in control versus periostin-knockdown spheroids. This would potentially increase cancer

cell proliferation in control spheroids as there is an established role for stiffened ECM in driving tumor proliferation (127), though we observe the opposite in vivo with depletion of periostin-expressing cells leading to a slightly increased primary tumor growth despite impaired collagen organization. This accelerated tumor growth following periostin^{+} cell depletion could be attributed to the loss of an organized collagen matrix, as there is evidence that fibrillar collagen can mechanically restrain tumor growth (238). Alternatively, it is possible that periostin-expressing cell depletion enhances primary tumor growth by shifting the immune landscape within tumors as has been previously observed upon CAF depletion in a model of pancreatic cancer (157). Therefore, an important future direction is to investigate the immune populations present in control versus periostin^{+} cell-depleted mammary tumors to determine if periostin-expressing CAFs perform immune-modulatory functions in addition to their roles in matrix remodeling.

Although our lineage tracing studies reveal that periostin-expressing cells make up a relatively small proportion of the total tumor tissue, they have a dramatic effect on the matrix architecture of the tumor microenvironment and lymphatic metastasis as evidenced by our periostin^{+} cell depletion tumor study. Our data reveal that periostin-expressing CAFs are instrumental in mediating lymphatic metastasis by depositing an organized collagen matrix and by promoting lymphovascular invasion of breast cancer cells. CAFs and collagen alignment have been shown to play a role in hematogenous metastasis (118, 119, 153, 154, 239-246), but our work shows that periostin-expressing CAFs

selectively promote lymphatic metastasis, as their depletion markedly reduces metastatic burden in the lymph node but does not significantly affect pulmonary metastasis. It could be that CAF-derived periostin generally promotes collagen remodeling and collective cell invasion towards both lymphatic and blood vessel interfaces within the primary tumor, but this enhanced invasion only leads to a difference in the number of cancer cells crossing lymphatic endothelial cell barriers and not blood endothelial cell barriers due to structural differences between the two types of vessels. Blood endothelial cells form tight junctions, making blood vessels inherently more restrictive and difficult to transverse, whereas lymphatic endothelial cells are characterized by discontinuous junctions that allow for the entry of fluid, macromolecules, and cells into lymphatic vessels during interstitial pressure regulation (96). This is reflected in our in vitro data with the median number of transmigrated cancer cells varying greatly in the control conditions between the assays performed with a monolayer of HUVECs (11 cells) versus assays performed with a monolayer of lymphatic endothelial cells (118 cells). These findings agree with and build upon recently published work showing that CAF-derived periostin can mediate metastasis by promoting lymphatic vessel permeability in an experimental model of popliteal lymph node metastasis (41), though this work used gain of function experiments to determine the effect of injected periostin on lymphatic metastasis of cervical squamous cell carcinoma whereas we have used genetic tools to determine the function of periostin^{+} cells in spontaneous breast cancer metastasis. Similarly, another study of periostin in experimental lymph node metastasis has shown an association

between periostin deposition and lymphangiogenesis within lymph nodes prior to colonization by murine melanoma cells (247). This finding is consistent with our lineage tracing results showing periostin activation in lymph nodes as part of premetastatic niche formation, though our work emphasizes an ECM-remodeling role for periostin within the primary tumor site. Our mouse model recapitulates the desmoplastic stromal reaction linked to poor prognosis of breast cancer patients and allows us to deplete the periostin^{+} CAFs that contribute to this desmoplasia in situ to reveal their critical role in collagen-mediated lymphovascular invasion. As our study is the first to lineage trace and deplete periostin-expressing cells in the tumor context, this strategy can and should be adapted to other orthotopic tumor models to reveal whether this CAF population is present and shares a similar role in promoting the lymphatic metastasis of other cancers, especially those also characterized by desmoplasia such as pancreatic and lung cancer (158, 248, 249).

Densely aligned fibrillar collagen distinguishes progressive breast tumors from in situ lesions and is associated with increased periostin deposition in human patients (121), so early targeting or re-programming of the periostin^{+} CAF population could be an intervention to help prevent breast tumors from advancing to invasive disease. An important therapeutic consideration would be the timing of targeting periostin^{+} cells, as we observe increased primary tumor growth rate following periostin^{+} cell depletion similar to the paradoxical results of other CAF depletion studies (156, 157). To avoid this effect and given that periostin is activated by tissue injury and inflammation, blocking periostin^{+} CAF activation

may be most effective around the time of surgical resection of the tumor, though further preclinical studies are required to examine the effect of periostin blockade at different timepoints during tumor progression and whether this could be an effective strategy to normalize the ECM and attenuate lymphatic metastasis. The ability of desmoplasia to drive breast cancer metastasis by promoting a mesenchymal phenotype in cancer cells to support cancer cell outgrowth at secondary sites has been established (116, 118), but attempts to target mediators of this process have been primarily preclinical with limited and largely unsuccessful clinical trials (250-252). Our study identifies a population of CAFs, including PVL-CAFs, responsible for the collagen remodeling that drives desmoplasia and demonstrates their role in promoting lymphovascular invasion and lymphatic metastasis, revealing a potential new avenue for therapeutic intervention in the metastatic cascade.

Chapter 3: Perspectives

3.1 Major findings

My thesis work identifies a population of CAFs, marked by the expression of the matricellular protein periostin, that is activated by metastatic breast cancer cells to remodel the ECM within the primary tumor microenvironment and promote lymphatic spread. While periostin-expressing myofibroblasts have previously been studied in the context of the injured heart (223), genetic lineage-tracing approaches have not been used to examine this population in the context of cancer progression. Therefore, we generated a lineage-tracing mouse model to probe the abundance and spatial distribution of periostin-expressing cells during breast cancer growth. Using these lineage-tracing mice, we have demonstrated that periostin-expressing cells are found in perivascular and periductal spaces within the naïve mammary gland and are enriched in the lymphatic vessel periphery. Using spatial transcriptomics, we characterized the gene expression profiles of these periostin-expressing populations and found that they are enriched in genes related to collagen organization and turnover, indicating that periostin-expressing cells work together to remodel the ECM within the mammary gland. We find that periostin-expressing cells are differentially activated in highly-metastatic mammary tumors compared to their low-metastatic counterparts and that this difference in periostin^{+} cell abundance coincides with changes to the intratumoral collagen architecture. Additionally, we observe an increased number of periostin-expressing cells in the axillary lymph nodes, lungs, and contralateral mammary glands of highly-metastatic tumor-bearing mice, indicating that periostin likely also functions within metastatic and

premetastatic niches although our work focuses on its role within the primary tumor microenvironment.

In order to determine the specific role of periostin-expressing cells in the tumor microenvironment, we performed a number of in vitro functional assays and in vivo depletion studies. We found that knocking down periostin expression in primary human breast CAFs in vitro impairs their ability to deposit and organize collagen matrices, thereby reducing cell spreading, migration, and collective cell invasion. Further, we have modeled lymphovascular invasion in vitro and found that knocking down periostin in primary human breast CAFs inhibits their ability to promote the migration of human breast cancer cells through a collagen matrix and across a lymphatic endothelial cell barrier. Similarly, if we deplete intratumoral periostin in vivo either by selectively ablating periostin-expressing cells or by attenuating TGFβ-mediated periostin expression we observe a reduction in collagen deposition and alignment as well as a significant decrease in lymphatic metastasis. Whereas previous studies of periostin in tumor progression have emphasized its ability to promote metastatic outgrowth within secondary microenvironments, this work establishes an earlier pro-metastatic role for periostin within the primary tumor as it promotes collagen alignment and invasion into the lymphatic vasculature (Figure 3.1).

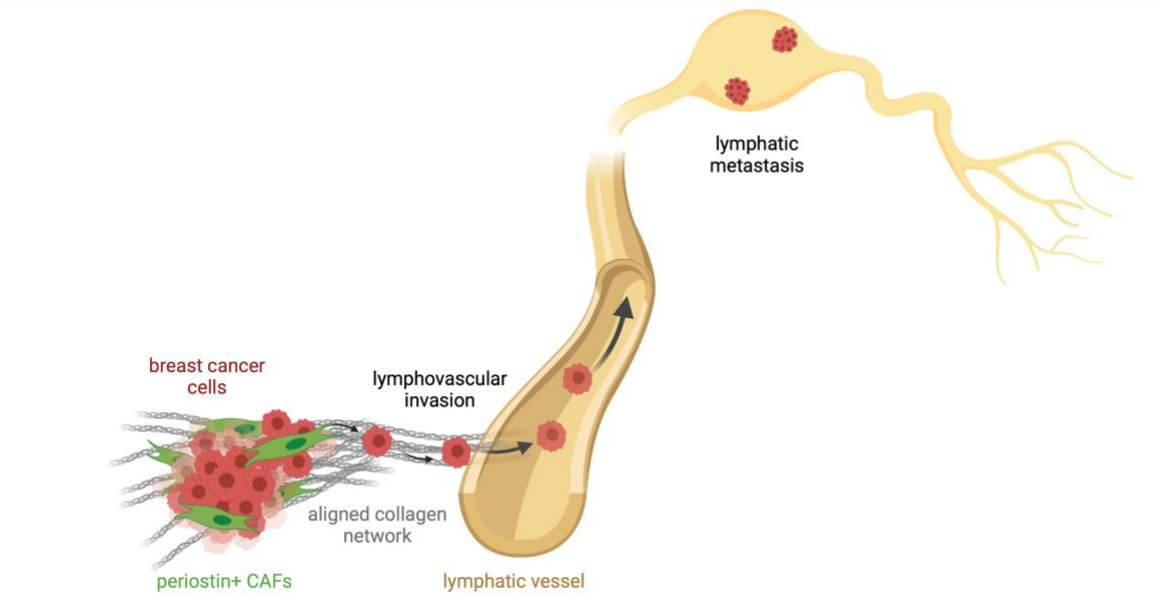

Figure 3.1. ***Periostin-expressing CAFs promote lymphatic metastasis by remodeling the ECM and directing lymphovascular invasion along collagen fibers.*** Summary model of the roles of periostin^{+} cells in breast cancer metastasis. Figure created using BioRender.

3.2 Future directions

3.2.1 Differential activation of periostin-expressing cells in breast cancer

In our lineage-tracing *Postn*^{iZSGreen} mice we observe a greater abundance of periostin-expressing cells in highly-metastatic mammary tumors compared to their low-metastatic counterparts, indicating that highly-metastatic cancer cells use an unknown mechanism to differentially activate periostin-expressing cells within the TME. It could be that highly-metastatic EO771.LMB tumor cells secrete a greater amount of a soluble factor that promotes periostin expression in tissue-resident fibroblasts compared to low-metastatic EO771 cells. To determine if this is the case, we could perform a transwell co-culture assay in which fibroblasts are cultured in the lower compartment of a transwell system with either low-metastatic or highly-metastatic breast cancer cells seeded in the upper compartment above a filter that does not allow for cells to transverse and reach the opposite compartment. Following incubation, the fibroblasts could be harvested and probed for periostin expression via qPCR and Western blot to determine whether soluble factors from highly-metastatic cancer cells increase periostin expression in fibroblasts to a greater degree than low-metastatic cancer cells as we would expect. This assay could be repeated with different cell types seeded in the upper chamber such as endothelial cells and fibroblasts to show that this effect on periostin expression is specific to highly-metastatic cancer cells. If there is no difference in periostin expression between the two conditions, it could be that periostin activation in fibroblasts is due to direct contact with cancer cells rather than a soluble factor. This alternative could be tested using a

co-culture system in which fibroblasts and low-metastatic or highly-metastatic cancer cells are cultured in direct contact on the same plate. As the cancer cell lines are labelled with mCherry, the fibroblasts could be separated from the co-cultures via flow cytometry and fibroblast periostin levels could be measured using qPCR and Western blot.

If the co-culture assays suggest that it is a tumor-secreted factor rather than direct cellular contact that differentially activates periostin expression in fibroblasts, we could revisit the sequencing data from the original paper that molecularly characterized the EO771 and EO771.LMB cell lines (232) to find candidate genes that are secreted factors differentially expressed between the two cell lines. These candidate genes could be evaluated in vitro by using siRNA to knock down their expression individually in the highly-metastatic EO771.LMB cells and performing the previously described transwell co-culture assay to determine the effects of target gene knockdown on periostin expression in fibroblasts. Once the soluble factor responsible for driving periostin expression in fibroblasts is identified using this in vitro approach, we could use CRISPR to knockout its expression in the highly-metastatic EO771.LMB cells and inject these cells into *Postn*^{iZSGreen} lineage-tracing mice to assess periostin^{+} cell abundance and metastatic burden in the lymph nodes. We would expect a reduction in the abundance of ZSGreen-labelled periostin-expressing cells in the knockout tumors compared to control EO771.LMB tumors and a subsequent reduction in metastatic spread to the lymph nodes. To complement this loss-of-function approach, we could also over-express the soluble factor in the low-

metastatic EO771 cells and inject them into *Postn*^{iZSGreen} lineage-tracing mice to determine if over-expressing the soluble factor is enough to increase the activation of periostin^{+} cells within the tumor and convert these tumors to a more highly-metastatic phenotype. Characterizing the mechanism of activation of periostin-expressing cells in highly-metastatic tumors could identify additional potential therapeutic targets that could be exploited to prevent periostin-mediated lymphovascular invasion and lymphatic metastasis.

In addition to identifying the factor responsible for the differential activation of periostin^{+} cells in low- and highly-metastatic tumors, it would be informative to use a transcriptomic approach in our *Postn*^{iZSGreen} lineage-tracing mouse model to characterize the different activation states of the ZSGreen-labelled periostin-expressing cells in the low- versus highly-metastatic tumors to better understand how the metastatic capacity of tumor cells influences the activity of periostin^{+} cells. Our previous studies suggest that there are likely differences in the expression of genes related to cytoskeletal remodeling and cell adhesion as well as ECM components as we observe phenotypic differences in cellular morphology and collagen matrix structure in low-metastatic (periostin^{low}) tumors compared to highly-metastatic (periostin^{high}) tumors. While our work establishes roles for periostin^{+} cells in collagen remodeling and collective cell invasion in highly-metastatic tumors, these cells may perform additional pro-metastatic functions that could be uncovered by transcriptomic analysis such as secreting pro-survival factors, promoting vascular permeability, or participating in immune suppression.

Periostin-expressing cells are very rare in low-metastatic EO771 tumors, so it would be technically challenging to recover the number of cells required to perform single-cell RNAseq of ZSGreen-labelled cells collected from low-metastatic tumors versus highly-metastatic tumors. Additionally, the tissue dissociation process can introduce transcriptional changes in cells that could skew gene expression results. Instead, we could assess the gene expression profiles of ZSGreen-labelled cells in situ using GeoMx digital spatial profiling. This approach would allow us to perform whole-transcriptome analysis of periostin$^+$ cells to uncover both intertumoral and intratumoral heterogeneity among periostin$^+$ populations. We could then compare our existing GeoMx profiling data of periostin$^+$ cells in the naïve mammary gland to the expression profiles of periostin$^+$ cells in low- and high-metastatic tumors to determine which molecular features are retained and which are altered following activation within the tumor microenvironment. Genes that are enriched in the periostin$^+$ cells in highly-metastatic tumors could be further explored as potential mediators of tumor cell metastasis or as biomarkers of reactive stroma.

In addition to characterizing differences among ZSGreen-labelled periostin$^+$ cells within primary tumors, we could use GeoMx to profile periostin$^+$ cells found in secondary sites including the lymph nodes, lungs, and contralateral mammary glands of highly-metastatic tumor-bearing mice. This would allow us to compare expression profiles between periostin$^+$ populations within the primary tumor and periostin$^+$ cells found in anatomically-distinct metastatic and premetastatic microenvironments and determine whether periostin$^+$ cells display

expression profiles that reflect tissue-specific functions. Gaining a broader understanding of the diverse functions of periostin-expressing cells and the way they contribute to disease progression in different tissue contexts is critical as it could inform future approaches to therapeutically target this population.

3.2.2 Source of periostin-expressing cells in secondary sites

Although we observe an increased abundance of periostin-expressing cells in the secondary sites of mice bearing highly-metastatic tumors compared to low-metastatic tumors, it remains unknown whether these ZSGreen-labelled periostin-expressing cells are tissue-resident fibroblasts that are activated during tumor progression or if these cells are recruited and migrate from other sources such as the primary tumor or bone marrow as has been reported for fibroblasts in other cancers (134, 253). This could be addressed by transplant experiments using our *Postn*^{iZSGreen} lineage-tracing mouse model. We could orthotopically inject tamoxifen-induced *Postn*^{iZSGreen} mice with highly metastatic EO771.LMB cells so that periostin-expressing cells within the primary tumor are labelled with ZSGreen. Then, these tumors could be transplanted into wild-type C57BL/6 mice and, following primary tumor growth, secondary sites can be harvested and evaluated for evidence of ZSGreen-labelled cells. If ZSGreen-labelled cells are detected in the lymph nodes, lungs, or contralateral mammary glands of these mice then this would indicate that periostin-expressing cells migrate from the primary tumor to premetastatic and/or metastatic microenvironments. Alternatively, we could orthotopically inject wild-type C57BL/6 mice with highly-

metastatic EO771.LMB cells, transplant these tumors into tamoxifen-induced *Postn*^{iZSGreen} lineage-tracing mice, and harvest secondary sites to determine whether there is evidence of ZSGreen-labelled cells in these tissues. The presence of ZSGreen-labelled cells within secondary sites would indicate that host periostin-expressing cells, either tissue-resident cells or recruited bone-marrow derived mesenchymal cells, are activated at secondary sites by primary tumor growth. To determine the contribution of the bone marrow to the periostin^{+} cell populations in secondary sites, we would perform bone marrow transplant experiments in which we engraft bone marrow from *Postn*^{iZSGreen} mice into irradiated wild-type recipients then inject the recipient mice with highly metastatic EO771.LMB cells and analyze secondary sites for evidence of bone marrow-derived ZSGreen-labelled cells that have been recruited to the metastatic microenvironments. Identifying the source(s) of periostin^{+} cells in metastatic microenvironments could allow for earlier targeting of these populations to prevent their previously established role in supporting the survival and metastatic outgrowth of disseminated breast cancer stem cells (72).

If these in vivo studies indicate that periostin^{+} cells in secondary sites are primarily tissue resident fibroblasts that are activated during tumor progression, then the next question to address would be what tumor-derived factors are responsible for driving this activation. Our data suggest that periostin-expressing cells are activated in premetastatic niches before evidence of tumor cell colonization and that an established primary tumor is required for periostin^{+} cell activation in lung metastases. Together, these findings indicate that systemic

signals from the primary tumor microenvironment likely promote changes in distant tissue microenvironments to activate periostin-expressing cells within premetastatic and metastatic niches. Tumor cells and stromal cells have been shown to secrete soluble factors including cytokines and chemokines that drive premetastatic niche formation (62, 71, 254). Additionally, tumor-derived extracellular vesicles (EVs) such as exosomes can transfer biological cargo including proteins, lipids, nucleic acids, and metabolites to tissue-resident recipient cells, thereby altering gene expression and signaling within in the recipient cells and driving formation of the premetastatic niche. While the pro-metastatic functions of tumor cell-derived exosomes are well-established (255-259), there are emerging roles for CAF-derived exosomes in promoting tumor cell proliferation, migration, and metastasis (260-265). Thus, it could be that activated periostin^{+} CAFs in the primary tumor shed EVs that contain periostin or other biomolecules that reach secondary organs and drive periostin activation in the premetastatic niches of these distant tissues. In order to evaluate this possibility in vivo, we could generate reporter mice by crossing our *Postn*^{MCM} mice with CD63-emGFP$^{loxP/stop/loxP}$ mice which have been previously characterized by our lab as a tool to audit cell type-specific EVs (266). It has been shown that fusions between CD63, a cell surface-associated membrane protein, and fluorescent optical reporters are secreted from cells via EVs (267, 268), so this reporter mouse system will enable us to track and isolate fluorescently-labelled EVs that originate from periostin-expressing cells. We could inject *Postn*^{MCM}:CD63-emGFP$^{loxP/stop/loxP}$ mice with low-metastatic

(periostin^{low}) EO771 and highly-metastatic (periostin^{high}) EO771.LMB tumors and collect blood samples, mammary glands, lymph nodes, and lungs to determine whether periostin-expressing cells in the primary tumor release EVs and if these EVs reach secondary tissue microenvironments. It could be that periostin-expressing cells in low-metastatic tumors release fewer EVs compared to highly-metastatic EO771.LMB tumors, and this could account for the reduced periostin^{+} cell activation in the secondary tissues of these mice. Additionally, the content of the EVs may vary between mice bearing highly-metastatic (periostin^{high}) tumors and low-metastatic (periostin^{low}) tumors and could also contribute to the differences we observe in periostin^{+} cell activation at pre-metastatic and metastatic microenvironments. Therefore, we could isolate these EVs and use transcriptomic microarrays and mass spectrometry to examine the EV cargo to identify what biomolecules may be activating periostin expression upon reaching secondary sites.

3.2.3 The effect of periostin^{+} cell depletion on the immune landscape

While our work demonstrates that depleting periostin-expressing cells inhibits tumor cell invasion by reducing the abundance and alignment of the intratumoral collagen matrix, alterations to the collagen architecture may also have immunomodulatory consequences within the tumor. Just as cancer cells migrate along collagen fibers, various immune cells have also been shown to accumulate and migrate within regions of dense fibrillar collagen (147, 153, 269). In addition to serving as a physical substrate for immune cell migration, collagen

can also mediate immune infiltration biochemically. Activation of discoidin domain receptor 1 (DDR1), a collagen receptor with tyrosine kinase activity, promotes macrophage infiltration in other pathological contexts (270, 271), and type I collagen and collagen fragments are chemotactic for monocytes (macrophage precursors) and neutrophils (147, 272, 273). In murine models of pancreatic carcinoma, reducing fibrillar collagen content either by depleting SMA^+ cells or knocking-out secreted protein acidic and cysteine rich (SPARC) expression decreased overall immune infiltration and increased the intratumoral frequency of pro-tumorigenic regulatory T cells and M2 macrophages (157, 274). Taken together, these findings suggest that depleting periostin-expressing cells could impair immune cell infiltration and the anti-tumor immune response.

However, contradictory roles for collagen in immune cell infiltration and activation have been reported. Although DDR1 mediates macrophage infiltration in some pathologies, it has recently been shown to instigate immune exclusion by aligning collagen in mouse models of triple-negative breast cancer (123). Additionally, collagen engages leukocyte-associated Ig-like receptors (LAIRs) which are highly expressed on most immune cells and can inhibit anti-tumor immunity by blocking NK cell, T cell, and phagocyte activity (275). Further, culturing macrophages on type I collagen reduces their cytotoxicity against cancer cells by inhibiting the polarization of monocytes to the tumoricidal M1-like macrophage type (276). Therefore, depleting periostin-expressing cells may instead improve immune infiltration and activity by reducing collagen-mediated inhibition of the anti-tumor immune response. To test whether $periostin^+$ cell

depletion enhances or impairs immune cell infiltration and activation, flow cytometry could be used to classify immune populations and quantify changes to the immune landscape in periostin$^+$ cell-depleted mammary tumors compared to control mammary tumors. Determining whether periostin-expressing cells display secondary immune-modulating functions will provide a more complete picture of their roles in cancer progression and could ultimately inform strategies for combinatory therapeutic approaches. Reducing desmoplasia by depleting periostin-expressing cells could make tumors more accessible to immune infiltrates, and treating them simultaneously with immunotherapies that enhance the activation and anti-tumor activity of these immune cells may attenuate the accelerated tumor growth we observe following depletion or may augment the reduction in lymphatic metastasis we observe in periostin cell-depleted mice.

3.2.4 Generation of a mutant periostin protein isoform that cannot bind collagen

The data presented in this thesis establish an association between periostin$^+$ cell abundance within primary mammary tumors and intratumoral collagen remodeling, lymphovascular invasion, and lymphatic metastasis. While we hypothesize that periostin-mediated collagen matrix remodeling is what permits these CAFs to promote invasion and metastasis, in vitro studies using a mutant periostin protein that cannot bind collagen and therefore cannot promote its assembly into an aligned matrix are critical to provide a mechanistic explanation for these observed associations. In order to achieve this, we could

perform site-directed mutagenesis to generate an isoform of human periostin that contains a mutated EMI domain, thus preventing its direct binding to collagen and inhibiting its ability to serve as a protein scaffold during collagen crosslinking and fiber assembly. We could purify this protein and use it in our in vitro spheroid assays and transwell migration assays to compare the ability of wild type periostin versus mutant periostin to rescue collective cell invasion and lymphovascular invasion defects that we observe following periostin knockdown in primary human breast CAFs. We would expect that the periostin isoform with a nonfunctional EMI domain would fail to rescue invasion as it cannot engage collagen and promote its organization into aligned fibers that cancer cells invade along. These experiments would provide the essential mechanistic link that is currently missing from our studies. Additionally, if our in vitro studies indicate that the EMI domain-mediated interactions between periostin and collagen are essential to promote collective cell invasion and lymphovascular invasion, we could design a small molecule inhibitor that targets this region of the periostin protein to interfere with periostin-collagen binding in vivo and measure any effects on tumor growth, collagen matrix organization, and lymphatic metastasis. We would hypothesize that blocking the EMI domain of periostin in vivo would impair intratumoral collagen matrix organization, thereby limiting lymphovascular invasion and lymphatic metastasis.

3.2.5 Periostin^{+} cell activation and function in other tumor models

Our work reveals an early pro-metastatic role for periostin-expressing cells in breast cancer, but it is important to determine whether these findings extend to other cancer types. A meta-analysis of the prognostic value of periostin across multiple cancer types demonstrated that high periostin expression is associated with lymph node metastasis, poor overall survival, and reduced disease-free survival in a cohort of 993 patients with cancer (277), indicating that periostin-expressing cells are likely activated and play a similar pro-metastatic role in other cancers. An advantage of our *Postn*^{iZSGreen} lineage-tracing mouse model and *Postn*^{DTA} depletion model is that they can be adapted to other orthotopic tumor models in order to test whether periostin-expressing cells are activated in primary and secondary sites and function similarly in other cancer types. High-priority cancer types are pancreatic ductal adenocarcinoma (PDAC) and lung carcinoma as they are characterized by a prominent desmoplastic reaction and display high periostin expression that associates with cancer cell proliferation, invasion, and poor prognosis (277-286). Using our lineage tracing and depletion mouse models we can determine whether our finding that periostin-expressing cells promote lymphovascular invasion of breast cancer cells can be generalized to other cancer types or whether periostin-expressing CAFs perform diverse and context-specific functions across different cancers.

3.2.6 Clinical relevance of periostin

Taken together, our in vitro functional assays and in vivo depletion studies implicate periostin-expressing CAFs in collagen-mediated collective cell invasion and lymphatic metastasis, thereby positioning these cells as a potential therapeutic target. In human breast cancer samples, periostin expression is associated with desmoplastic stroma and is predictive of progressive invasive disease (121). Thus, targeting periostin^{+} cells early in the course of disease may promote the normalization of the intratumoral ECM and could prevent lymphatic metastasis of breast cancer cells. Previous attempts to develop treatments that normalize tumor ECM have shown promise in preclinical tumor models but have been largely unsuccessful in clinical trials due to off-target side effects that compromise their therapeutic value and prevent their clinical application (287, 288). For example, therapies designed to suppress tumor fibrosis and LOX-mediated collagen cross-linking are associated with severe cardiac disfunction and high toxicity in patients, precluding their clinical adoption (289, 290). These clinical challenges in targeting intratumoral collagen can be attributed to two critical limitations. First, collagen is expressed abundantly throughout the body and is essential for maintaining normal tissues, so targeting a factor whose expression is not restricted to the tumor stroma leads to widespread side effects in other organs. Secondly, when tested in clinical trials, these collagen-targeted therapies are administered to late-stage patients who already present with metastatic disease and, therefore, do not result in clinically meaningful improvement in these patients as their cancer cells have already exploited the

aberrant intratumoral ECM to disseminate and reach secondary sites. In other words, while anti-fibrotic cancer therapies may effectively prevent or reduce metastatic spread, previous clinical trials were not designed in a way that could capture any potential anti-metastatic effect.

Since periostin is less abundant in normal tissues and is upregulated in the tumor microenvironment, it could serve as a more effective and safer target for anti-cancer therapies. Pre-clinical studies have shown that targeting periostin using antibodies and nucleic acid aptamers can reduce tumor growth and metastasis in patient-derived xenografts and syngeneic breast cancer models (221, 291, 292), but periostin blockade has not yet been evaluated in human cancer patients. As evidenced by the lack of success in the previous clinical trials of ECM-normalizing therapies, an important consideration when designing clinical trials of periostin-targeted therapies will be the timing of treatment. Periostin blockade may only be useful in patients who present with localized disease that has yet to reach distant lymph nodes. Since we observe periostin^{+} cell activation within the premetastatic niche, anti-periostin treatments could be used as an early intervention aimed at interfering with formation of the premetastatic niche and therefore preventing metastasis at an earlier stage. Additionally, since periostin-expressing cells are also detected in metastatic microenvironments and have been implicated in supporting the outgrowth of disseminated cancer cells into macrometastases in the lung (72), attenuating periostin's activity before there are clinically detectable metastatic lesions may limit cancer stem cell outgrowth in secondary sites and reduce disease

recurrence. Given the observed increase in primary tumor growth rate following periostin^{+} cell depletion in our orthotopic breast cancer model and the fact that tissue injury and inflammation can drive periostin activation, blocking periostin may be most effective around the time of surgical resection of the primary tumor.

If directly blocking periostin's activity proves to be ineffective at reducing metastasis or improving outcomes in cancer patients, periostin and its abundance in primary tumors could still be leveraged in other valuable clinical applications. For example, periostin could be used in the design of antibody-drug conjugates (ADCs) that target the tumor stroma. ADCs are a class of emerging therapeutics that consist of a cytotoxic drug payload chemically linked to an antibody that is directed toward a specific target found in the tumor microenvironment in order to enhance drug delivery within tumors and reduce the off-target toxicities that characterize systemic cytotoxic therapies like chemotherapy (293). While ADCs have traditionally been designed to bind to cell surface proteins expressed by cancer cells, there is growing evidence that ADCs targeting stromal factors may be an effective alternative approach to improve intratumoral drug delivery and limit tumor growth by eliminating nearby tumor cells via bystander killing (294-296). Given that periostin is upregulated in the tumor microenvironments of diverse cancer types and displays relatively low expression in normal tissues, it is a candidate target for future ADCs. Another potential clinical application of periostin is its utility as a biomarker of advanced disease. Serum periostin level has been evaluated as a biomarker in advanced lung cancer patients and associates with poor patient prognosis. Median serum

periostin level was higher in patients with bone metastases than those with localized disease, and patients with high periostin displayed reduced overall survival (279, 280). Future clinical studies should examine whether this association between serum periostin and metastatic burden holds true in other cancer types, especially breast cancer. Given our preclinical findings, we would predict that serum periostin levels would be higher in patients who already have metastatic disease or who have localized disease but are at risk for developing metastatic disease as periostin can be activated in the premetastatic niche and in secondary sites that harbor micrometastatic cancer colonies. Thus, liquid biopsies to measure circulating periostin levels could be used to identify cancers that have a propensity to metastasize or could indicate early metastatic disease before it is detected by the traditional imaging techniques that are currently used to monitor metastatic lesions.

3.3 Conclusion and significance

Collectively, the data presented in this thesis highlight a population of cancer stromal cells, marked by their expression of the matrisomal protein periostin, that remodel the ECM within the primary tumor microenvironment and promote the collective invasion of breast cancer cells into lymphatic vessels, allowing for their metastatic dissemination and colonization of nearby lymph nodes. We have used multiple genetically-engineered mouse models to label and ablate periostin-expressing cells in order to characterize their functions during breast cancer progression. We report that periostin-expressing stromal cells are

located surrounding mammary ducts and vasculature in the tumor-naïve mammary gland and are enriched at the peripheries of lymphatic vessels. These cells are differentially activated by highly-metastatic cancer cells within primary tumors, premetastatic niches, and secondary sites of metastasis, and their increased abundance within primary tumors is associated with enhanced collagen matrix remodeling and organization. Genetically depleting periostin^{+} cells in vivo impairs intratumoral collagen organization and inhibits lymphatic metastasis of highly-metastatic breast cancer cells, and periostin ablation in primary human breast CAFs in vitro reduces their ability to deposit aligned collagen matrices and inhibits cancer cell invasion across lymphatic endothelial cell barriers. Together, these findings implicate periostin-expressing CAFs in the collagen-mediated lymphovascular invasion of breast cancer cells and suggest that this population may be a suitable target for future therapeutics with the goal of improving patient outcomes by preventing metastatic spread.

References

1. Sung H, Ferlay J, Siegel RL, Laversanne M, Soerjomataram I, Jemal A, Bray F. 2021. Global Cancer Statistics 2020: GLOBOCAN Estimates of Incidence and Mortality Worldwide for 36 Cancers in 185 Countries. CA Cancer J Clin 71:209-249.
2. Siegel RL, Miller KD, Wagle NS, Jemal A. 2023. Cancer statistics, 2023. CA: A Cancer Journal for Clinicians 73:17-48.
3. Waks AG, Winer EP. 2019. Breast Cancer Treatment: A Review. Jama 321:288-300.
4. Siegel RL, Miller KD, Fuchs HE, Jemal A. 2022. Cancer statistics, 2022. CA Cancer J Clin 72:7-33.
5. Nelson CM, Bissell MJ. 2006. Of extracellular matrix, scaffolds, and signaling: tissue architecture regulates development, homeostasis, and cancer. Annu Rev Cell Dev Biol 22:287-309.
6. Place AE, Jin Huh S, Polyak K. 2011. The microenvironment in breast cancer progression: biology and implications for treatment. Breast Cancer Research 13:227.
7. Burstein HJ, Polyak K, Wong JS, Lester SC, Kaelin CM. 2004. Ductal Carcinoma in Situ of the Breast. New England Journal of Medicine 350:1430-1441.
8. Riggio AI, Varley KE, Welm AL. The lingering mysteries of metastatic recurrence in breast cancer.
9. Chiang AC, Massagué J. 2008. Molecular Basis of Metastasis. New England Journal of Medicine 359:2814-2823.
10. Welch DR, Hurst DR. 2019. Defining the Hallmarks of Metastasis. Cancer Res 79:3011-3027.
11. Redig AJ, McAllister SS. 2013. Breast cancer as a systemic disease: a view of metastasis. J Intern Med 274:113-26.
12. Cichon MA, Degnim AC, Visscher DW, Radisky DC. 2010. Microenvironmental influences that drive progression from benign breast disease to invasive breast cancer. J Mammary Gland Biol Neoplasia 15:389-97.
13. van Dooijeweert C, van Diest PJ, Ellis IO. 2022. Grading of invasive breast carcinoma: the way forward. Virchows Archiv 480:33-43.
14. Bleiweiss IJ. 2021. Pathology of Breast Cancer. *In* (ed), UpToDate. https://www.uptodate.com/contents/pathology-of-breast-cancer/print.
15. Eliyatkın N, Yalçın E, Zengel B, Aktaş S, Vardar E. 2015. Molecular Classification of Breast Carcinoma: From Traditional, Old-Fashioned Way to A New Age, and A New Way. The journal of breast health 11:59-66.

16. Yersal O, Barutca S. 2014. Biological subtypes of breast cancer: Prognostic and therapeutic implications. World J Clin Oncol 5:412-24.
17. Carroll JS, Hickey TE, Tarulli GA, Williams M, Tilley WD. 2017. Deciphering the divergent roles of progestogens in breast cancer. Nature Reviews Cancer 17:54-64.
18. Ballaré C, Uhrig M, Bechtold T, Sancho E, Di Domenico M, Migliaccio A, Auricchio F, Beato M. 2003. Two domains of the progesterone receptor interact with the estrogen receptor and are required for progesterone activation of the c-Src/Erk pathway in mammalian cells. Mol Cell Biol 23:1994-2008.
19. Boonyaratanakornkit V, Scott MP, Ribon V, Sherman L, Anderson SM, Maller JL, Miller WT, Edwards DP. 2001. Progesterone Receptor Contains a Proline-Rich Motif that Directly Interacts with SH3 Domains and Activates c-Src Family Tyrosine Kinases. Molecular Cell 8:269-280.
20. Callahan R, Hurvitz S. 2011. Human epidermal growth factor receptor-2-positive breast cancer: Current management of early, advanced, and recurrent disease. Current opinion in obstetrics & gynecology 23:37-43.
21. Weigelt B, Mackay A, A'Hern R, Natrajan R, Tan DSP, Dowsett M, Ashworth A, Reis-Filho JS. 2010. Breast cancer molecular profiling with single sample predictors: a retrospective analysis. The Lancet Oncology 11:339-349.
22. Hart CD, Migliaccio I, Malorni L, Guarducci C, Biganzoli L, Di Leo A. 2015. Challenges in the management of advanced, ER-positive, HER2-negative breast cancer. Nature Reviews Clinical Oncology 12:541-552.
23. Perou CM, Sørlie T, Eisen MB, van de Rijn M, Jeffrey SS, Rees CA, Pollack JR, Ross DT, Johnsen H, Akslen LA, Fluge Ø, Pergamenschikov A, Williams C, Zhu SX, Lønning PE, Børresen-Dale A-L, Brown PO, Botstein D. 2000. Molecular portraits of human breast tumours. Nature 406:747-752.
24. Cejalvo JM, Martínez de Dueñas E, Galván P, García-Recio S, Burgués Gasión O, Paré L, Antolín S, Martinello R, Blancas I, Adamo B, Guerrero-Zotano Á, Muñoz M, Nucíforo P, Vidal M, Pérez RM, Chacón López-Muniz JI, Caballero R, Peg V, Carrasco E, Rojo F, Perou CM, Cortés J, Adamo V, Albanell J, Gomis RR, Lluch A, Prat A. 2017. Intrinsic Subtypes and Gene Expression Profiles in Primary and Metastatic Breast Cancer. Cancer Research 77:2213-2221.
25. Hortobagyi GN, Edge SB, Giuliano A. 2018. New and Important Changes in the TNM Staging System for Breast Cancer. American Society of Clinical Oncology Educational Book:457-467.

26. Burstein HJ. 2022. Tumor, node, metastasis (TNM) staging classification for breast cancer, UpToDate.
27. Greene FL, Sobin LH. 2008. The Staging of Cancer: A Retrospective and Prospective Appraisal. CA: A Cancer Journal for Clinicians 58:180-190.
28. Goutsouliak K, Veeraraghavan J, Sethunath V, De Angelis C, Osborne CK, Rimawi MF, Schiff R. 2020. Towards personalized treatment for early stage HER2-positive breast cancer. Nature Reviews Clinical Oncology 17:233-250.
29. Wilson FR, Coombes ME, Brezden-Masley C, Yurchenko M, Wylie Q, Douma R, Varu A, Hutton B, Skidmore B, Cameron CA-OX. Herceptin® (trastuzumab) in HER2-positive early breast cancer: a systematic review and cumulative network meta-analysis.
30. Bianchini G, De Angelis C, Licata L, Gianni L. 2022. Treatment landscape of triple-negative breast cancer — expanded options, evolving needs. Nature Reviews Clinical Oncology 19:91-113.
31. Bianchini G, Balko JM, Mayer IA, Sanders ME, Gianni L. 2016. Triple-negative breast cancer: challenges and opportunities of a heterogeneous disease. Nature Reviews Clinical Oncology 13:674-690.
32. Bareche Y, Buisseret L, Gruosso T, Girard E, Venet D, Dupont F, Desmedt C, Larsimont D, Park M, Rothé F, Stagg J, Sotiriou C. 2020. Unraveling Triple-Negative Breast Cancer Tumor Microenvironment Heterogeneity: Towards an Optimized Treatment Approach. J Natl Cancer Inst 112:708-719.
33. Dent R, Trudeau M, Pritchard KI, Hanna WM, Kahn HK, Sawka CA, Lickley LA, Rawlinson E, Sun P, Narod SA. 2007. Triple-negative breast cancer: clinical features and patterns of recurrence. Clin Cancer Res 13:4429-34.
34. Howlader N, Cronin KA, Kurian AW, Andridge R. 2018. Differences in Breast Cancer Survival by Molecular Subtypes in the United States. Cancer Epidemiology, Biomarkers & Prevention 27:619-626.
35. Aguirre-Ghiso JA. 2007. Models, mechanisms and clinical evidence for cancer dormancy. Nat Rev Cancer 7:834-46.
36. Hüsemann Y, Geigl JB, Schubert F, Musiani P, Meyer M, Burghart E, Forni G, Eils R, Fehm T, Riethmüller G, Klein CA. 2008. Systemic Spread Is an Early Step in Breast Cancer. Cancer Cell 13:58-68.
37. Chaffer CL, Weinberg RA. 2011. A Perspective on Cancer Cell Metastasis. Science 331:1559-1564.
38. Klein CA. 2009. Parallel progression of primary tumours and metastases. Nature Reviews Cancer 9:302-312.

39. Ghajar CM, Peinado H, Mori H, Matei IR, Evason KJ, Brazier H, Almeida D, Koller A, Hajjar KA, Stainier DY, Chen EI, Lyden D, Bissell MJ. 2013. The perivascular niche regulates breast tumour dormancy. Nat Cell Biol 15:807-17.
40. Sosa MS, Bragado P, Aguirre-Ghiso JA. 2014. Mechanisms of disseminated cancer cell dormancy: an awakening field. Nat Rev Cancer 14:611-22.
41. Meng S, Tripathy D, Frenkel EP, Shete S, Naftalis EZ, Huth JF, Beitsch PD, Leitch M, Hoover S, Euhus D, Haley B, Morrison L, Fleming TP, Herlyn D, Terstappen LW, Fehm T, Tucker TF, Lane N, Wang J, Uhr JW. 2004. Circulating tumor cells in patients with breast cancer dormancy. Clin Cancer Res 10:8152-62.
42. Gerratana L, Fanotto V, Bonotto M, Bolzonello S, Minisini AM, Fasola G, Puglisi F. 2015. Pattern of metastasis and outcome in patients with breast cancer. Clinical & Experimental Metastasis 32:125-133.
43. Pastushenko I, Brisebarre A, Sifrim A, Fioramonti M, Revenco T, Boumahdi S, Van Keymeulen A, Brown D, Moers V, Lemaire S, De Clercq S, Minguijón E, Balsat C, Sokolow Y, Dubois C, De Cock F, Scozzaro S, Sopena F, Lanas A, D'Haene N, Salmon I, Marine J-C, Voet T, Sotiropoulou PA, Blanpain C. 2018. Identification of the tumour transition states occurring during EMT. Nature 556:463-468.
44. Aceto N, Bardia A, Miyamoto David T, Donaldson Maria C, Wittner Ben S, Spencer Joel A, Yu M, Pely A, Engstrom A, Zhu H, Brannigan Brian W, Kapur R, Stott Shannon L, Shioda T, Ramaswamy S, Ting David T, Lin Charles P, Toner M, Haber Daniel A, Maheswaran S. 2014. Circulating Tumor Cell Clusters Are Oligoclonal Precursors of Breast Cancer Metastasis. Cell 158:1110-1122.
45. Ye X, Weinberg RA. 2015. Epithelial-Mesenchymal Plasticity: A Central Regulator of Cancer Progression. Trends Cell Biol 25:675-686.
46. Nieto MA. 2013. Epithelial Plasticity: A Common Theme in Embryonic and Cancer Cells. Science 342:1234850.
47. Cheung KJ, Ewald AJ. 2016. A collective route to metastasis: Seeding by tumor cell clusters. Science 352:167-169.
48. Yu M, Bardia A, Wittner BS, Stott SL, Smas ME, Ting DT, Isakoff SJ, Ciciliano JC, Wells MN, Shah AM, Concannon KF, Donaldson MC, Sequist LV, Brachtel E, Sgroi D, Baselga J, Ramaswamy S, Toner M, Haber DA, Maheswaran S. 2013. Circulating breast tumor cells exhibit dynamic changes in epithelial and mesenchymal composition. Science 339:580-4.

49. Wyckoff JB, Jones JG, Condeelis JS, Segall JE. 2000. A critical step in metastasis: in vivo analysis of intravasation at the primary tumor. Cancer Res 60:2504-11.
50. Reymond N, d'Água BB, Ridley AJ. 2013. Crossing the endothelial barrier during metastasis. Nat Rev Cancer 13:858-70.
51. Kienast Y, von Baumgarten L, Fuhrmann M, Klinkert WE, Goldbrunner R, Herms J, Winkler F. 2010. Real-time imaging reveals the single steps of brain metastasis formation. Nat Med 16:116-22.
52. Lambert AW, Pattabiraman DR, Weinberg RA. 2017. Emerging Biological Principles of Metastasis. Cell 168:670-691.
53. Talmadge JE, Fidler IJ. 2010. AACR centennial series: the biology of cancer metastasis: historical perspective. Cancer Res 70:5649-69.
54. Valastyan S, Weinberg Robert A. 2011. Tumor Metastasis: Molecular Insights and Evolving Paradigms. Cell 147:275-292.
55. Gupta GP, Massagué J. 2006. Cancer Metastasis: Building a Framework. Cell 127:679-695.
56. Steeg PS. 2006. Tumor metastasis: mechanistic insights and clinical challenges. Nature Medicine 12:895-904.
57. Massagué J, Obenauf AC. 2016. Metastatic colonization by circulating tumour cells. Nature 529:298-306.
58. Langley RR, Fidler IJ. 2011. The seed and soil hypothesis revisited--the role of tumor-stroma interactions in metastasis to different organs. Int J Cancer 128:2527-35.
59. Paget S. 1889. THE DISTRIBUTION OF SECONDARY GROWTHS IN CANCER OF THE BREAST. The Lancet 133:571-573.
60. Fidler IJ. 2003. The pathogenesis of cancer metastasis: the 'seed and soil' hypothesis revisited. Nature Reviews Cancer 3:453-458.
61. Zomer A, Maynard C, Verweij Frederik J, Kamermans A, Schäfer R, Beerling E, Schiffelers Raymond M, de Wit E, Berenguer J, Ellenbroek Saskia Inge J, Wurdinger T, Pegtel Dirk M, van Rheenen J. 2015. In Vivo Imaging Reveals Extracellular Vesicle-Mediated Phenocopying of Metastatic Behavior. Cell 161:1046-1057.
62. Peinado H, Zhang H, Matei IR, Costa-Silva B, Hoshino A, Rodrigues G, Psaila B, Kaplan RN, Bromberg JF, Kang Y, Bissell MJ, Cox TR, Giaccia AJ, Erler JT, Hiratsuka S, Ghajar CM, Lyden D. 2017. Pre-metastatic niches: organ-specific homes for metastases. Nature Reviews Cancer 17:302-317.
63. Psaila B, Lyden D. 2009. The metastatic niche: adapting the foreign soil, p 285-93, Nat Rev Cancer, vol 9.

64. Hiratsuka S, Nakamura K, Iwai S, Murakami M, Itoh T, Kijima H, Shipley JM, Senior RM, Shibuya M. 2002. MMP9 induction by vascular endothelial growth factor receptor-1 is involved in lung-specific metastasis. Cancer Cell 2:289-300.
65. Hiratsuka S, Watanabe A, Aburatani H, Maru Y. 2006. Tumour-mediated upregulation of chemoattractants and recruitment of myeloid cells predetermines lung metastasis. Nat Cell Biol 8:1369-75.
66. Kaplan RN, Riba RD, Zacharoulis S, Bramley AH, Vincent L, Costa C, MacDonald DD, Jin DK, Shido K, Kerns SA, Zhu Z, Hicklin D, Wu Y, Port JL, Altorki N, Port ER, Ruggero D, Shmelkov SV, Jensen KK, Rafii S, Lyden D. 2005. VEGFR1-positive haematopoietic bone marrow progenitors initiate the pre-metastatic niche. Nature 438:820-7.
67. Orimo A, Gupta PB, Sgroi DC, Arenzana-Seisdedos F, Delaunay T, Naeem R, Carey VJ, Richardson AL, Weinberg RA. 2005. Stromal Fibroblasts Present in Invasive Human Breast Carcinomas Promote Tumor Growth and Angiogenesis through Elevated SDF-1/CXCL12 Secretion. Cell 121:335-348.
68. Karnoub AE, Dash AB, Vo AP, Sullivan A, Brooks MW, Bell GW, Richardson AL, Polyak K, Tubo R, Weinberg RA. 2007. Mesenchymal stem cells within tumour stroma promote breast cancer metastasis. Nature 449:557-63.
69. Erler JT, Bennewith KL, Cox TR, Lang G, Bird D, Koong A, Le QT, Giaccia AJ. 2009. Hypoxia-induced lysyl oxidase is a critical mediator of bone marrow cell recruitment to form the premetastatic niche. Cancer Cell 15:35-44.
70. McAllister SS, Gifford AM, Greiner AL, Kelleher SP, Saelzler MP, Ince TA, Reinhardt F, Harris LN, Hylander BL, Repasky EA, Weinberg RA. 2008. Systemic endocrine instigation of indolent tumor growth requires osteopontin. Cell 133:994-1005.
71. Kaplan RN, Rafii S, Lyden D. 2006. Preparing the "soil": the premetastatic niche. Cancer Res 66:11089-93.
72. Malanchi I, Santamaria-Martínez A, Susanto E, Peng H, Lehr H-A, Delaloye J-F, Huelsken J. 2012. Interactions between cancer stem cells and their niche govern metastatic colonization. Nature 481:85-89.
73. Hanahan D, Coussens Lisa M. 2012. Accessories to the Crime: Functions of Cells Recruited to the Tumor Microenvironment. Cancer Cell 21:309-322.
74. Oskarsson T, Acharyya S, Zhang XHF, Vanharanta S, Tavazoie SF, Morris PG, Downey RJ, Manova-Todorova K, Brogi E, Massagué J. 2011.

Breast cancer cells produce tenascin C as a metastatic niche component to colonize the lungs. Nature Medicine 17:867-874.
75. DeNardo DG, Johansson M, Coussens LM. 2008. Immune cells as mediators of solid tumor metastasis. Cancer Metastasis Rev 27:11-8.
76. Joyce JA, Pollard JW. 2009. Microenvironmental regulation of metastasis. Nat Rev Cancer 9:239-52.
77. Obenauf AC, Massagué J. 2015. Surviving at a Distance: Organ-Specific Metastasis. Trends Cancer 1:76-91.
78. Kitamura T, Qian BZ, Pollard JW. 2015. Immune cell promotion of metastasis. Nat Rev Immunol 15:73-86.
79. Chatterjee A, Serniak N, Czerniecki BJ. 2015. Sentinel lymph node biopsy in breast cancer: a work in progress. Cancer J 21:7-10.
80. Maguire A, Brogi E. 2016. Sentinel Lymph Nodes for Breast Carcinoma: A Paradigm Shift. Arch Pathol Lab Med 140:791-8.
81. Carter CL, Allen C, Henson DE. 1989. Relation of tumor size, lymph node status, and survival in 24,740 breast cancer cases. Cancer 63:181-7.
82. Sleeman J, Schmid A, Thiele W. 2009. Tumor lymphatics. Semin Cancer Biol 19:285-97.
83. Pereira ER, Kedrin D, Seano G, Gautier O, Meijer EFJ, Jones D, Chin SM, Kitahara S, Bouta EM, Chang J, Beech E, Jeong HS, Carroll MC, Taghian AG, Padera TP. 2018. Lymph node metastases can invade local blood vessels, exit the node, and colonize distant organs in mice. Science 359:1403-1407.
84. Brown M, Assen FP, Leithner A, Abe J, Schachner H, Asfour G, Bago-Horvath Z, Stein JV, Uhrin P, Sixt M, Kerjaschki D. 2018. Lymph node blood vessels provide exit routes for metastatic tumor cell dissemination in mice. Science 359:1408-1411.
85. Nathanson SD, Kwon D, Kapke A, Alford SH, Chitale D. 2009. The Role of Lymph Node Metastasis in the Systemic Dissemination of Breast Cancer. Annals of Surgical Oncology 16:3396-3405.
86. Ubellacker JM, Tasdogan A, Ramesh V, Shen B, Mitchell EC, Martin-Sandoval MS, Gu Z, McCormick ML, Durham AB, Spitz DR, Zhao Z, Mathews TP, Morrison SJ. 2020. Lymph protects metastasizing melanoma cells from ferroptosis. Nature 585:113-118.
87. Reticker-Flynn NE, Zhang W, Belk JA, Basto PA, Escalante NK, Pilarowski GOW, Bejnood A, Martins MM, Kenkel JA, Linde IL, Bagchi S, Yuan R, Chang S, Spitzer MH, Carmi Y, Cheng J, Tolentino LL, Choi O, Wu N, Kong CS, Gentles AJ, Sunwoo JB, Satpathy AT, Plevritis SK, Engleman EG. 2022. Lymph node colonization induces tumor-immune tolerance to promote distant metastasis. Cell 185:1924-1942.e23.

88. Mohammed RAA, Martin SG, Gill MS, Green AR, Paish EC, Ellis IO. 2007. Improved Methods of Detection of Lymphovascular Invasion Demonstrate That It is the Predominant Method of Vascular Invasion in Breast Cancer and has Important Clinical Consequences. The American Journal of Surgical Pathology 31.
89. Houvenaeghel G, Cohen M, Classe JM, Reyal F, Mazouni C, Chopin N, Martinez A, Daraï E, Coutant C, Colombo PE, Gimbergues P, Chauvet MP, Azuar AS, Rouzier R, Tunon de Lara C, Muracciole X, Agostini A, Bannier M, Charaffe Jauffret E, De Nonneville A, Goncalves A. 2021. Lymphovascular invasion has a significant prognostic impact in patients with early breast cancer, results from a large, national, multicenter, retrospective cohort study. ESMO Open 6.
90. Rakha EA, Martin S, Lee AH, Morgan D, Pharoah PD, Hodi Z, Macmillan D, Ellis IO. 2012. The prognostic significance of lymphovascular invasion in invasive breast carcinoma. Cancer 118:3670-80.
91. Sabatier R, Jacquemier J, Bertucci F, Esterni B, Finetti P, Azario F, Birnbaum D, Viens P, Gonçalves A, Extra J-M. 2011. Peritumoural vascular invasion: A major determinant of triple-negative breast cancer outcome. European Journal of Cancer 47:1537-1545.
92. Pepper MS, Skobe M. 2003. Lymphatic endothelium: morphological, molecular and functional properties. J Cell Biol 163:209-13.
93. Podgrabinska S, Braun P, Velasco P, Kloos B, Pepper MS, Jackson DG, Skobe M. 2002. Molecular characterization of lymphatic endothelial cells. Proceedings of the National Academy of Sciences 99:16069-16074.
94. Alitalo K. 2011. The lymphatic vasculature in disease. Nature Medicine 17:1371-1380.
95. Stacker SA, Williams SP, Karnezis T, Shayan R, Fox SB, Achen MG. 2014. Lymphangiogenesis and lymphatic vessel remodelling in cancer. Nature Reviews Cancer 14:159-172.
96. Zhang F, Zarkada G, Yi S, Eichmann A. 2020. Lymphatic Endothelial Cell Junctions: Molecular Regulation in Physiology and Diseases. Front Physiol 11:509.
97. Padera TP, Stoll BR, Tooredman JB, Capen D, di Tomaso E, Jain RK. 2004. Pathology: cancer cells compress intratumour vessels. Nature 427:695.
98. Baluk P, Fuxe J, Hashizume H, Romano T, Lashnits E, Butz S, Vestweber D, Corada M, Molendini C, Dejana E, McDonald DM. 2007. Functionally specialized junctions between endothelial cells of lymphatic vessels. J Exp Med 204:2349-62.

99. Aleskandarany MA, Sonbul SN, Mukherjee A, Rakha EA. 2015. Molecular Mechanisms Underlying Lymphovascular Invasion in Invasive Breast Cancer. Pathobiology 82:113-123.
100. Christiansen A, Detmar M. 2011. Lymphangiogenesis and cancer. Genes Cancer 2:1146-58.
101. Issa A, Le TX, Shoushtari AN, Shields JD, Swartz MA. 2009. Vascular endothelial growth factor-C and C-C chemokine receptor 7 in tumor cell-lymphatic cross-talk promote invasive phenotype. Cancer Res 69:349-57.
102. Shields JD, Fleury ME, Yong C, Tomei AA, Randolph GJ, Swartz MA. 2007. Autologous chemotaxis as a mechanism of tumor cell homing to lymphatics via interstitial flow and autocrine CCR7 signaling. Cancer Cell 11:526-38.
103. Alitalo A, Detmar M. 2012. Interaction of tumor cells and lymphatic vessels in cancer progression. Oncogene 31:4499-508.
104. Kariri YA, Aleskandarany MA, Joseph C, Kurozumi S, Mohammed OJ, Toss MS, Green AR, Rakha EA. 2020. Molecular Complexity of Lymphovascular Invasion: The Role of Cell Migration in Breast Cancer as a Prototype. Pathobiology 87:218-231.
105. Ran S, Volk L, Hall K, Flister MJ. 2010. Lymphangiogenesis and lymphatic metastasis in breast cancer. Pathophysiology 17:229-51.
106. Farnsworth RH, Achen MG, Stacker SA. 2006. Lymphatic endothelium: an important interactive surface for malignant cells. Pulm Pharmacol Ther 19:51-60.
107. Wong SY, Hynes RO. 2006. Lymphatic or hematogenous dissemination: how does a metastatic tumor cell decide? Cell Cycle 5:812-7.
108. Junttila MR, de Sauvage FJ. 2013. Influence of tumour micro-environment heterogeneity on therapeutic response. Nature 501:346-354.
109. Allinen M, Beroukhim R, Cai L, Brennan C, Lahti-Domenici J, Huang H, Porter D, Hu M, Chin L, Richardson A, Schnitt S, Sellers WR, Polyak K. 2004. Molecular characterization of the tumor microenvironment in breast cancer. Cancer Cell 6:17-32.
110. Wagner J, Rapsomaniki MA, Chevrier S, Anzeneder T, Langwieder C, Dykgers A, Rees M, Ramaswamy A, Muenst S, Soysal SD, Jacobs A, Windhager J, Silina K, van den Broek M, Dedes KJ, Rodríguez Martínez M, Weber WP, Bodenmiller B. 2019. A Single-Cell Atlas of the Tumor and Immune Ecosystem of Human Breast Cancer. Cell 177:1330-1345.e18.
111. McAllister SS, Weinberg RA. 2010. Tumor-Host Interactions: A Far-Reaching Relationship. Journal of Clinical Oncology 28:4022-4028.
112. Keren L, Bosse M, Marquez D, Angoshtari R, Jain S, Varma S, Yang S-R, Kurian A, Van Valen D, West R, Bendall SC, Angelo M. 2018. A

Structured Tumor-Immune Microenvironment in Triple Negative Breast Cancer Revealed by Multiplexed Ion Beam Imaging. Cell 174:1373-1387.e19.
113. Jackson HW, Fischer JR, Zanotelli VRT, Ali HR, Mechera R, Soysal SD, Moch H, Muenst S, Varga Z, Weber WP, Bodenmiller B. 2020. The single-cell pathology landscape of breast cancer. Nature 578:615-620.
114. Bourgot I, Primac I, Louis T, Noël A, Maquoi E. 2020. Reciprocal Interplay Between Fibrillar Collagens and Collagen-Binding Integrins: Implications in Cancer Progression and Metastasis. Frontiers in Oncology 10.
115. Cox TR. 2021. The matrix in cancer. Nature Reviews Cancer 21:217-238.
116. Cox TR, Bird D, Baker AM, Barker HE, Ho MW, Lang G, Erler JT. 2013. LOX-mediated collagen crosslinking is responsible for fibrosis-enhanced metastasis. Cancer Res 73:1721-32.
117. Winkler J, Abisoye-Ogunniyan A, Metcalf KJ, Werb Z. 2020. Concepts of extracellular matrix remodelling in tumour progression and metastasis. Nature Communications 11:5120.
118. Dumont N, Liu B, Defilippis RA, Chang H, Rabban JT, Karnezis AN, Tjoe JA, Marx J, Parvin B, Tlsty TD. 2013. Breast fibroblasts modulate early dissemination, tumorigenesis, and metastasis through alteration of extracellular matrix characteristics. Neoplasia 15:249-62.
119. Wang W, Wyckoff JB, Frohlich VC, Oleynikov Y, Hüttelmaier S, Zavadil J, Cermak L, Bottinger EP, Singer RH, White JG, Segall JE, Condeelis JS. 2002. Single cell behavior in metastatic primary mammary tumors correlated with gene expression patterns revealed by molecular profiling. Cancer Res 62:6278-88.
120. Friedman G, Levi-Galibov O, David E, Bornstein C, Giladi A, Dadiani M, Mayo A, Halperin C, Pevsner-Fischer M, Lavon H, Mayer S, Nevo R, Stein Y, Balint-Lahat N, Barshack I, Ali HR, Caldas C, Nili-Gal-Yam E, Alon U, Amit I, Scherz-Shouval R. 2020. Cancer-associated fibroblast compositions change with breast cancer progression linking the ratio of S100A4+ and PDPN+ CAFs to clinical outcome. Nature Cancer 1:692-708.
121. Risom T, Glass DR, Averbukh I, Liu CC, Baranski A, Kagel A, McCaffrey EF, Greenwald NF, Rivero-Gutiérrez B, Strand SH, Varma S, Kong A, Keren L, Srivastava S, Zhu C, Khair Z, Veis DJ, Deschryver K, Vennam S, Maley C, Hwang ES, Marks JR, Bendall SC, Colditz GA, West RB, Angelo M. 2022. Transition to invasive breast cancer is associated with progressive changes in the structure and composition of tumor stroma. Cell 185:299-310.e18.

122. Provenzano PP, Eliceiri KW, Campbell JM, Inman DR, White JG, Keely PJ. 2006. Collagen reorganization at the tumor-stromal interface facilitates local invasion. BMC Medicine 4:38.
123. Sun X, Wu B, Chiang H-C, Deng H, Zhang X, Xiong W, Liu J, Rozeboom AM, Harris BT, Blommaert E, Gomez A, Garcia RE, Zhou Y, Mitra P, Prevost M, Zhang D, Banik D, Isaacs C, Berry D, Lai C, Chaldekas K, Latham PS, Brantner CA, Popratiloff A, Jin VX, Zhang N, Hu Y, Pujana MA, Curiel TJ, An Z, Li R. 2021. Tumour DDR1 promotes collagen fibre alignment to instigate immune exclusion. Nature 599:673-678.
124. Wu SZ, Roden DL, Wang C, Holliday H, Harvey K, Cazet AS, Murphy KJ, Pereira B, Al-Eryani G, Bartonicek N, Hou R, Torpy JR, Junankar S, Chan C-L, Lam CE, Hui MN, Gluch L, Beith J, Parker A, Robbins E, Segara D, Mak C, Cooper C, Warrier S, Forrest A, Powell J, O'Toole S, Cox TR, Timpson P, Lim E, Liu XS, Swarbrick A. 2020. Stromal cell diversity associated with immune evasion in human triple-negative breast cancer. The EMBO Journal 39:e104063.
125. Erdogan B, Ao M, White LM, Means AL, Brewer BM, Yang L, Washington MK, Shi C, Franco OE, Weaver AM, Hayward SW, Li D, Webb DJ. 2017. Cancer-associated fibroblasts promote directional cancer cell migration by aligning fibronectin. J Cell Biol 216:3799-3816.
126. Labernadie A, Kato T, Brugués A, Serra-Picamal X, Derzsi S, Arwert E, Weston A, González-Tarragó V, Elosegui-Artola A, Albertazzi L, Alcaraz J, Roca-Cusachs P, Sahai E, Trepat X. 2017. A mechanically active heterotypic E-cadherin/N-cadherin adhesion enables fibroblasts to drive cancer cell invasion. Nature Cell Biology 19:224-237.
127. Levental KR, Yu H, Kass L, Lakins JN, Egeblad M, Erler JT, Fong SF, Csiszar K, Giaccia A, Weninger W, Yamauchi M, Gasser DL, Weaver VM. 2009. Matrix crosslinking forces tumor progression by enhancing integrin signaling. Cell 139:891-906.
128. Danenberg E, Bardwell H, Zanotelli VRT, Provenzano E, Chin S-F, Rueda OM, Green A, Rakha E, Aparicio S, Ellis IO, Bodenmiller B, Caldas C, Ali HR. 2022. Breast tumor microenvironment structures are associated with genomic features and clinical outcome. Nature Genetics 54:660-669.
129. Soysal SD, Tzankov A, Muenst SE. 2015. Role of the Tumor Microenvironment in Breast Cancer. Pathobiology 82:142-52.
130. Schoppmann SF, Birner P, Stöckl J, Kalt R, Ullrich R, Caucig C, Kriehuber E, Nagy K, Alitalo K, Kerjaschki D. 2002. Tumor-associated macrophages express lymphatic endothelial growth factors and are related to peritumoral lymphangiogenesis. Am J Pathol 161:947-56.

131. Kerjaschki D. 2005. The crucial role of macrophages in lymphangiogenesis. J Clin Invest 115:2316-9.
132. Egeblad M, Nakasone ES, Werb Z. 2010. Tumors as Organs: Complex Tissues that Interface with the Entire Organism. Developmental Cell 18:884-901.
133. Quail DF, Joyce JA. 2013. Microenvironmental regulation of tumor progression and metastasis. Nat Med 19:1423-37.
134. Direkze NC, Hodivala-Dilke K, Jeffery R, Hunt T, Poulsom R, Oukrif D, Alison MR, Wright NA. 2004. Bone marrow contribution to tumor-associated myofibroblasts and fibroblasts. Cancer Res 64:8492-5.
135. LeBleu VS, Kalluri R. 2018. A peek into cancer-associated fibroblasts: origins, functions and translational impact. Disease Models & Mechanisms 11.
136. Xue M, Jackson CJ. 2015. Extracellular Matrix Reorganization During Wound Healing and Its Impact on Abnormal Scarring. Adv Wound Care (New Rochelle) 4:119-136.
137. Shoulders MD, Raines RT. 2009. Collagen structure and stability. Annu Rev Biochem 78:929-58.
138. DeLeon-Pennell KY, Barker TH, Lindsey ML. 2020. Fibroblasts: The arbiters of extracellular matrix remodeling. Matrix Biology 91-92:1-7.
139. Lu P, Weaver VM, Werb Z. 2012. The extracellular matrix: a dynamic niche in cancer progression. J Cell Biol 196:395-406.
140. Kalluri R. 2016. The biology and function of fibroblasts in cancer. Nature Reviews Cancer 16:582-598.
141. Dvorak HF. 1986. Tumors: Wounds That Do Not Heal. New England Journal of Medicine 315:1650-1659.
142. Deyell M, Garris CS, Laughney AM. 2021. Cancer metastasis as a non-healing wound. British Journal of Cancer 124:1491-1502.
143. Hanahan D, Weinberg Robert A. 2011. Hallmarks of Cancer: The Next Generation. Cell 144:646-674.
144. Pickup MW, Mouw JK, Weaver VM. 2014. The extracellular matrix modulates the hallmarks of cancer. EMBO Rep 15:1243-53.
145. Lopez JI, Kang I, You WK, McDonald DM, Weaver VM. 2011. In situ force mapping of mammary gland transformation. Integr Biol (Camb) 3:910-21.
146. Bhowmick NA, Neilson EG, Moses HL. 2004. Stromal fibroblasts in cancer initiation and progression. Nature 432:332-337.
147. Egeblad M, Rasch MG, Weaver VM. 2010. Dynamic interplay between the collagen scaffold and tumor evolution. Curr Opin Cell Biol 22:697-706.

148. Poltavets V, Kochetkova M, Pitson SM, Samuel MS. 2018. The Role of the Extracellular Matrix and Its Molecular and Cellular Regulators in Cancer Cell Plasticity. Front Oncol 8:431.
149. Miles FL, Sikes RA. 2014. Insidious Changes in Stromal Matrix Fuel Cancer Progression. Molecular Cancer Research 12:297-312.
150. Erdogan B, Webb DJ. 2017. Cancer-associated fibroblasts modulate growth factor signaling and extracellular matrix remodeling to regulate tumor metastasis. Biochem Soc Trans 45:229-236.
151. Brassart-Pasco S, Brézillon S, Brassart B, Ramont L, Oudart JB, Monboisse JC. 2020. Tumor Microenvironment: Extracellular Matrix Alterations Influence Tumor Progression. Front Oncol 10:397.
152. Gaggioli C, Hooper S, Hidalgo-Carcedo C, Grosse R, Marshall JF, Harrington K, Sahai E. 2007. Fibroblast-led collective invasion of carcinoma cells with differing roles for RhoGTPases in leading and following cells. Nature Cell Biology 9:1392-1400.
153. Condeelis J, Segall JE. 2003. Intravital imaging of cell movement in tumours. Nature Reviews Cancer 3:921-930.
154. Han W, Chen S, Yuan W, Fan Q, Tian J, Wang X, Chen L, Zhang X, Wei W, Liu R, Qu J, Jiao Y, Austin RH, Liu L. 2016. Oriented collagen fibers direct tumor cell intravasation. Proceedings of the National Academy of Sciences 113:11208-11213.
155. Conklin MW, Eickhoff JC, Riching KM, Pehlke CA, Eliceiri KW, Provenzano PP, Friedl A, Keely PJ. 2011. Aligned collagen is a prognostic signature for survival in human breast carcinoma. Am J Pathol 178:1221-32.
156. Rhim AD, Oberstein PE, Thomas DH, Mirek ET, Palermo CF, Sastra SA, Dekleva EN, Saunders T, Becerra CP, Tattersall IW, Westphalen CB, Kitajewski J, Fernandez-Barrena MG, Fernandez-Zapico ME, Iacobuzio-Donahue C, Olive KP, Stanger BZ. 2014. Stromal elements act to restrain, rather than support, pancreatic ductal adenocarcinoma. Cancer Cell 25:735-47.
157. Özdemir BC, Pentcheva-Hoang T, Carstens JL, Zheng X, Wu CC, Simpson TR, Laklai H, Sugimoto H, Kahlert C, Novitskiy SV, De Jesus-Acosta A, Sharma P, Heidari P, Mahmood U, Chin L, Moses HL, Weaver VM, Maitra A, Allison JP, LeBleu VS, Kalluri R. 2014. Depletion of carcinoma-associated fibroblasts and fibrosis induces immunosuppression and accelerates pancreas cancer with reduced survival. Cancer Cell 25:719-34.
158. Lambrechts D, Wauters E, Boeckx B, Aibar S, Nittner D, Burton O, Bassez A, Decaluwé H, Pircher A, Van den Eynde K, Weynand B, Verbeken E, De

Leyn P, Liston A, Vansteenkiste J, Carmeliet P, Aerts S, Thienpont B. 2018. Phenotype molding of stromal cells in the lung tumor microenvironment. Nat Med 24:1277-1289.

159. Chen S, Zhu G, Yang Y, Wang F, Xiao Y-T, Zhang N, Bian X, Zhu Y, Yu Y, Liu F, Dong K, Mariscal J, Liu Y, Soares F, Loo Yau H, Zhang B, Chen W, Wang C, Chen D, Guo Q, Yi Z, Liu M, Fraser M, De Carvalho DD, Boutros PC, Di Vizio D, Jiang Z, van der Kwast T, Berlin A, Wu S, Wang J, He HH, Ren S. 2021. Single-cell analysis reveals transcriptomic remodellings in distinct cell types that contribute to human prostate cancer progression. Nature Cell Biology 23:87-98.
160. Puram SV, Tirosh I, Parikh AS, Patel AP, Yizhak K, Gillespie S, Rodman C, Luo CL, Mroz EA, Emerick KS, Deschler DG, Varvares MA, Mylvaganam R, Rozenblatt-Rosen O, Rocco JW, Faquin WC, Lin DT, Regev A, Bernstein BE. 2017. Single-Cell Transcriptomic Analysis of Primary and Metastatic Tumor Ecosystems in Head and Neck Cancer. Cell 171:1611-1624.e24.
161. Davidson S, Efremova M, Riedel A, Mahata B, Pramanik J, Huuhtanen J, Kar G, Vento-Tormo R, Hagai T, Chen X, Haniffa MA, Shields JD, Teichmann SA. 2020. Single-Cell RNA Sequencing Reveals a Dynamic Stromal Niche That Supports Tumor Growth. Cell Reports 31:107628.
162. Wu SZ, Al-Eryani G, Roden DL, Junankar S, Harvey K, Andersson A, Thennavan A, Wang C, Torpy JR, Bartonicek N, Wang T, Larsson L, Kaczorowski D, Weisenfeld NI, Uytingco CR, Chew JG, Bent ZW, Chan C-L, Gnanasambandapillai V, Dutertre C-A, Gluch L, Hui MN, Beith J, Parker A, Robbins E, Segara D, Cooper C, Mak C, Chan B, Warrier S, Ginhoux F, Millar E, Powell JE, Williams SR, Liu XS, O'Toole S, Lim E, Lundeberg J, Perou CM, Swarbrick A. 2021. A single-cell and spatially resolved atlas of human breast cancers. Nature Genetics 53:1334-1347.
163. Bartoschek M, Oskolkov N, Bocci M, Lövrot J, Larsson C, Sommarin M, Madsen CD, Lindgren D, Pekar G, Karlsson G, Ringnér M, Bergh J, Björklund Å, Pietras K. 2018. Spatially and functionally distinct subclasses of breast cancer-associated fibroblasts revealed by single cell RNA sequencing. Nature Communications 9:5150.
164. Bernard V, Semaan A, Huang J, San Lucas FA, Mulu FC, Stephens BM, Guerrero PA, Huang Y, Zhao J, Kamyabi N, Sen S, Scheet PA, Taniguchi CM, Kim MP, Tzeng CW, Katz MH, Singhi AD, Maitra A, Alvarez HA. 2019. Single-Cell Transcriptomics of Pancreatic Cancer Precursors Demonstrates Epithelial and Microenvironmental Heterogeneity as an Early Event in Neoplastic Progression. Clin Cancer Res 25:2194-2205.

165. Biffi G, Oni TE, Spielman B, Hao Y, Elyada E, Park Y, Preall J, Tuveson DA. 2019. IL1-Induced JAK/STAT Signaling Is Antagonized by TGFβ to Shape CAF Heterogeneity in Pancreatic Ductal Adenocarcinoma. Cancer Discov 9:282-301.
166. Helms EJ, Berry MW, Chaw RC, DuFort CC, Sun D, Onate MK, Oon C, Bhattacharyya S, Sanford-Crane H, Horton W, Finan JM, Sattler A, Makar R, Dawson DW, Xia Z, Hingorani SR, Sherman MH. 2021. Mesenchymal Lineage Heterogeneity Underlies Non-Redundant Functions of Pancreatic Cancer-Associated Fibroblasts. Cancer Discovery:candisc.0601.2021.
167. Brechbuhl HM, Finlay-Schultz J, Yamamoto TM, Gillen AE, Cittelly DM, Tan AC, Sams SB, Pillai MM, Elias AD, Robinson WA, Sartorius CA, Kabos P. 2017. Fibroblast Subtypes Regulate Responsiveness of Luminal Breast Cancer to Estrogen. Clin Cancer Res 23:1710-1721.
168. Takeshita S, Kikuno R, Tezuka K, Amann E. 1993. Osteoblast-specific factor 2: cloning of a putative bone adhesion protein with homology with the insect protein fasciclin I. Biochem J 294 (Pt 1):271-8.
169. Horiuchi K, Amizuka N, Takeshita S, Takamatsu H, Katsuura M, Ozawa H, Toyama Y, Bonewald LF, Kudo A. 1999. Identification and characterization of a novel protein, periostin, with restricted expression to periosteum and periodontal ligament and increased expression by transforming growth factor beta. J Bone Miner Res 14:1239-49.
170. Dorafshan S, Razmi M, Safaei S, Gentilin E, Madjd Z, Ghods R. 2022. Periostin: biology and function in cancer. Cancer Cell Int 22:315.
171. Murota H, Lingli Y, Katayama I. 2017. Periostin in the pathogenesis of skin diseases. Cell Mol Life Sci 74:4321-4328.
172. Sonnenberg-Riethmacher E, Miehe M, Riethmacher D. 2021. Periostin in Allergy and Inflammation. Front Immunol 12:722170.
173. Kudo A. 2017. Introductory review: periostin-gene and protein structure. Cell Mol Life Sci 74:4259-4268.
174. Maruhashi T, Kii I, Saito M, Kudo A. 2010. Interaction between periostin and BMP-1 promotes proteolytic activation of lysyl oxidase. J Biol Chem 285:13294-303.
175. Kii I, Ito H. 2017. Periostin and its interacting proteins in the construction of extracellular architectures. Cell Mol Life Sci 74:4269-4277.
176. Kii I, Nishiyama T, Li M, Matsumoto K, Saito M, Amizuka N, Kudo A. 2010. Incorporation of tenascin-C into the extracellular matrix by periostin underlies an extracellular meshwork architecture. J Biol Chem 285:2028-39.
177. Norris RA, Damon B, Mironov V, Kasyanov V, Ramamurthi A, Moreno-Rodriguez R, Trusk T, Potts JD, Goodwin RL, Davis J, Hoffman S, Wen X,

Sugi Y, Kern CB, Mjaatvedt CH, Turner DK, Oka T, Conway SJ, Molkentin JD, Forgacs G, Markwald RR. 2007. Periostin regulates collagen fibrillogenesis and the biomechanical properties of connective tissues. J Cell Biochem 101:695-711.

178. Kii I. 2019. Periostin Functions as a Scaffold for Assembly of Extracellular Proteins. Adv Exp Med Biol 1132:23-32.
179. Qin X, Yan M, Zhang J, Wang X, Shen Z, Lv Z, Li Z, Wei W, Chen W. 2016. TGFβ3-mediated induction of Periostin facilitates head and neck cancer growth and is associated with metastasis. Sci Rep 6:20587.
180. Shriver Z, Capila I, Venkataraman G, Sasisekharan R. 2012. Heparin and heparan sulfate: analyzing structure and microheterogeneity. Handb Exp Pharmacol:159-76.
181. Hamilton DW. 2008. Functional role of periostin in development and wound repair: implications for connective tissue disease. J Cell Commun Signal 2:9-17.
182. Jackson-Boeters L, Wen W, Hamilton DW. 2009. Periostin localizes to cells in normal skin, but is associated with the extracellular matrix during wound repair. J Cell Commun Signal 3:125-33.
183. Zhou HM, Wang J, Elliott C, Wen W, Hamilton DW, Conway SJ. 2010. Spatiotemporal expression of periostin during skin development and incisional wound healing: lessons for human fibrotic scar formation. J Cell Commun Signal 4:99-107.
184. Conway SJ, Izuhara K, Kudo Y, Litvin J, Markwald R, Ouyang G, Arron JR, Holweg CT, Kudo A. 2014. The role of periostin in tissue remodeling across health and disease. Cell Mol Life Sci 71:1279-88.
185. Ontsuka K, Kotobuki Y, Shiraishi H, Serada S, Ohta S, Tanemura A, Yang L, Fujimoto M, Arima K, Suzuki S, Murota H, Toda S, Kudo A, Conway SJ, Narisawa Y, Katayama I, Izuhara K, Naka T. 2012. Periostin, a matricellular protein, accelerates cutaneous wound repair by activating dermal fibroblasts. Exp Dermatol 21:331-6.
186. Nakama T, Yoshida S, Ishikawa K, Kobayashi Y, Abe T, Kiyonari H, Shioi G, Katsuragi N, Ishibashi T, Morishita R, Taniyama Y. 2016. Different roles played by periostin splice variants in retinal neovascularization. Exp Eye Res 153:133-140.
187. Hoersch S, Andrade-Navarro MA. 2010. Periostin shows increased evolutionary plasticity in its alternatively spliced region. BMC Evol Biol 10:30.
188. Kim CJ, Isono T, Tambe Y, Chano T, Okabe H, Okada Y, Inoue H. 2008. Role of alternative splicing of periostin in human bladder carcinogenesis. Int J Oncol 32:161-9.

189. Shimamura M, Taniyama Y, Katsuragi N, Koibuchi N, Kyutoku M, Sato N, Allahtavakoli M, Wakayama K, Nakagami H, Morishita R. 2012. Role of Central Nervous System Periostin in Cerebral Ischemia. Stroke 43:1108-1114.
190. Morra L, Rechsteiner M, Casagrande S, Duc Luu V, Santimaria R, Diener PA, Sulser T, Kristiansen G, Schraml P, Moch H, Soltermann A. 2011. Relevance of periostin splice variants in renal cell carcinoma. Am J Pathol 179:1513-21.
191. Morra L, Rechsteiner M, Casagrande S, von Teichman A, Schraml P, Moch H, Soltermann A. 2012. Characterization of periostin isoform pattern in non-small cell lung cancer. Lung Cancer 76:183-90.
192. Ikeda-Iwabu Y, Taniyama Y, Katsuragi N, Sanada F, Koibuchi N, Shibata K, Shimazu K, Rakugi H, Morishita R. 2021. Periostin Short Fragment with Exon 17 via Aberrant Alternative Splicing Is Required for Breast Cancer Growth and Metastasis. Cells 10.
193. Sidhu SS, Yuan S, Innes AL, Kerr S, Woodruff PG, Hou L, Muller SJ, Fahy JV. 2010. Roles of epithelial cell-derived periostin in TGF-beta activation, collagen production, and collagen gel elasticity in asthma. Proc Natl Acad Sci U S A 107:14170-5.
194. Yuyama N, Davies DE, Akaiwa M, Matsui K, Hamasaki Y, Suminami Y, Yoshida NL, Maeda M, Pandit A, Lordan JL, Kamogawa Y, Arima K, Nagumo F, Sugimachi M, Berger A, Richards I, Roberds SL, Yamashita T, Kishi F, Kato H, Arai K, Ohshima K, Tadano J, Hamasaki N, Miyatake S, Sugita Y, Holgate ST, Izuhara K. 2002. Analysis of novel disease-related genes in bronchial asthma. Cytokine 19:287-96.
195. Izuhara K, Nunomura S, Nanri Y, Ono J, Takai M, Kawaguchi A. 2019. Periostin: An emerging biomarker for allergic diseases. Allergy 74:2116-2128.
196. O'Dwyer DN, Moore BB. 2017. The role of periostin in lung fibrosis and airway remodeling. Cell Mol Life Sci 74:4305-4314.
197. Naik PK, Bozyk PD, Bentley JK, Popova AP, Birch CM, Wilke CA, Fry CD, White ES, Sisson TH, Tayob N, Carnemolla B, Orecchia P, Flaherty KR, Hershenson MB, Murray S, Martinez FJ, Moore BB. 2012. Periostin promotes fibrosis and predicts progression in patients with idiopathic pulmonary fibrosis. Am J Physiol Lung Cell Mol Physiol 303:L1046-56.
198. Ohta S, Okamoto M, Fujimoto K, Sakamoto N, Takahashi K, Yamamoto H, Kushima H, Ishii H, Akasaka K, Ono J, Kamei A, Azuma Y, Matsumoto H, Yamaguchi Y, Aihara M, Johkoh T, Kawaguchi A, Ichiki M, Sagara H, Kadota JI, Hanaoka M, Hayashi SI, Kohno S, Hoshino T, Izuhara K. 2017.

The usefulness of monomeric periostin as a biomarker for idiopathic pulmonary fibrosis. PLoS One 12:e0174547.
199. Yang L, Serada S, Fujimoto M, Terao M, Kotobuki Y, Kitaba S, Matsui S, Kudo A, Naka T, Murota H, Katayama I. 2012. Periostin facilitates skin sclerosis via PI3K/Akt dependent mechanism in a mouse model of scleroderma. PLoS One 7:e41994.
200. Makino K, Makino T, Stawski L, Mantero JC, Lafyatis R, Simms R, Trojanowska M. 2017. Blockade of PDGF Receptors by Crenolanib Has Therapeutic Effect in Patient Fibroblasts and in Preclinical Models of Systemic Sclerosis. J Invest Dermatol 137:1671-1681.
201. Turczyn A, Pańczyk-Tomaszewska M. 2021. The role of periostin in kidney diseases. Cent Eur J Immunol 46:494-501.
202. Wallace DP. 2019. Periostin in the Kidney. Adv Exp Med Biol 1132:99-112.
203. Guerrot D, Dussaule JC, Mael-Ainin M, Xu-Dubois YC, Rondeau E, Chatziantoniou C, Placier S. 2012. Identification of periostin as a critical marker of progression/reversal of hypertensive nephropathy. PLoS One 7:e31974.
204. Satirapoj B, Tassanasorn S, Charoenpitakchai M, Supasyndh O. 2015. Periostin as a tissue and urinary biomarker of renal injury in type 2 diabetes mellitus. PLoS One 10:e0124055.
205. Hixson JE, Shimmin LC, Montasser ME, Kim DK, Zhong Y, Ibarguen H, Follis J, Malcom G, Strong J, Howard T, Langefeld C, Liu Y, Rotter JI, Johnson C, Herrington D. 2011. Common variants in the periostin gene influence development of atherosclerosis in young persons. Arterioscler Thromb Vasc Biol 31:1661-7.
206. Hakuno D, Kimura N, Yoshioka M, Mukai M, Kimura T, Okada Y, Yozu R, Shukunami C, Hiraki Y, Kudo A, Ogawa S, Fukuda K. 2010. Periostin advances atherosclerotic and rheumatic cardiac valve degeneration by inducing angiogenesis and MMP production in humans and rodents. J Clin Invest 120:2292-306.
207. Soikkeli J, Podlasz P, Yin M, Nummela P, Jahkola T, Virolainen S, Krogerus L, Heikkilä P, von Smitten K, Saksela O, Hölttä E. 2010. Metastatic outgrowth encompasses COL-I, FN1, and POSTN up-regulation and assembly to fibrillar networks regulating cell adhesion, migration, and growth. Am J Pathol 177:387-403.
208. Wang Z, Xiong S, Mao Y, Chen M, Ma X, Zhou X, Ma Z, Liu F, Huang Z, Luo Q, Ouyang G. 2016. Periostin promotes immunosuppressive premetastatic niche formation to facilitate breast tumour metastasis. J Pathol 239:484-95.

209. Siriwardena BS, Kudo Y, Ogawa I, Kitagawa M, Kitajima S, Hatano H, Tilakaratne WM, Miyauchi M, Takata T. 2006. Periostin is frequently overexpressed and enhances invasion and angiogenesis in oral cancer. Br J Cancer 95:1396-403.
210. Ruan K, Bao S, Ouyang G. 2009. The multifaceted role of periostin in tumorigenesis. Cell Mol Life Sci 66:2219-30.
211. Kudo Y, Ogawa I, Kitajima S, Kitagawa M, Kawai H, Gaffney PM, Miyauchi M, Takata T. 2006. Periostin promotes invasion and anchorage-independent growth in the metastatic process of head and neck cancer. Cancer Res 66:6928-35.
212. Erkan M, Kleeff J, Gorbachevski A, Reiser C, Mitkus T, Esposito I, Giese T, Büchler MW, Giese NA, Friess H. 2007. Periostin creates a tumor-supportive microenvironment in the pancreas by sustaining fibrogenic stellate cell activity. Gastroenterology 132:1447-64.
213. Zhou W, Ke SQ, Huang Z, Flavahan W, Fang X, Paul J, Wu L, Sloan AE, McLendon RE, Li X, Rich JN, Bao S. 2015. Periostin secreted by glioblastoma stem cells recruits M2 tumour-associated macrophages and promotes malignant growth. Nature Cell Biology 17:170-182.
214. Wu G, Wang X, Zhang X. 2013. Clinical implications of periostin in the liver metastasis of colorectal cancer. Cancer Biother Radiopharm 28:298-302.
215. Tilman G, Mattiussi M, Brasseur F, van Baren N, Decottignies A. 2007. Human periostin gene expression in normal tissues, tumors and melanoma: evidences for periostin production by both stromal and melanoma cells. Mol Cancer 6:80.
216. Ratajczak-Wielgomas K, Grzegrzolka J, Piotrowska A, Gomulkiewicz A, Witkiewicz W, Dziegiel P. 2016. Periostin expression in cancer-associated fibroblasts of invasive ductal breast carcinoma. Oncol Rep 36:2745-2754.
217. Liu AY, Zheng H, Ouyang G. 2014. Periostin, a multifunctional matricellular protein in inflammatory and tumor microenvironments. Matrix Biol 37:150-6.
218. Cui D, Huang Z, Liu Y, Ouyang G. 2017. The multifaceted role of periostin in priming the tumor microenvironments for tumor progression. Cell Mol Life Sci 74:4287-4291.
219. González-González L, Alonso J. 2018. Periostin: A Matricellular Protein With Multiple Functions in Cancer Development and Progression. Front Oncol 8:225.
220. Michaylira CZ, Wong GS, Miller CG, Gutierrez CM, Nakagawa H, Hammond R, Klein-Szanto AJ, Lee JS, Kim SB, Herlyn M, Diehl JA, Gimotty P, Rustgi AK. 2010. Periostin, a cell adhesion molecule, facilitates

invasion in the tumor microenvironment and annotates a novel tumor-invasive signature in esophageal cancer. Cancer Res 70:5281-92.
221. Nakazawa Y, Taniyama Y, Sanada F, Morishita R, Nakamori S, Morimoto K, Yeung KT, Yang J. 2018. Periostin blockade overcomes chemoresistance via restricting the expansion of mesenchymal tumor subpopulations in breast cancer. Scientific Reports 8:4013.
222. Rios H, Koushik SV, Wang H, Wang J, Zhou HM, Lindsley A, Rogers R, Chen Z, Maeda M, Kruzynska-Frejtag A, Feng JQ, Conway SJ. 2005. periostin null mice exhibit dwarfism, incisor enamel defects, and an early-onset periodontal disease-like phenotype. Mol Cell Biol 25:11131-44.
223. Kanisicak O, Khalil H, Ivey MJ, Karch J, Maliken BD, Correll RN, Brody MJ, J. Lin S-C, Aronow BJ, Tallquist MD, Molkentin JD. 2016. Genetic lineage tracing defines myofibroblast origin and function in the injured heart. Nature Communications 7:12260.
224. Liu T, Zhou L, Li D, Andl T, Zhang Y. 2019. Cancer-Associated Fibroblasts Build and Secure the Tumor Microenvironment. Frontiers in Cell and Developmental Biology 7.
225. Marusyk A, Tabassum DP, Janiszewska M, Place AE, Trinh A, Rozhok AI, Pyne S, Guerriero JL, Shu S, Ekram M, Ishkin A, Cahill DP, Nikolsky Y, Chan TA, Rimawi MF, Hilsenbeck S, Schiff R, Osborne KC, Letai A, Polyak K. 2016. Spatial Proximity to Fibroblasts Impacts Molecular Features and Therapeutic Sensitivity of Breast Cancer Cells Influencing Clinical Outcomes. Cancer Res 76:6495-6506.
226. Hirata E, Girotti MR, Viros A, Hooper S, Spencer-Dene B, Matsuda M, Larkin J, Marais R, Sahai E. 2015. Intravital imaging reveals how BRAF inhibition generates drug-tolerant microenvironments with high integrin β1/FAK signaling. Cancer Cell 27:574-88.
227. Öhlund D, Handly-Santana A, Biffi G, Elyada E, Almeida AS, Ponz-Sarvise M, Corbo V, Oni TE, Hearn SA, Lee EJ, Chio, II, Hwang CI, Tiriac H, Baker LA, Engle DD, Feig C, Kultti A, Egeblad M, Fearon DT, Crawford JM, Clevers H, Park Y, Tuveson DA. 2017. Distinct populations of inflammatory fibroblasts and myofibroblasts in pancreatic cancer. J Exp Med 214:579-596.
228. Brauer HA, Makowski L, Hoadley KA, Casbas-Hernandez P, Lang LJ, Romàn-Pèrez E, D'Arcy M, Freemerman AJ, Perou CM, Troester MA. 2013. Impact of Tumor Microenvironment and Epithelial Phenotypes on Metabolism in Breast Cancer. Clinical Cancer Research 19:571-585.
229. Xiao L, Kim DJ, Davis CL, McCann JV, Dunleavey JM, Vanderlinden AK, Xu N, Pattenden SG, Frye SV, Xu X, Onaitis M, Monaghan-Benson E, Burridge K, Dudley AC. 2015. Tumor Endothelial Cells with Distinct

Patterns of TGFβ-Driven Endothelial-to-Mesenchymal Transition. Cancer Research 75:1244.
230. Wershof E, Park D, Barry DJ, Jenkins RP, Rullan A, Wilkins A, Schlegelmilch K, Roxanis I, Anderson KI, Bates PA, Sahai E. 2021. A FIJI macro for quantifying pattern in extracellular matrix. Life Sci Alliance 4.
231. Püspöki Z, Storath M, Sage D, Unser M. 2016. Transforms and Operators for Directional Bioimage Analysis: A Survey. Adv Anat Embryol Cell Biol 219:69-93.
232. Johnstone CN, Smith YE, Cao Y, Burrows AD, Cross RS, Ling X, Redvers RP, Doherty JP, Eckhardt BL, Natoli AL, Restall CM, Lucas E, Pearson HB, Deb S, Britt KL, Rizzitelli A, Li J, Harmey JH, Pouliot N, Anderson RL. 2015. Functional and molecular characterisation of EO771.LMB tumours, a new C57BL/6-mouse-derived model of spontaneously metastatic mammary cancer. Dis Model Mech 8:237-51.
233. Alkner S, Tang M-HE, Brueffer C, Dahlgren M, Chen Y, Olsson E, Winter C, Baker S, Ehinger A, Rydén L, Saal LH, Fernö M, Gruvberger-Saal SK. 2015. Contralateral breast cancer can represent a metastatic spread of the first primary tumor: determination of clonal relationship between contralateral breast cancers using next-generation whole genome sequencing. Breast Cancer Research 17:102.
234. Vichapat V, Garmo H, Holmberg L, Fentiman IS, Tutt A, Gillett C, Lüchtenborg M. 2012. Patterns of metastasis in women with metachronous contralateral breast cancer. British Journal of Cancer 107:221-223.
235. van Helvert S, Storm C, Friedl P. 2018. Mechanoreciprocity in cell migration. Nat Cell Biol 20:8-20.
236. Friedl P, Alexander S. 2011. Cancer invasion and the microenvironment: plasticity and reciprocity. Cell 147:992-1009.
237. Ősz Á, Lánczky A, Győrffy B. 2021. Survival analysis in breast cancer using proteomic data from four independent datasets. Scientific Reports 11:16787.
238. Bhattacharjee S, Hamberger F, Ravichandra A, Miller M, Nair A, Affo S, Filliol A, Chin L, Savage TM, Yin D, Wirsik NM, Mehal A, Arpaia N, Seki E, Mack M, Zhu D, Sims PA, Kalluri R, Stanger BZ, Olive KP, Schmidt T, Wells RG, Mederacke I, Schwabe RF. 2021. Tumor restriction by type I collagen opposes tumor-promoting effects of cancer-associated fibroblasts. J Clin Invest 131.
239. Goetz Jacky G, Minguet S, Navarro-Lérida I, Lazcano Juan J, Samaniego R, Calvo E, Tello M, Osteso-Ibáñez T, Pellinen T, Echarri A, Cerezo A, Klein-Szanto Andres JP, Garcia R, Keely Patricia J, Sánchez-Mateos P,

Cukierman E, Del Pozo Miguel A. 2011. Biomechanical Remodeling of the Microenvironment by Stromal Caveolin-1 Favors Tumor Invasion and Metastasis. Cell 146:148-163.
240. Wullkopf L, West AV, Leijnse N, Cox TR, Madsen CD, Oddershede LB, Erler JT. 2018. Cancer cells' ability to mechanically adjust to extracellular matrix stiffness correlates with their invasive potential. Mol Biol Cell 29:2378-2385.
241. Barker HE, Chang J, Cox TR, Lang G, Bird D, Nicolau M, Evans HR, Gartland A, Erler JT. 2011. LOXL2-mediated matrix remodeling in metastasis and mammary gland involution. Cancer Res 71:1561-72.
242. Alexander S, Weigelin B, Winkler F, Friedl P. 2013. Preclinical intravital microscopy of the tumour-stroma interface: invasion, metastasis, and therapy response. Curr Opin Cell Biol 25:659-71.
243. Wolf K, Alexander S, Schacht V, Coussens LM, von Andrian UH, van Rheenen J, Deryugina E, Friedl P. 2009. Collagen-based cell migration models in vitro and in vivo. Semin Cell Dev Biol 20:931-41.
244. Ilina O, Bakker GJ, Vasaturo A, Hofmann RM, Friedl P. 2011. Two-photon laser-generated microtracks in 3D collagen lattices: principles of MMP-dependent and -independent collective cancer cell invasion. Phys Biol 8:015010.
245. Lee HO, Mullins SR, Franco-Barraza J, Valianou M, Cukierman E, Cheng JD. 2011. FAP-overexpressing fibroblasts produce an extracellular matrix that enhances invasive velocity and directionality of pancreatic cancer cells. BMC Cancer 11:245.
246. Venning FA, Wullkopf L, Erler JT. 2015. Targeting ECM Disrupts Cancer Progression. Front Oncol 5:224.
247. Gillot L, Lebeau A, Baudin L, Pottier C, Louis T, Durré T, Longuespée R, Mazzucchelli G, Nizet C, Blacher S, Kridelka F, Noël A. 2022. Periostin in lymph node pre-metastatic niches governs lymphatic endothelial cell functions and metastatic colonization. Cell Mol Life Sci 79:295.
248. Whatcott CJ, Diep CH, Jiang P, Watanabe A, LoBello J, Sima C, Hostetter G, Shepard HM, Von Hoff DD, Han H. 2015. Desmoplasia in Primary Tumors and Metastatic Lesions of Pancreatic Cancer. Clinical Cancer Research 21:3561-3568.
249. Altorki NK, Markowitz GJ, Gao D, Port JL, Saxena A, Stiles B, McGraw T, Mittal V. 2019. The lung microenvironment: an important regulator of tumour growth and metastasis. Nature Reviews Cancer 19:9-31.
250. Ferreira S, Saraiva N, Rijo P, Fernandes AS. 2021. LOXL2 Inhibitors and Breast Cancer Progression. Antioxidants (Basel) 10.

251. Nandi T, Pradyuth S, Singh AK, Chitkara D, Mittal A. 2020. Therapeutic agents for targeting desmoplasia: current status and emerging trends. Drug Discovery Today 25:2046-2055.
252. Huang J, Zhang L, Wan D, Zhou L, Zheng S, Lin S, Qiao Y. 2021. Extracellular matrix and its therapeutic potential for cancer treatment. Signal Transduction and Targeted Therapy 6:153.
253. Duda DG, Duyverman AMMJ, Kohno M, Snuderl M, Steller EJA, Fukumura D, Jain RK. 2010. Malignant cells facilitate lung metastasis by bringing their own soil. Proceedings of the National Academy of Sciences 107:21677-21682.
254. Peinado H, Lavotshkin S, Lyden D. 2011. The secreted factors responsible for pre-metastatic niche formation: old sayings and new thoughts. Semin Cancer Biol 21:139-46.
255. Hoshino A, Costa-Silva B, Shen TL, Rodrigues G, Hashimoto A, Tesic Mark M, Molina H, Kohsaka S, Di Giannatale A, Ceder S, Singh S, Williams C, Soplop N, Uryu K, Pharmer L, King T, Bojmar L, Davies AE, Ararso Y, Zhang T, Zhang H, Hernandez J, Weiss JM, Dumont-Cole VD, Kramer K, Wexler LH, Narendran A, Schwartz GK, Healey JH, Sandstrom P, Labori KJ, Kure EH, Grandgenett PM, Hollingsworth MA, de Sousa M, Kaur S, Jain M, Mallya K, Batra SK, Jarnagin WR, Brady MS, Fodstad O, Muller V, Pantel K, Minn AJ, Bissell MJ, Garcia BA, Kang Y, Rajasekhar VK, Ghajar CM, et al. 2015. Tumour exosome integrins determine organotropic metastasis. Nature 527:329-35.
256. Wortzel I, Dror S, Kenific CM, Lyden D. 2019. Exosome-Mediated Metastasis: Communication from a Distance. Developmental Cell 49:347-360.
257. Fu Q, Zhang Q, Lou Y, Yang J, Nie G, Chen Q, Chen Y, Zhang J, Wang J, Wei T, Qin H, Dang X, Bai X, Liang T. 2018. Primary tumor-derived exosomes facilitate metastasis by regulating adhesion of circulating tumor cells via SMAD3 in liver cancer. Oncogene 37:6105-6118.
258. Bai S, Wang Z, Wang M, Li J, Wei Y, Xu R, Du J. 2022. Tumor-Derived Exosomes Modulate Primary Site Tumor Metastasis. Front Cell Dev Biol 10:752818.
259. Zhou W, Fong MY, Min Y, Somlo G, Liu L, Palomares MR, Yu Y, Chow A, O'Connor ST, Chin AR, Yen Y, Wang Y, Marcusson EG, Chu P, Wu J, Wu X, Li AX, Li Z, Gao H, Ren X, Boldin MP, Lin PC, Wang SE. 2014. Cancer-secreted miR-105 destroys vascular endothelial barriers to promote metastasis. Cancer Cell 25:501-15.

260. Peng L, Wang D, Han Y, Huang T, He X, Wang J, Ou C. 2021. Emerging Role of Cancer-Associated Fibroblasts-Derived Exosomes in Tumorigenesis. Front Immunol 12:795372.
261. Li B-L, Lu W, Qu J-J, Ye L, Du G-Q, Wan X-P. 2019. Loss of exosomal miR-148b from cancer-associated fibroblasts promotes endometrial cancer cell invasion and cancer metastasis. Journal of Cellular Physiology 234:2943-2953.
262. Yang F, Yan Y, Yang Y, Hong X, Wang M, Yang Z, Liu B, Ye L. 2020. MiR-210 in exosomes derived from CAFs promotes non-small cell lung cancer migration and invasion through PTEN/PI3K/AKT pathway. Cellular Signalling 73:109675.
263. Zarin B, Rafiee L, Daneshpajouhnejad P, Haghjooy Javanmard S. 2021. A review on the role of CAFs and CAF-derived exosomes in progression and metastasis of digestive system cancers. Tumour Biol 43:141-157.
264. Li Y, Gao S, Hu Q, Wu F. 2022. Functional Properties of Cancer Epithelium and Stroma-Derived Exosomes in Head and Neck Squamous Cell Carcinoma. Life. 12(5):doi:10.3390/life12050757.
265. Luga V, Zhang L, Viloria-Petit AM, Ogunjimi AA, Inanlou MR, Chiu E, Buchanan M, Hosein AN, Basik M, Wrana JL. 2012. Exosomes mediate stromal mobilization of autocrine Wnt-PCP signaling in breast cancer cell migration. Cell 151:1542-56.
266. McCann JV, Bischoff SR, Zhang Y, Cowley DO, Sanchez-Gonzalez V, Daaboul GD, Dudley AC. 2020. Reporter mice for isolating and auditing cell type-specific extracellular vesicles in vivo. Genesis 58:e23369.
267. Verweij FJ, Bebelman MP, Jimenez CR, Garcia-Vallejo JJ, Janssen H, Neefjes J, Knol JC, de Goeij-de Haas R, Piersma SR, Baglio SR, Verhage M, Middeldorp JM, Zomer A, van Rheenen J, Coppolino MG, Hurbain I, Raposo G, Smit MJ, Toonen RFG, van Niel G, Pegtel DM. 2018. Quantifying exosome secretion from single cells reveals a modulatory role for GPCR signaling. J Cell Biol 217:1129-1142.
268. Pols MS, Klumperman J. 2009. Trafficking and function of the tetraspanin CD63. Experimental Cell Research 315:1584-1592.
269. Egeblad M, Ewald AJ, Askautrud HA, Truitt ML, Welm BE, Bainbridge E, Peeters G, Krummel MF, Werb Z. 2008. Visualizing stromal cell dynamics in different tumor microenvironments by spinning disk confocal microscopy. Dis Model Mech 1:155-67; discussion 165.
270. Franco C, Britto K, Wong E, Hou G, Zhu SN, Chen M, Cybulsky MI, Bendeck MP. 2009. Discoidin domain receptor 1 on bone marrow-derived cells promotes macrophage accumulation during atherogenesis. Circ Res 105:1141-8.

271. Guerrot D, Kerroch M, Placier S, Vandermeersch S, Trivin C, Mael-Ainin M, Chatziantoniou C, Dussaule JC. 2011. Discoidin domain receptor 1 is a major mediator of inflammation and fibrosis in obstructive nephropathy. Am J Pathol 179:83-91.
272. Postlethwaite AE, Kang AH. 1976. Collagen-and collagen peptide-induced chemotaxis of human blood monocytes. J Exp Med 143:1299-307.
273. Weathington NM, van Houwelingen AH, Noerager BD, Jackson PL, Kraneveld AD, Galin FS, Folkerts G, Nijkamp FP, Blalock JE. 2006. A novel peptide CXCR ligand derived from extracellular matrix degradation during airway inflammation. Nat Med 12:317-23.
274. Arnold SA, Rivera LB, Miller AF, Carbon JG, Dineen SP, Xie Y, Castrillon DH, Sage EH, Puolakkainen P, Bradshaw AD, Brekken RA. 2010. Lack of host SPARC enhances vascular function and tumor spread in an orthotopic murine model of pancreatic carcinoma. Dis Model Mech 3:57-72.
275. Meyaard L. 2008. The inhibitory collagen receptor LAIR-1 (CD305). J Leukoc Biol 83:799-803.
276. Kaplan G. 1983. In vitro differentiation of human monocytes. Monocytes cultured on glass are cytotoxic to tumor cells but monocytes cultured on collagen are not. J Exp Med 157:2061-72.
277. Yang T, Deng Z, Pan Z, Qian Y, Yao W, Wang J. 2020. Prognostic value of periostin in multiple solid cancers: A systematic review with meta-analysis. J Cell Physiol 235:2800-2808.
278. Yamato H, Kimura K, Fukui E, Kanou T, Ose N, Funaki S, Minami M, Shintani Y. 2021. Periostin secreted by activated fibroblasts in idiopathic pulmonary fibrosis promotes tumorigenesis of non-small cell lung cancer. Scientific Reports 11:21114.
279. Massy E, Rousseau JC, Gueye M, Bonnelye E, Brevet M, Chambard L, Duruisseaux M, Borel O, Roger C, Guelminger R, Pialat JB, Gineyts E, Bouazza L, Millet M, Maury JM, Clézardin P, Girard N, Confavreux CB. 2021. Serum total periostin is an independent marker of overall survival in bone metastases of lung adenocarcinoma. Journal of Bone Oncology 29:100364.
280. Zhang Y, Yuan D, Yao Y, Sun W, Shi Y, Su X. 2017. Predictive and prognostic value of serum periostin in advanced non-small cell lung cancer patients receiving chemotherapy. Tumour Biol 39:1010428317698367.
281. Liu Y, Li F, Gao F, Xing L, Qin P, Liang X, Zhang J, Qiao X, Lin L, Zhao Q, Du L. 2017. Role of microenvironmental periostin in pancreatic cancer progression. Oncotarget 8:89552-89565.

282. Fukushima N, Kikuchi Y, Nishiyama T, Kudo A, Fukayama M. 2008. Periostin deposition in the stroma of invasive and intraductal neoplasms of the pancreas. Mod Pathol 21:1044-53.
283. Ben QW, Jin XL, Liu J, Cai X, Yuan F, Yuan YZ. 2011. Periostin, a matrix specific protein, is associated with proliferation and invasion of pancreatic cancer. Oncol Rep 25:709-16.
284. Foster DS, Januszyk M, Delitto D, Yost KE, Griffin M, Guo J, Guardino N, Delitto AE, Chinta M, Burcham AR, Nguyen AT, Bauer-Rowe KE, Titan AL, Salhotra A, Jones RE, da Silva O, Lindsay HG, Berry CE, Chen K, Henn D, Mascharak S, Talbott HE, Kim A, Nosrati F, Sivaraj D, Ransom RC, Matthews M, Khan A, Wagh D, Coller J, Gurtner GC, Wan DC, Wapnir IL, Chang HY, Norton JA, Longaker MT. 2022. Multiomic analysis reveals conservation of cancer-associated fibroblast phenotypes across species and tissue of origin. Cancer Cell 40:1392-1406.e7.
285. Chijimatsu R, Kobayashi S, Takeda Y, Kitakaze M, Tatekawa S, Arao Y, Nakayama M, Tachibana N, Saito T, Ennishi D, Tomida S, Sasaki K, Yamada D, Tomimaru Y, Takahashi H, Okuzaki D, Motooka D, Ohshiro T, Taniguchi M, Suzuki Y, Ogawa K, Mori M, Doki Y, Eguchi H, Ishii H. 2022. Establishment of a reference single-cell RNA sequencing dataset for human pancreatic adenocarcinoma. iScience 25:104659.
286. Okazaki T, Tamai K, Shibuya R, Nakamura M, Mochizuki M, Yamaguchi K, Abe J, Takahashi S, Sato I, Kudo A, Okada Y, Satoh K. 2018. Periostin is a negative prognostic factor and promotes cancer cell proliferation in non-small cell lung cancer. Oncotarget 9:31187-31199.
287. Kai F, Drain AP, Weaver VM. 2019. The Extracellular Matrix Modulates the Metastatic Journey. Developmental Cell 49:332-346.
288. Xiao Y, Yu D. 2021. Tumor microenvironment as a therapeutic target in cancer. Pharmacol Ther 221:107753.
289. Smith AL, Robin TP, Ford HL. 2012. Molecular Pathways: Targeting the TGF-β Pathway for Cancer Therapy. Clinical Cancer Research 18:4514-4521.
290. Keiser HR, Sjoerdsma A. 1967. Studies on beta-aminopropionitrile in patients with scleroderma. Clinical Pharmacology & Therapeutics 8:593-602.
291. Lee YJ, Kim IS, Park S-A, Kim Y, Lee JE, Noh D-Y, Kim K-T, Ryu SH, Suh P-G. 2013. Periostin-binding DNA Aptamer Inhibits Breast Cancer Growth and Metastasis. Molecular Therapy 21:1004-1013.
292. Kyutoku M, Taniyama Y, Katsuragi N, Shimizu H, Kunugiza Y, Iekushi K, Koibuchi N, Sanada F, Oshita Y, Morishita R. 2011. Role of periostin in cancer progression and metastasis: Inhibition of breast cancer

progression and metastasis by anti-periostin antibody in a murine model. Int J Mol Med 28:181-186.
293. Fu Z, Li S, Han S, Shi C, Zhang Y. 2022. Antibody drug conjugate: the “biological missile” for targeted cancer therapy. Signal Transduction and Targeted Therapy 7:93.
294. Szot C, Saha S, Zhang XM, Zhu Z, Hilton MB, Morris K, Seaman S, Dunleavey JM, Hsu KS, Yu GJ, Morris H, Swing DA, Haines DC, Wang Y, Hwang J, Feng Y, Welsch D, DeCrescenzo G, Chaudhary A, Zudaire E, Dimitrov DS, St Croix B. 2018. Tumor stroma-targeted antibody-drug conjugate triggers localized anticancer drug release. J Clin Invest 128:2927-2943.
295. Boni V, Sharma MR, Patnaik A. 2020. The Resurgence of Antibody Drug Conjugates in Cancer Therapeutics: Novel Targets and Payloads. American Society of Clinical Oncology Educational Book:e58-e74.
296. Staudacher AH, Brown MP. 2017. Antibody drug conjugates and bystander killing: is antigen-dependent internalisation required? British Journal of Cancer 117:1736-1742.